Optimal Control based Image Sequence Interpolation

von Kanglin Chen

Dissertation

zur Erlangung des Grades eines Doktors der Naturwissenschaften

– Dr. rer. nat. –

Vorgelegt im Fachbereich 3 (Mathematik & Informatik)

der Universität Bremen

im September 2011

Datum des Promotionskolloquiums: 27. September 2011

Gutachter: Prof. Dr. Dirk Lorenz (TU Braunschweig)
Prof. Dr. Peter Maaß (Universität Bremen)

Zusammenfassung

Die vorliegende Arbeit entstand im Rahmen einer dreijährige Promotionsforschung im Bereich der Interpolation einer Bildsequenz. Die vorgestellten Interpolationsmethoden sind hauptsächlich auf der Suche nach einem passenden optischen Flussfeld, mit dem die Objekte im Anfangsbild zu einem bestimmten Zeitpunkt „transportiert“ und „verzerrt“ werden können. Um das optische Flussfeld zu identifizieren, wird das Interpolationsproblem im Rahmen der optimalen Steuerung mit Hilfe der Transportgleichung gesteuert. Um die Qualität der Interpolation zu verbessern, werden die Modellen vorgestellt, so dass die optischen Flusskanten bleiben erhalten und die Vorwärts- bzw. Rückwärts-Interpolation lokal ausgewertet werden können. Grundlegend dabei ist die Verwendung einer geglätteten Version der totalen Variation und der aktiven Konturen für die Segmentierung. Aus theoretischer Sicht wird die Lösungstheorie der Transportgleichung unter verschiedenen Regularitätsvoraussetzungen an den optischen Fluss untersucht. Die resultierenden Ergebnisse ermöglichen dann den Nachweis der Existenz eines Minimierers des geweiligen Minimierungsproblems.

Abstract

This thesis includes my three-year doctoral research in the field of image sequence interpolation. The introduced interpolation methods are mainly based on finding an appropriate optical flow field, with which the objects in an initial image can be "transported" and "warped" to a certain time. To identify the optical flow field the interpolation problem is considered in the framework of optimal control governed by the transport equation. To improve the interpolation quality, the models are introduced so that the edges of the optical flow are preserved, the forward and backward interpolation are locally selected. Basically the smooth version of total variation and the active contours for segmentation are used. In the theoretical part, the solution theory of transport equation is investigated under different settings on the regularity of the optical flow, and applied in the proof of the existence of a minimizer to the associated minimization problems.

Acknowledgements

I would like to acknowledge that my doctoral research is supported by the Zentrale Forschungsförderung, Universität Bremen within the Ph.D group "Scientific Computing in Engineering" (SCiE).

I would like to thank my supervisor Prof. Dirk Lorenz for his encouragement and patient supervision, Prof. Peter Maaß for his evaluation of my thesis, all the people of the "AG Technomathematik", all the colleagues of SCiE, in particular Bastian Kanning, Thanh Son Nguyen, Quy Muoi Pham, Majid Salmani in the same office of me for their help both in the research and private life. Last but not the least, I would like to thank my family for their permanent support of my study.

Contents

List of Figures

Chapter 1

Introduction

Image sequence interpolation is the generation of intermediate images between two given consecutive images, a process which is, for example, relevant if the image acquisition is slow or expensive and has broad applications in the fields of video compression, medical imaging and so on. In video compression, the knowledge of motions helps to remove the non-moving parts of images and compress video sequences with high compression rates. For example in the MPEG format, motion estimation is the most computationally expensive portion of the video encoder and normally solved by mesh-based matching techniques [57]. While decompressing a video, intermediate images are generated by warping the image sequence with motion vectors. In the field of medical imaging image sequence interpolation is also desired. For example, the diagnostic requires a point-by-point correspondence between the same tissue from the image sequence taken at different time [50]. Similarly, in disease diagnostics an image of a patient's tissue may need to be compared with a healthy tissue [31]. This is an example of how image sequence interpolation in some cases can be used to solve the problem normally classified as image registration. In addition, image sequence interpolation is also able to improve the quality of historic movies by increasing the frame-rate to the modern standard.

1.1 Outline of the Thesis

We divide this thesis into 6 chapters. In the second chapter we give a brief introduction of functions of bounded variation, for short BV, and introduce some important

properties of BV. Then we introduce the concept of mollifiers and their approximate properties, in particular we prove the convergence of a mollified sequence in the L^p-norm defined in the whole domain. Finally, we consider two-dimensional Stokes equations and propose the mixed finite element method for solving them.

In the third chapter we propose the first model of image sequence interpolation in the framework of optimal control governed by a transport equation. According to the classic solution theory of transport equations we model the cost functional regularized by an H^3-term of optical flow, and we prove the existence of a minimizer to the associated minimization problem. In the application we substitute the H^3-regularization with an H^1-regularization and propose two different segregation loops for solving the first-order optimality conditions system.

Since the H^1-regularization is too smooth to preserve the discontinuities of the optical flow, we introduce in Chapter 4 the ε-smooth total variation to regularize the optical flow in the cost functional. According to the theory of DiPerna and Lions the transport equation is still well-posed if the optical flow enjoys the Sobolev regularity. Thanks to this solution theory of transport equations we are able to prove the existence of a minimizer to the associated minimization problem.

The last model we propose in Chapter 5 combines the segmentation by active contours with the previous model such that the domain is divided into the covered parts and disclosed parts, which are suitable for the forward image interpolation and backward image interpolation, respectively. We also prove the existence of a minimizer to the associated minimization problem and evaluate our model with the experiments based on human visual perception.

1.2 Optical Flow

The optical flow plays a decisive role in our modeling of image sequence interpolation, so we give here a brief overview of it. As mentioned in [8], we are not able to measure the 2d motion field (the projection on the image plane of the 3d velocity of the scene), what we are able to perceive is just an apparent motion, also called the optical flow. By apparent, we mean that this 2d motion is observable only through intensity variations. Although the optical flow and the 2d motion field are quantitatively different, they often share the same motion discontinuities, and the optical flow gives a rich source of information about real 3d kinematic behavior of

objects.

Horn and Schunck are the first who proposed a variational method based on gradients to estimate the optical flow in their celebrated work [36]. The optical flow constraint equation

$$u_t + b \cdot \nabla u = 0 \tag{1.1}$$

derived from a Taylor expansion of the conservation equation

$$u(t, x) = u_0(x - bt), \tag{1.2}$$

where u_0 is an initial image, $b := (v, w)$ is the optical flow, and u is image intensity function defined in time and space. Define that Ω is a bounded domain of $\mathbb{R}^2$, and λ is the regularization parameter to trade off the fidelity term and regularization term, combined (1.1) with a global smoothness term to constrain the estimated flow field b, minimizing

$$\int_\Omega \left(u_t + b \cdot \nabla u\right)^2 dx + \lambda \int_\Omega |\nabla v|^2 + |\nabla w|^2 \, dx$$

yields the first-order optimality conditions system

$$\begin{cases} \Delta v - \dfrac{1}{\lambda}\left(u_x^2 v + u_x u_y w + u_x u_t\right) = 0, \\ \Delta w - \dfrac{1}{\lambda}\left(u_y^2 w + u_x u_y v + u_y u_t\right) = 0. \end{cases}$$

Until now, the gradient-based methods for optical flow estimation have been widely developed. For instance, in [14] the local Lukas & Kanade method , is combined with the Horn & Schunck method, because the local differential method has advantage of robustness against noises and the global differential method is able to produce a dense optical flow. Since the Horn & Schunck method penalizes the optical flow in a quadratic way, it does not allow discontinuities in the flow field, and it does not handle outliers in the fidelity term robustly. To overcome these limitations, the TV-L^1 model [59, 58] was proposed such that the TV constraint makes the optical flow piece-wise constant, and the fidelity term endowed with the L^1-norm can be regarded as applying methods from robust statistics where outliers are penalized less severely than in quadratic methods [14]. Finally, it is worthy mentioning the

work of Ito et al. [11]. They estimated the optical flow in the framework of optimal control governed by the transport equation (3.1). The cost functional is defined as

$$\frac{1}{2}\|u(T)-u_T\|^2_{L^2(\Omega)} + \int_0^T\int_\Omega \frac{\alpha}{2}\Phi(|\partial_t b|^2)+\frac{\beta}{2}\Psi(|\nabla v|^2+|\nabla w|^2)+\frac{\gamma}{2}|\mathrm{div} b|^2\,dxdt$$

where u_T is another given image at time T, and α, β, γ are positive regularization parameters, and Φ, Ψ are specially chosen functions which make the optical flow smooth in time and piece-wise smooth in space (see [11] for details). Using the optimal control makes the optical flow estimation more stable compared to the Horn & Schunck method and this method is also quite similar to our image sequence interpolation methods [22] to be proposed.

For visualization of the optical flow we use the color coding scheme proposed in [9] (see Figure 1.1).

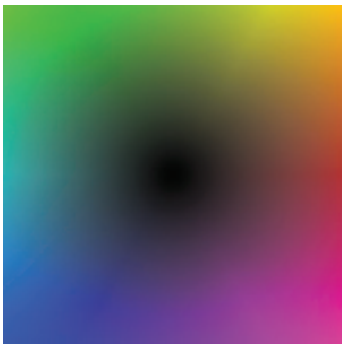

Figure 1.1: Color coding map of the optical flow: Direction is coded by hue, length is coded by saturation.

1.3 Recent Results of Image Sequence Interpolation

There are several existing variational methods to interpolate the missing intermediate images. In [39] the variational method penalized by the elastic regularization

is considered:

$$J_{\text{rigid}}(u,b) = \int\limits_{[0,T]\times\Omega} (u_t + b\cdot\nabla u)^2 + \lambda\left|\nabla b' + \nabla b\right|^2 dxdt, \tag{1.3}$$

where b' is the transpose of b. Minimizing (1.3) gives the interpolated images with maximal rigidity, and has applications in the field of medical image registration, e.g. registration of magnetic resonance images. In [34] the authors keep the conservation equation (1.2) without differentiating it and apply the time dependent Horn & Schunck functional:

$$J_{\text{cons}}(b) = \frac{\lambda}{2}\int\limits_0^T \|u(t) - u_T\|^2_{L^2(\Omega)}\, dt + \frac{1}{2}\int\limits_0^T\int\limits_\Omega |\nabla b|^2\, dxdt,$$

where $u(0) = u_0$ and u_T are the given two images. After calculating the time-dependent optical flow one can warp the initial image u_0 to a certain time.

Different from the global variational methods, some introduce the per-pixel-wise methods. In [42] the path-based interpolation sequence method is considered. They search where every pixel comes from and trace out the path of every pixel from the given two images. To stabilize the interpolation they have to post-process the occlusions by means of verification of the displacement flow. The group Compute Graphics at TU Braunschweig introduced another per-pixel-wise method, namely the perception-based interpolation [51, 52]. They simulate human visual perception in the following way: To begin with, they detect the edges and homogeneous region, and then they estimate the translets by matching edges, finally they use the forward warping and feather the interpolated images.

Chapter 2

Basic Theory

2.1 Total Variation

In this section we give the concept of functions of bounded variation (BV) and list some important properties of BV which will be applied in the following chapters. For the literature of BV we refer to [8, 7, 30, 5].

Definition 2.1. *Let Ω be a bounded open subset of $\mathbb{R}^d$ and f be a function in $L^1(\Omega)$. We say a function f has* bounded variation *if*

$$\int_\Omega |Df| := \sup\left\{ \int_\Omega f \mathrm{div}\varphi \, dx \;\middle|\; \varphi \in C_0^1(\Omega)^d, \;\; \|\varphi\|_{L^\infty(\Omega)^d} \le 1 \right\} < \infty,$$

where $C_0^1(\Omega)^d$ is the space of continuously differential functions with compact support in Ω, endowed with the uniform norm $\|\varphi\|_{L^\infty(\Omega)^d} = \left(\sum_{i=1}^d \sup_{x\in\Omega} |\varphi_i(x)|^2\right)^{1/2}$.

An important example is the case $f = \chi_A$, the characteristic function of a subset A of $\mathbb{R}^d$:

$$\int_\Omega |Df| = \sup\left\{ \int_A \mathrm{div}\varphi \, dx \;\middle|\; \varphi \in C_0^1(\Omega)^d, \;\; \|\varphi\|_{L^\infty(\Omega)^d} \le 1 \right\}.$$

If this supremum is finite, A is called a set of finite perimeter in Ω, and we write

$$\int_{\Omega} |D\chi_A| = \mathrm{Per}_{\Omega}(A).$$

If ∂A is smooth, then $\mathrm{Per}_{\Omega}(A)$ coincides with classical length ($d = 2$) or surface area ($d = 3$).

Definition 2.2. *We define* $BV(\Omega)$*,* the space of functions of bounded variation*, as*

$$BV(\Omega) = \left\{ f \in L^1(\Omega) \;\middle|\; \int_{\Omega} |Df| < \infty \right\}.$$

The associated BV *norm of an* $f \in BV(\Omega)$ *is given by*

$$\|f\|_{BV(\Omega)} = \|f\|_{L^1(\Omega)} + \int_{\Omega} |Df|.$$

The Sobolev space $W^{1,1}(\Omega)$ is a closed subspace of $BV(\Omega)$. Indeed, unlike Sobolev functions the BV functions are piecewise continuous, i.e. allow discontinuities in hypersurfaces of dimension $d-1$. Due to such advantage BV has been very successfully applied in many subfields of image processing, such as image denoising [48], image deblurring [21], image inpainting [19] and so on.

Every BV function can be approximated by C^∞ functions but not in BV norm, since the closure of of the set of C^∞ functions in this norm is $W^{1,1}(\Omega)$. However, the weak* topology of BV defined as

$$f_n \xrightarrow[BV(\Omega)]{*} f \iff \begin{cases} f_n \longrightarrow f \quad \text{in } L^1(\Omega), \\ \displaystyle\int_{\Omega} \varphi\, Df_n \longrightarrow \int_{\Omega} \varphi\, Df \quad \text{for all } \varphi \text{ in } C_0(\Omega)^d, \end{cases}$$

possesses good compactness properties. Assume that Ω is a bounded open subset of $\mathbb{R}^d$ and $\partial\Omega$ is Lipschitz in the following context of this chapter. We give another characterization of the weak* topology of BV in the following theorem:

Theorem 2.1. *Let* $(f_n) \subset BV(\Omega)$*. Then* (f_n) *converges weakly* to* f *in* $BV(\Omega)$ *if and only if* (f_n) *is uniformly bounded in* $BV(\Omega)$ *and converges to* f *in* $L^1(\Omega)$*.*

The compactness properties of BV in the weak* topology is concluded in the following theorem:

Theorem 2.2. *Let (f_n) be uniformly bounded in $BV(\Omega)$. Then there exists a subsequence (f_{n_k}) of (f_n) and $f \in BV(\Omega)$ with $1 \leq p < \frac{d}{d-1}$ such that*

$$f_{n_k} \longrightarrow f \quad \text{in } L^p(\Omega),$$
$$\int_\Omega \varphi \, Df_{n_k} \longrightarrow \int_\Omega \varphi \, Df \quad \text{for all } \varphi \text{ in } C_0(\Omega)^d.$$

Moreover, $BV(\Omega)$ is continuously embedded in $L^p(\Omega)$ with $p = \infty$ if $d = 1$, and $p = \frac{d}{d-1}$ otherwise.

The lower semi-continuity of total variation of BV functions is often used to prove the existence of a minimizer to a total variation minimization problem.

Corollary 2.1. *Let $(f_n) \subset BV(\Omega)$ and (f_n) converge to f in $L^1(\Omega)$. Then*

$$\int_\Omega |Df| \leq \liminf_{n\to\infty} \int_\Omega |Df_n|.$$

We also want to introduce the generalized Gauss-Green theorem of $BV(\Omega)$.

Theorem 2.3. *There exists a bounded linear mapping*

$$K : BV(\Omega) \to L^1(\partial\Omega; \mathcal{H}^{d-1})$$

such that

$$\int_\Omega f \mathrm{div}\varphi \, dx = -\int_\Omega \varphi \, dDf + \int_{\partial\Omega} (\varphi \cdot \nu) Kf \, d\mathcal{H}^{d-1},$$

for all $f \in BV(\Omega)$, $\varphi \in C^1(\mathbb{R}^d)^d$ and ν denoting the unit outer normal to $\partial\Omega$. The function Kf, which is uniquely defined up to sets of $d-1$ dimensional Hausdorff measure $\mathcal{H}^{d-1}$ equal to zero, is called the trace *of f on $\partial\Omega$.*

2.2 Mollifier

Definition 2.3 (Mollifier)**.** *Define a C^∞ function $\eta : \mathbb{R}^d \to \mathbb{R}$ as follows:*

$$\eta(x) = \begin{cases} c \exp\left(\dfrac{1}{|x|^2 - 1}\right) & \text{if } |x| < 1, \\ 0 & \text{if } |x| \geq 1, \end{cases}$$

the constant c is chosen such that

$$\int_{\mathbb{R}^d} \eta(x)\, dx = 1.$$

Let $\varepsilon > 0$ and then define

$$\eta_\varepsilon(x) = \frac{1}{\varepsilon^d} \eta\left(\frac{x}{\varepsilon}\right), \quad x \in \mathbb{R}^d,$$

here η_ε denotes the standard mollifier*. Let us define the convolution of the mollifier η_ε and a function f as*

$$f_\varepsilon(x) = \eta_\varepsilon * f(x) = \int_\Omega \eta_\varepsilon(x - y) f(y)\, dy. \tag{2.1}$$

We list some important properties of mollifier [30, 8] in the following theorem:

Theorem 2.4. *Let $1 \leq p < \infty$ and $f \in L^p(\Omega)$. Then*

1. *$\eta_\varepsilon * f \in C^\infty(\Omega)$;*
2. *$\eta_\varepsilon * f \to f$ a.e. as $\varepsilon \to 0$;*
3. *$\|\eta_\varepsilon * f\|_{L^p(\Omega)} \leq \|f\|_{L^p(\Omega)}$;*
4. *$\lim\limits_{\varepsilon \downarrow 0} \|f * \eta_\varepsilon - f\|_{L^p(\Omega)} = 0$.*

In view of these properties, mollifiers are also called *approximate identities*. The convergence property of mollifiers in norm is normally given in a subset of Ω. We want to verify it in Ω with definition (2.1):

Proof. We prove the convergence property in L^p-nom. First of all, we use without proof the result that $C_c(\Omega)$ is dense in $L^p(\Omega)$. It means that for every $\tau > 0$ there exists $g \in C_c(\Omega)$ with $\|f - g\|_{L^p(\Omega)} < \tau$. Let us check the statement for g first:

$$\begin{aligned}\int\limits_\Omega |\eta_\varepsilon * g(x) - g(x)|^p \, dx = \int\limits_\Omega \Bigg| \int\limits_\Omega \eta_\varepsilon(x-y)g(y)\,dy \\ - \int\limits_\Omega \eta_\varepsilon(x-y)g(x)\,dy - \int\limits_{\mathbb{R}^d\setminus\Omega} \eta_\varepsilon(x-y)g(x)\,dy\Bigg|^p dx. \\ \overset{\text{Lemma 2.1}}{\leq} 2^{p-1}\Bigg(\int\limits_\Omega \Bigg| \int\limits_\Omega \eta_\varepsilon(x-y)(g(y)-g(x))\,dy\Bigg|^p dx \\ + \int\limits_\Omega \Bigg| \int\limits_{\mathbb{R}^d\setminus\Omega} \eta_\varepsilon(x-y)g(x)\,dy\Bigg|^p dx\Bigg). \qquad (2.2)\end{aligned}$$

Consider the second summand of the right-hand side of (2.2):

$$\begin{aligned}&\int\limits_\Omega \Bigg| \int\limits_{\mathbb{R}^d\setminus\Omega} \eta_\varepsilon(x-y)g(x)\,dy\Bigg|^p dx \\ &\leq \int\limits_\Omega |B_\varepsilon(x)|^p |g(x)|^p dx \\ &= |B_\varepsilon|^p \, \|g\|^p_{L^p(\Omega)}\,,\end{aligned}$$

where $B_\varepsilon(x)$ denotes the set of all points $y \in \mathbb{R}^d$ such that $|x-y| < \varepsilon$. Consider the first summand of the right-hand side of (2.2):

$$\begin{aligned}\int\limits_\Omega \Bigg| \int\limits_\Omega \eta_\varepsilon(x-y)(g(y)-g(x))\,dy\Bigg|^p dx &= \int\limits_\Omega \Bigg| \int\limits_{B_\varepsilon(x)\cap\Omega} \eta_\varepsilon(x-y)(g(y)-g(x))\,dy\Bigg|^p dx \\ &\leq \sup_{|x-y|<\varepsilon} |g(y)-g(x)|^p \int\limits_\Omega \Bigg| \int\limits_{B_\varepsilon(x)\cap\Omega} \eta_\varepsilon(x-y)\,dy\Bigg|^p dx \\ &\leq \sup_{|x-y|<\varepsilon} |g(y)-g(x)|^p \, |B_\varepsilon(x)\cap\Omega|^p \, |\Omega|.\end{aligned}$$

Since g has compact support and it is uniformly continuous, one has

$$\lim_{\varepsilon \to 0} \|\eta_\varepsilon * g - g\|_{L^p(\Omega)} = 0. \tag{2.3}$$

Finally,

$$\begin{aligned} \|\eta_\varepsilon * f - f\|_{L^p(\Omega)} &\leq \|\eta_\varepsilon * g - g\|_{L^p(\Omega)} + \|\eta_\varepsilon * (f-g) - (f-g)\|_{L^p(\Omega)} \\ &\leq \|\eta_\varepsilon * g - g\|_{L^p(\Omega)} + 2\|f-g\|_{L^p(\Omega)} \end{aligned}$$

Since $C_c(\Omega)$ is dense in $L^p(\Omega)$, together with (2.3) we derive the statement: □

Lemma 2.1. *The following inequality is valid for every $a, b \in \mathbb{R}$ and $p \in \mathbb{R}^+$*

$$|a+b|^p \leq 2^{p-1}(|a|^p + |b|^p).$$

2.3 Saddle Point Problems

We consider a simplified model of two dimensional Stokes equations [12]:

$$\begin{cases} -\Delta u + \nabla p = f \quad \text{in } \Omega, \\ \text{div} u = 0 \quad \text{in } \Omega, \\ u = 0 \quad \text{on } \partial\Omega. \end{cases} \tag{2.4}$$

Here, u and p can be regarded as the velocity and the pressure of a viscous flow. In view of the fact that the pressure part of the solution is unique only up to a constant, we choose for p the space

$$Q := \left\{ q \in L^2(\Omega) \;\middle|\; \int_\Omega q \, dxdy = 0 \right\}.$$

Define $V = H_0^1(\Omega)^2$. Then, the variation problem of (2.4) is formulated as: Find a weak solution $(u, p) \in V \times Q$ satisfying

$$\begin{cases} a(u,v) + b(v,p) = (f,v), \;\; \forall v \in V, \\ b(u,q) = 0, \;\; \forall q \in Q, \end{cases} \tag{2.5}$$

where the bilinear forms are defined by

$$
\begin{aligned}
(f, v) &= \int_{\Omega} f \cdot v \, dxdy, \quad v \in V, \\
a(u, v) &= \int_{\Omega} \nabla u : \nabla v \, dxdy, \quad u, v \in V, \\
b(v, p) &= -\int_{\Omega} (\mathrm{div} v) \, p \, dxdy, \quad v \in V, p \in Q,
\end{aligned}
$$

where $\nabla u : \nabla v$ represents the component-wise scalar product of matrix. In order to prove the existence and uniqueness of a solution, the so-called inf-sup condition is required: There exists a constant $\beta > 0$ so that

$$
\inf_{p \in Q} \sup_{v \in V} \frac{b(v, p)}{\|v\|_V \, \|p\|_Q} \geqslant \beta. \tag{2.6}
$$

For a proof we refer to the seminal work [13]. Next we want to illustrate why the inf-sup condition is so important to the solvability of the Stokes equations in the discrete case. Using some finite element method we can discretize the variation problem (2.5) into the block form

$$
\begin{pmatrix} A & B' \\ B & 0 \end{pmatrix} \begin{pmatrix} u_N \\ p_M \end{pmatrix} = \begin{pmatrix} f_N \\ 0 \end{pmatrix}.
$$

The coefficient vectors u_N, p_M, f_N of u, p, f are calculated with respect to some finite element basics. Unfortunately, the matrix of the block form is not positive definite. These problems are called mixed problems, or saddle point problems, and performing a block-wise Gaussian elimination we obtain the pressure Schur complement

$$
BA^{-1}B'p_M = BA^{-1}f_N.
$$

Since A^{-1} is invertible in this case, we only need to consider whether BB' is invertible. For BB' to be invertible it requires that

$$
\mathrm{kernel}(B') = 0.
$$

It means that B' must have full column rank and it is equivalent to requiring that

$$\max_{v_N}(v_N, B'p_M) = \max_{v_N}(Bv_N, p_M) > 0, \ \ \forall p_M \neq 0. \tag{2.7}$$

The natural translation of (2.7) into the framework of the finite element method is

$$\max_{v \in V_h} \frac{(\nabla \cdot v, p_h)}{\|v\|_{V_h} \|p_h\|_{Q_h}} > 0, \ \ p_h \in Q_h. \tag{2.8}$$

The finite element spaces V_h, Q_h are specified introduced in next section. The condition (2.8) allows BB' to degenerate towards a singular system as the spatial resolution $h \to 0$ and this does not lead to optimal error estimates. The stricter version of (2.8), namely the inf-sup condition (2.6) ensures that BB' does not degenerate towards zeros as h vanishes.

2.4 Mixed Finite Element Method for Stokes Equations

Applying some finite element method we derive the following discrete variation problem: find $(u_h, p_h) \in V_h \times Q_h$ such that

$$\begin{cases} a(u_h, v) + b(v, p_h) = (f, v), \ \ \forall v \in V_h \subset V, \\ b(u_h, q) = 0, \ \ \forall q \in Q_h \subset Q. \end{cases} \tag{2.9}$$

The discrete variation problem (2.9) is also carefully investigated by Brezzi and Fortin in [13]. In order to guarantee the existence and uniqueness of solutions to (2.9), we have to specify adequate finite element subspaces V_h and Q_h such that the inf-sup condition (2.6) is fulfilled. As introduced in [13, 28], we choose the P2-P1 approximation, so-called Taylor and Hood elements (see Figure 2.1). The velocity u and pressure p are approximated respectively by polynomial of second order (P2) and first order (P1). Let the domain Ω be discretized by a triangulation T_h, i.e. there exists a sequence of triangles $\triangle_k \in T_h, k = 1 \cdots K$ satisfying

$$\bigcup_k \overline{\triangle}_k = \overline{\Omega} \quad \text{and} \quad \triangle_l \cap \triangle_m = \emptyset \quad \text{with } l \neq m \ \ \forall\, l, m \in \{1, \cdots, K\}\,.$$

The approximation of u and p are carried out in every triangle of the triangulation T_h and the finite element spaces V_h and Q_h are characterized in the following:

$$V_h := \left\{ v \in C^0(\overline{\Omega})^2 \;\middle|\; v|_{\triangle_k} \in P_2(\Omega)^2,\ \forall \triangle_k \in T_h \right\} \cap H_0^1(\Omega)^2,$$

$$Q_h := \left\{ q \in C^0(\overline{\Omega}) \;\middle|\; q|_{\triangle_k} \in P_1(\Omega),\ \forall \triangle_k \in T_h \text{ and } \int_\Omega q\, dxdy = 0 \right\}.$$

Suppose that the inf-sup condition is fulfilled, the following error estimate is valid [32]: When (u, p) belongs to $(H^{m+1}(\Omega)^2 \cap H_0^1(\Omega)^2) \times (H^m(\Omega) \cap Q)$ with $1 \le m < \infty$, we have the error bounds

$$\|u - u_h\|_{H^1(\Omega)^2} + \|p - p_h\|_{L^2(\Omega)} \le Ch^m \left(\|u\|_{H^{m+1}(\Omega)^2} + \|p\|_{H^m(\Omega)} \right),$$

$$\|u - u_h\|_{L^2(\Omega)^2} \le Ch^{m+1} \left(\|u\|_{H^{m+1}(\Omega)^2} + \|p\|_{H^m(\Omega)} \right).$$

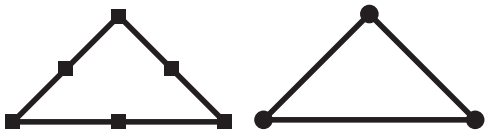

Figure 2.1: P2-P1

Let the set $\{\Phi_i, 1 \le i \le N\}$ be a basic of V_h and the set $\{\psi_i, 1 \le i \le M\}$ be a basic of Q_h. Then, the solution $(u_h, p_h) \in V_h \times Q_h$ to (2.9) has the following decomposition

$$u_h = \sum_{i=1}^{N} \alpha_i \Phi_i, \qquad p_h = \sum_{i=1}^{M} \gamma_i \psi_i.$$

Define further

$$\begin{aligned}
&A_{N\times N} = (a_{i,j}),\ \ a_{i,j} = a(\Phi_i, \Phi_j),\\
&B_{M\times N} = (b_{i,j}),\ \ b_{i,j} = b(\psi_i, \Phi_j),\\
&f_N = (f_i),\ \ f_i = (f, \Phi_i),\\
&u_N = (\alpha_i),\\
&p_M = (\gamma_i).
\end{aligned}$$

The discretization of variation problem (2.9) using previously introduced finite element method produces a linear system of the form

$$\begin{pmatrix} A & B' \\ B & 0 \end{pmatrix} \begin{pmatrix} u_N \\ p_M \end{pmatrix} = \begin{pmatrix} f_N \\ 0 \end{pmatrix}. \tag{2.10}$$

The matrix in (2.10) is sparse and symmetric, but not positive definite. Suppose that every triangle of T_h is isosceles right with length $2h$ and N, M are the number of measurement points of velocity and pressure. Let the two dimensional basic function Φ_i of V_h in each dimension be made of basic function φ_i. It follows

$$\begin{aligned}
&a\left(\begin{pmatrix}\varphi_i\\0\end{pmatrix},\begin{pmatrix}\varphi_j\\0\end{pmatrix}\right) = \int_\Omega \nabla\varphi_i\cdot\nabla\varphi_j\,dxdy,\ \ i,j=1,\cdots,N,\\
&a\left(\begin{pmatrix}\varphi_i\\0\end{pmatrix},\begin{pmatrix}0\\\varphi_j\end{pmatrix}\right) = 0,\ \ i=1,\cdots,N;\ j=N+1,\cdots,2N,\\
&a\left(\begin{pmatrix}0\\\varphi_i\end{pmatrix},\begin{pmatrix}\varphi_j\\0\end{pmatrix}\right) = 0,\ \ i=N+1,\cdots,2N;\ j=1,\cdots,N,\\
&a\left(\begin{pmatrix}0\\\varphi_i\end{pmatrix},\begin{pmatrix}0\\\varphi_j\end{pmatrix}\right) = \int_\Omega \nabla\varphi_i\cdot\nabla\varphi_j\,dxdy,\ \ i,j=N+1,\cdots,2N.
\end{aligned}$$

The stiffness matrix A has the following block form

$$A = \begin{pmatrix} A_1 & 0 \\ 0 & A_1 \end{pmatrix},$$

where $A_1 = \left(\int_\Omega \nabla\varphi_i\cdot\nabla\varphi_j\,dxdy\right), i,j=1,\cdots,N$. The matrix B' has also a block form

$$B' = \begin{pmatrix} B'_1 \\ B'_2 \end{pmatrix},$$

$$B'_1 = \left\{ -\int_\Omega \frac{\partial\varphi_i}{\partial x}\psi_j\,dxdy,\ \ i=1,\cdots,N;\ j=1,\cdots,M \right\},$$

$$B'_2 = \left\{ -\int_\Omega \frac{\partial\varphi_i}{\partial y}\psi_j\,dxdy,\ \ i=1,\cdots,N;\ j=1,\cdots,M \right\}.$$

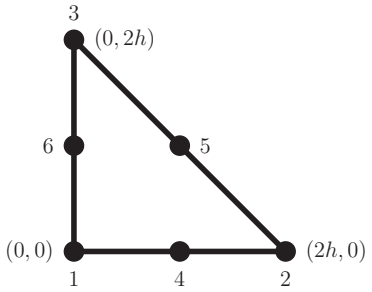

Figure 2.2: A basic triangulation element, denoted by E.

We create now the basic functions on the triangular elements, the procedure refers to [60]. In a basic triangulation element E (see Figure 2.2) the basic functions of V_h are given by

$$\begin{aligned}
\varphi_1(x,y) &= \left(1-\frac{x}{h}-\frac{y}{h}\right)\left(1-\frac{x}{2h}-\frac{y}{2h}\right),\\
\varphi_2(x,y) &= \frac{x}{2h}\left(\frac{x}{h}-1\right),\\
\varphi_3(x,y) &= \frac{y}{2h}\left(\frac{y}{h}-1\right),\\
\varphi_4(x,y) &= \frac{x}{h}\left(2-\frac{x}{h}-\frac{y}{h}\right),\\
\varphi_5(x,y) &= \frac{xy}{h^2},\\
\varphi_6(x,y) &= \frac{y}{h}\left(2-\frac{x}{h}-\frac{y}{h}\right)
\end{aligned}$$

satisfying $\varphi_i(x_j, y_j) = \delta_{i,j}$ where (x_j, y_j) is the coordinate of node j in element E in Figure 2.2. Analogously, the basic functions of Q_h in element E are given by

$$\begin{aligned}
\psi_1(x,y) &= 1-\frac{x}{2h}-\frac{y}{2h},\\
\psi_2(x,y) &= \frac{x}{2h},\\
\psi_3(x,y) &= \frac{y}{2h}.
\end{aligned}$$

The element stiffness matrix is

$$A_1^E = \begin{pmatrix}
1 & \frac{1}{6} & \frac{1}{6} & -\frac{2}{3} & 0 & -\frac{2}{3}\\
\frac{1}{6} & \frac{1}{2} & 0 & -\frac{2}{3} & 0 & 0\\
\frac{1}{6} & 0 & \frac{1}{2} & 0 & 0 & -\frac{2}{3}\\
-\frac{2}{3} & -\frac{2}{3} & 0 & \frac{8}{3} & -\frac{4}{3} & 0\\
0 & 0 & 0 & -\frac{4}{3} & \frac{8}{3} & -\frac{4}{3}\\
-\frac{2}{3} & 0 & -\frac{2}{3} & 0 & -\frac{4}{3} & \frac{8}{3}
\end{pmatrix}.$$

The matrix B_1' and B_2' consist of element matrix b_1^E and b_2^E given by

$$b_1^E = \begin{pmatrix} 0 & 0 & 0 & 0 & -\frac{2}{3}h & \frac{2}{3}h \\ 0 & -\frac{1}{3}h & 0 & \frac{1}{3}h & -\frac{1}{3}h & \frac{1}{3}h \\ \frac{1}{3}h & 0 & 0 & -\frac{1}{3}h & -\frac{1}{3}h & \frac{1}{3}h \end{pmatrix}', \quad b_2^E = \begin{pmatrix} 0 & 0 & -\frac{1}{3}h & \frac{1}{3}h & -\frac{1}{3}h & \frac{1}{3}h \\ 0 & 0 & 0 & \frac{2}{3}h & -\frac{2}{3}h & 0 \\ \frac{1}{3}h & 0 & 0 & \frac{1}{3}h & -\frac{1}{3}h & -\frac{1}{3}h \end{pmatrix}'.$$

The vector $f = (f_1, f_2)'$ is composed of the scalarproducts (f_1, φ_i) and (f_2, φ_i) for $i = 1, \cdots, N$. We derive the interpolation polynomial of f_1, f_2 with respect to the basic

$$f_1^h = \sum_{i=1}^{N} f_1(x_i)\varphi_i,$$
$$f_2^h = \sum_{i=1}^{N} f_2(x_i)\varphi_i,$$

where x_i is the corresponding measurement point of φ_i. Consequently,

$$f_i = (f_1^h, \varphi_i) = \sum_{j=1}^{N} f_1(x_j) \int_\Omega \varphi_j\varphi_i \, dxdy, \ i = 1, \cdots, N,$$
$$f_i = (f_2^h, \varphi_i) = \sum_{j=1}^{N} f_2(x_j) \int_\Omega \varphi_j\varphi_i \, dxdy, \ i = N+1, \cdots, 2N.$$

The vector f is made of the entries of the element mass matrix

$$Mass^E = h^2 \begin{pmatrix} \frac{1}{15} & -\frac{1}{90} & -\frac{1}{90} & 0 & -\frac{2}{45} & 0 \\ -\frac{1}{90} & \frac{1}{15} & -\frac{1}{90} & 0 & 0 & -\frac{2}{45} \\ -\frac{1}{90} & -\frac{1}{90} & \frac{1}{15} & -\frac{2}{45} & 0 & 0 \\ 0 & 0 & -\frac{2}{45} & \frac{16}{45} & \frac{8}{45} & \frac{8}{45} \\ -\frac{2}{45} & 0 & 0 & \frac{8}{45} & \frac{16}{45} & \frac{8}{45} \\ 0 & -\frac{2}{45} & 0 & \frac{8}{45} & \frac{8}{45} & \frac{16}{45} \end{pmatrix}.$$

The entries of matrix $Mass^E$ consist of the scalarproducts

$$m_{i,j} = \int_\Omega \varphi_i\varphi_j \, dxdy.$$

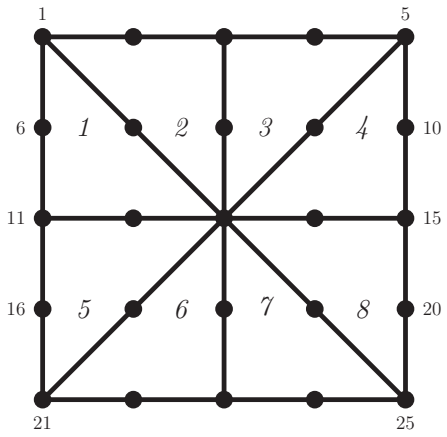

Figure 2.3: Numbering a mesh with the time new roman font for nodes and the italics font for triangle elements.

The main computational issue is to ensure that the element contributions are put into the correct locations in the stiffness matrix A, B', B and vector f_N. The simplest way of implementing the process is to represent the mapping between local and global entities using a connectivity matrix. In connectivity matrix $P(k,i)$ specifies the global node number of local node i in triangle k. And for each row of P the global numbers form the same orientation corresponding to the nodes number $1, \cdots, 6$ in element E. Then, we are able to find for each triangle the right contributions for global node $P(k,i)$ and add them together. For example, the connectivity matrix P of the triangulation in Figure (2.3) is given by

$$P = \begin{pmatrix} 11 & 13 & 1 & 12 & 7 & 6 \\ 3 & 1 & 13 & 2 & 7 & 8 \\ 3 & 5 & 13 & 4 & 9 & 8 \\ 15 & 13 & 5 & 14 & 9 & 10 \\ 11 & 13 & 21 & 12 & 17 & 16 \\ 23 & 21 & 13 & 22 & 17 & 18 \\ 23 & 25 & 13 & 24 & 19 & 18 \\ 15 & 13 & 25 & 14 & 19 & 20 \end{pmatrix}.$$

The element stiffness matrix A_1^E can be assembled into the global stiffness matrix using a set of nested loops described in the following pseudocode:

```
for k = 1 : 8
    for i = 1 : 6
        for j = 1 : 6

            A(P(k,i),P(k,j)) = A(P(k,i),P(k,j)) + A_1^E(i,j)

        end
    end
end
```

In similar way we can also assemble the stiffness matrices b_1^E, b_2^E and $Mass^E$ into global matrices B_1', B_2' and the right-hand side f_N.

Chapter 3

Lipschitzian Flow based Optimal Control

3.1 Modeling

We are interested in finding an optical flow field, which is suitable for image sequence interpolation, especially, instead of minimizing the optical flow constraint equation (1.1) directly, since the linearization of (1.2) is only valid in the case that the displacement between two images is small. Thus, more naturally we utilize the transport equation to fit a given image u_0 to another given image u_T in the sense of some predefined norm.

Let us model the optimal control problem governed by the transport equation. Consider the Cauchy problem for the transport equation in $[0,T] \times \Omega$, $\Omega \subset \mathbb{R}^d$ (generally $d = 2$):

$$\begin{cases} \partial_t u(t,x) + b(t,x) \cdot \nabla_x u(t,x) = 0 \quad \text{in }]0,T] \times \Omega, \\ u(0,x) = u_0(x) \quad \text{in } \Omega, \\ u_n(x) = 0 \quad \text{on } [0,T] \times \partial\Omega. \end{cases} \tag{3.1}$$

Here $b : [0,T] \times \Omega \longrightarrow \mathbb{R}^d$ is an optical flow field, u_0 is a given initial condition and u is an unknown function depending on t and x. The normal derivative u_n of u is not essential in our context, since we will assume later that b vanishes on $\partial\Omega$ for

a.e. $t \in [0, T]$. We define the nonlinear solution operator of (3.1)

$$\begin{aligned} G : X \times Y &\longrightarrow Z, \\ (u_0, b) &\longmapsto u, \end{aligned}$$

where X, Y, Z are normed spaces to be specified. Then, we define a linear "observation operator" $E_T : u \mapsto u(T)$, which observes the value of u at time T. By the chain $(u_0, b) \mapsto u \mapsto u(T)$ we have the "control-to-state" operator $S := E_T \circ G$, namely

$$\begin{aligned} S : X \times Y &\longrightarrow U, \\ (u_0, b) &\longmapsto u(T). \end{aligned} \tag{3.2}$$

The space U is a subspace of Z, which does not involve time. Our intention is to find a flow field b such that the corresponding image $S(u_0, b)$ matches the image u_T as well as possible. This motivates us to minimize the functional $\frac{1}{2} \|S(u_0, b) - u_T\|_U^2$. However, this problem is ill-posed, and hence we add an additional regularization term in the cost functional. In addition, we add the divergence-free constraint of b. Thus, this regularized optimal control problem is formulated as the following minimization problem for a given $\lambda > 0$:

$$\inf_{b \in Y} J(b) = \frac{1}{2} \|S(u_0, b) - u_T\|_U^2 + \frac{\lambda}{2} \|b\|_Y^2 , \tag{3.3}$$

$$\text{subject to} \quad \text{div} b = 0. \tag{3.4}$$

In the framework of optimal control [41, 55] we call b the control and u the state. According to the conservation law [35] and the divergence theorem [47], the divergence-free constraint of b makes the flow volume conserving, smooth and varying not too much inside the flow field of a moving object. At least the last two properties are desirable for computation of the optical flow. Moreover, the divergence-free constraint is a somehow technical assumption as it implies that the equation for the dual variable of u is also a transport equation (see Section 3.5 for details), and hence simplifies the numerical implementation. Such constraint is not new for optical flow estimation and was similarly introduced as a regularization constraint, e.g. in [53, 37, 11]. However, note that a divergence-free constraint excludes sources and

sinks in the flow field and the feature of volume preservation may be undesirable.

We emphasize, that our model is considerably different from the Horn & Schunck method which is based on the optical flow constraint. There one has a given image u and a given derivative $\partial_t u$ (both at time t_0) and one finds a flow field $b := (v, w)$ by minimizing

$$\int_\Omega (\partial_t u + b \cdot \nabla u)^2 dx + \int_\Omega |\nabla v|^2 + |\nabla w|^2 dx.$$

The main conceptual difference between this approach and ours is that Horn and Schunck just considered one time t_0 and matched the flow field only to that time. Hence, it is unclear in what sense the produced flow field could be useful to match a given image with another one. Our approach uses two given images and tries to find a flow field b which transports the first image as close as possible to the second image. The "optical flow constraint equation" now enters as a constraint to the optimization problem and is not in the cost functional itself.

In the next chapters we will investigate the solution theory of transport equations and choose adequate spaces for u and b. Especially, we are interested in images u_0 and u_T which are of bounded total variation. Hence, we introduce the solution theory of transport equations equipped with a smooth flow field and a BV image as the initial value. Especially, we need to work out conditions under which the BV-regularity is propagated by the optical flow. Then, we will analyze the existence of a minimizer to (3.3) restricted to (3.1) and (3.4).

3.2 Solution Theory of Ordinary Differential Equations

The classic solution theory of transport equations is based on the characteristics [29], which are derived from the associated ordinary differential equation (ODE). Gaining the uniqueness of the characteristics requests normally that the velocity field of the transport equation needs to enjoy the Lipschitz regularity in space. We give next a brief introduction of solution theory of ODEs [33, 24, 6]. We consider

the following ODE which characterizes the characteristic $\gamma(t)$ related to b:

$$\begin{cases} \dot{\gamma}(t) = b(t, \gamma(t)), \ \ t \in I, \\ \gamma(a) = x_0 \quad \text{in } \Omega. \end{cases} \tag{3.5}$$

Regarding the solution theory of (3.5), the existence and uniqueness of a solution is derived by the theorem of Picard-Lindelöf [33], if b is Lipschitz continuous in space and uniformly continuous in time. We can also relax the assumption on b with respect to t to be integrable by the Carathéodory theorem [6], which is a general version of the Picard-Lindelöf theorem:

Theorem 3.1 (Carathéodory)**.** *Define $I = [a, c]$ and Ω is a bounded subset in $\mathbb{R}^d$. Suppose that $b : I \times \Omega \to \mathbb{R}^d$ satisfies*

1. *$t \to b(t, x)$ is measurable in I for every $x \in \Omega$;*
2. *There exists a $C \geq 0$ with $|b(t, x) - b(t, x')| \leq C|x - x'|$ for a.e. $t \in I$ and every $x, x' \in \overline{\Omega}$;*
3. *$b(t, x) = 0$ for a.e. $t \in I$ and every $x \in \partial\Omega$;*
4. *The function $m(t) = |b(t, x_0)|$ is integrable in I for $x_0 \in \Omega$.*

Then there exists a unique solution

$$\gamma^* : [a, c] \to \Omega$$

to the Cauchy problem (3.5)*.*

Proof. We choose the interval I with $q := C|c - a| < 1$, where C is the Lipschitz constant of b, and $\alpha > 0$ with $q\alpha + C \|m\|_{L^1([a,c])} \leq \alpha$. Assume $X := C^0(I; \Omega)$ endowed with the supremum norm. Consider the closed subset Y of X

$$Y := \{\gamma \in X \mid \ \gamma(a) = x_0\} \cap \bigcap_{s,t \in I, s<t} \left\{ \gamma \in X \ \middle| \ |\gamma(s) - \gamma(t)| \leq \int_s^t m(x) + \alpha \, dx \right\}.$$

Let us define

$$R\gamma(t) = x_0 + \int_a^t b(s, \gamma(s)) \, ds, \ \ t \in I, \tag{3.6}$$

the operator R maps X into X, since b is equal to zero on $\partial\Omega$ and by Lusin's theorem [30] the measurable function $t \to b(t,x)$ is continuous a.e. in $[a,c]$, taking the integral over t derives the continuity of the right-hand side of (3.6). Let us verify the operator R is a contraction in Y. If $\gamma \in Y$, then

$$\begin{aligned}
|(R\gamma)'(t)| &= |b(t,\gamma(t))| \\
&\leq |b(t,\gamma(a))| + C|\gamma(t) - \gamma(a)| \\
&= |b(t,x_0)| + C|\gamma(t) - \gamma(a)| \\
&\leq m(t) + C|\gamma(t) - \gamma(a)| \\
&\leq m(t) + C\int_a^t m(\tau) + \alpha\, d\tau \\
&\leq m(t) + C\int_a^c m(\tau)\, d\tau + C\alpha|c-a| \\
&= m(t) + C\,\|m\|_{L^1([a,c])} + C\alpha|c-a| \\
&= m(t) + C\,\|m\|_{L^1([a,c])} + q\alpha \\
&\leq m(t) + \alpha.
\end{aligned}$$

Hence, by the Lebesgue differentiation theorem [30] one has R maps Y into Y. Moreover,

$$\begin{aligned}
\sup_{t\in I}|R\gamma_1(t) - R\gamma_2(t)| &\leq \sup_{t\in I}\int_a^t |b(s,\gamma_1(s)) - b(s,\gamma_2(s))|\, ds \\
&\leq C\sup_{t\in I}\int_a^t |\gamma_1(s) - \gamma_2(s)|\, ds \\
&\leq C|c-a|\sup_{s\in I}|\gamma_1(s) - \gamma_2(s)|,
\end{aligned}$$

and since $C|c-a| < 1$, we apply the Banach fixed point theorem [49] to get the existence of a unique fixed point $\gamma^* \in Y$ such that $R\gamma^* = \gamma^*$. That is the unique solution to (3.5). □

Remark 3.1. As a consequence of the proof, the flow $\gamma^*(t)$ is absolutely continuous

in $[a, c]$. Generally, if we consider the solution in $[0, T]$ with $T > c$, we can restart γ^* at $(c, \gamma^*(c))$ until the unique continuous solution arrives at time T. The backward flow is the special case when the time t is smaller than the initial time a, and the uniqueness of the backward flow is obvious by Theorem 3.1.

We want to choose an appropriate function space for b, which is easy to be applied in the control problem. Actually, the space of Lipschitz functions and $W^{1,\infty}(\Omega)$ are equivalent under some assumptions of Ω explained in the following theorem [5]:

Theorem 3.2. *Let $\Omega \subset \mathbb{R}^d$ be a bounded, convex, open set, and $f : \Omega \to \mathbb{R}$. Then, $f \in W^{1,\infty}(\Omega)$ if and only if*

$$\mathrm{Lip}(f, \Omega) := \sup \left\{ \frac{|f(x) - f(y)|}{|x - y|} \;\middle|\; x \neq y,\ \ x, y \in \Omega \right\} < \infty,$$

and $\|\nabla f\|_{L^\infty(\Omega)} = \mathrm{Lip}(f, \Omega)$.

However, the norm of $W^{1,\infty}$ is not well suited as a penalty term since it is difficult to determine the necessary conditions system in this situation. Thus, we assume additionally that the domain Ω enjoys the strong local Lipschitz condition [2], then $H_0^3(\Omega)^2$ is continuously embedded into $W^{1,\infty}(\Omega)^2$ when $d = 2$. We want a priori to set the flow field b divergence-free and we denote that

$$H_0^{3,\mathrm{div}}(\Omega)^2 = \left\{ f \in H_0^3(\Omega)^2 \;\middle|\; \mathrm{div} f = 0 \right\}.$$

Adjusting the assumption on the time of b in Theorem 3.1 and previous conditions on Ω, we assume that

– $\Omega \subset \mathbb{R}^2$ is a bounded, convex, open set, which satisfies the strong local Lipschitz condition;

– $b \in L^2(0, T; H_0^{3,\mathrm{div}}(\Omega)^2)$,

throughout this chapter. In order to formulate the solution to transport equations in a convenient way, we give the concept of classical flow [24].

Definition 3.1 (Classical flow of a vector field)**.** The classical flow of the vector field b *is a map*

$$\Phi(t, x) : [0, T] \times \Omega \longrightarrow \Omega,$$

which satisfies

$$\begin{cases} \dfrac{\partial \Phi}{\partial t}(t,x) = b(t,\Phi(t,x)) \quad \textit{in } (0,T]\times\Omega, \\ \Phi(0,x) = x \quad \textit{in } \Omega. \end{cases} \tag{3.7}$$

The classical flow is a generalization of the flow, whose initial value can be varied. For every fixed $x \in \Omega$ the flow $\Phi(\cdot, x)$ is uniquely determined by Theorem 3.1 and the solution is given by

$$\Phi(t,x) = x + \int_0^t b(s,\Phi(s,x))\,ds.$$

In the following we gain some helpful properties of Φ.

Corollary 3.1. *The mapping $\Phi(t,\cdot) : \Omega \to \Omega$ is bijective for every $t \in [0,T]$.*

Proof. The injectivity is derived from the uniqueness of the backward flow: If the flow Φ starts from two points $x_1 \neq x_2$ and arrives at some t in the same point $\Phi(t,x_1) = \Phi(t,x_2) = \overline{x}$, then the backward flow starting from $(t,\overline{x})$ is not unique. Regarding the surjectivity: for every point $y \in \Omega$ we can find a backward flow starting from (t,y) such that

$$\gamma(t') = y + \int_t^{t'} b(s,\gamma(s))\,ds = x \in \Omega,$$

in the case $t' = 0$ implies that $\Phi(t,x) = y$. □

Here Φ^{-1} denotes the backward flow of Φ, and $\Phi^{-1}(t,\cdot)(x)$ maps to the initial value, from which Φ arrives in point x at time t. Now we will discuss the regularity of Φ in x. As a preparation we need Gronwall's inequality.

Lemma 3.1 (Gronwall's lemma)**.** *Let f and g be real-valued continuous functions defined on $[a,c]$. If f is differentiable and satisfies the differential inequality*

$$f'(t) \leq g(t)f(t), \quad t \in [a,c],$$

then f is bounded by

$$f(t) \leq f(a) \exp\left(\int_a^t g(s)\, ds\right)$$

for all $t \in [a, c]$.

Corollary 3.2 (Lipschitz regularity of Φ)**.** *$\Phi(t, \cdot)$ is Lipschitz continuous.*

Proof. The following inequality is valid for every $t \in [0, T]$ and $x, y \in \Omega$:

$$\begin{aligned}\frac{\partial}{\partial t} |\Phi(t,x) - \Phi(t,y)|^2 &= 2 \langle b(t, \Phi(t,x)) - b(t, \Phi(t,y)), \Phi(t,x) - \Phi(t,y) \rangle \\ &\leq 2C |\Phi(t,x) - \Phi(t,y)|^2,\end{aligned}$$

where C is the Lipschitz constant of b. According to Gronwall's lemma, it implies

$$|\Phi(t,x) - \Phi(t,y)|^2 \leq |x - y|^2 e^{2Ct}.$$

Then it yields

$$\mathrm{Lip}(\Phi(t, \cdot)) \leq e^{Ct}.$$

□

Besides the Lipschitz regularity, we can say more about the differentiability of Φ in x, which deals with the spatial regularity of b.

Corollary 3.3. *The mapping $\Phi(t, \cdot) : \Omega \to \Omega$ is a diffeomorphism.*

Proof. Since the Lipschitz continuity gives only the local C^1-regularity, for the C^1-regularity of $\Phi(t, \cdot)$ in Ω one follows the result in [24], which states that if b has the C^1-regularity in space, then the flow $\Phi(t, \cdot)$ is also C^1 in space. In fact, $H_0^3(\Omega)^2$ is continuously embedded into $C^1(\overline{\Omega})^2$ and $\Phi(t, \cdot), \Phi^{-1}(t, \cdot)$ have the same regularity, then together with the bijectivity of $\Phi(t, \cdot)$ we derive the statement. □

3.3 Solution Theory of Transport Equations with Smooth Setting

In this section we consider the transport equation with an initial value in BV. However, the propagation of BV regularity is a delicate matter. We first formulate

the solution to the transport equation with a smooth initial value.

Corollary 3.4. *Let $u_0 \in C^1(\Omega)$. Then*

$$u(t,x) := u_0 \circ \Phi^{-1}(t,\cdot)(x) \tag{3.8}$$

is the unique solution to (3.1).

Proof. Let us test the equation (3.1) along the characteristics $(t, \Phi(t,x))$:

$$\begin{aligned} 0 &= \frac{\partial u}{\partial t}(t,\Phi(t,x)) + b(t,\Phi(t,x)) \cdot \nabla u(t,\Phi(t,x)) \\ &= \frac{\partial u}{\partial t}(t,\Phi(t,x)) + \frac{\partial \Phi}{\partial t}(t,x) \cdot \nabla u(t,\Phi(t,x)) \\ &= \frac{\partial}{\partial t}(u(t,\cdot) \circ \Phi(t,x)). \end{aligned}$$

This implies that every solution is constant along the characteristics. Adjusting the initial value we derive that (3.8) is a solution to (3.1) and the uniqueness follows immediately from the uniqueness of Φ. □

Equipped with a non-differentiable initial value, the classic solution (3.8) breaks down. Thus, we give the definition of the solution to the transport equation in the weak sense.

Definition 3.2 (Weak solution)**.** *If b and u_0 are summable functions and b is divergence-free in space, then we say that a function $u : [0,T] \times \Omega \to \mathbb{R}$ is a weak solution to* (3.1) *if the following identity holds for every function $\varphi \in C_c^\infty([0,T[\times\Omega)$:*

$$\int_0^T \int_\Omega u\left(\partial_t \varphi + b \cdot \nabla \varphi\right) dxdt = -\int_\Omega u_0(x)\varphi(0,x)\, dx. \tag{3.9}$$

To prove that (3.8) is a weak solution to (3.1) it is common to use the technique of mollifiers introduced in Chapter 2. In short, we smooth the initial value with a mollifier η_ε with variance ε, let ε converge to zero and investigate the convergence of the solution with a smooth initial value to a non-smooth initial value. This process is clarified in the next theorem:

Theorem 3.3. *Assume $u_0 \in BV(\Omega), \varphi$ and φ^{-1} are diffeomorphisms in Ω. Then, the sequence $((u_0 * \eta_\varepsilon) \circ \varphi)$ converges to $u_0 \circ \varphi$ in the weak*-topology of $BV(\Omega)$.*

Proof. Let us verify first the L^1-convergence of $((u_0 * \eta_\varepsilon) \circ \varphi)$ and set $\varphi(x) = y$

$$\begin{aligned}
&\int_\Omega |(u_0 * \eta_\varepsilon) \circ \varphi(x) - u_0 \circ \varphi(x)|\, dx \\
&= \int_\Omega |u_0 * \eta_\varepsilon(y) - u_0(y)| \left|\det \nabla \varphi^{-1}(y)\right| dy \\
&\leq \|u_0 * \eta_\varepsilon - u_0\|_{L^1(\Omega)} \left\|\det \nabla \varphi^{-1}\right\|_{L^\infty(\Omega)}.
\end{aligned}$$

Let L be the Lipschitz constant of φ^{-1}, i.e. $L = \|\nabla \varphi^{-1}\|_{L^\infty(\Omega)^4}$, then $\|\det \nabla \varphi^{-1}\|_{L^\infty(\Omega)}$ is bounded from above by $2L^2$. Together with the approximation property of mollifiers it gives the L^1-convergence. Regarding the weak*-convergence of Radon measures $(\nabla(u_0 * \eta_\varepsilon))$ we observe that for every $\psi \in C_c^\infty(\Omega)^2$ it holds that

$$\begin{aligned}
&\int_\Omega \nabla((u_0 * \eta_\varepsilon) \circ \varphi)\psi\, dx \\
&= -\int_\Omega (u_0 * \eta_\varepsilon) \circ \varphi \mathrm{div}\psi\, dx \\
&= -\int_\Omega (u_0 * \eta_\varepsilon)(y) \mathrm{div}(\psi \circ \varphi^{-1}(y))| \det \nabla \varphi^{-1}(y)|\, dy \\
&= -\int_\Omega \left(\int_\Omega \eta_\varepsilon(y - s) u_0(s)\, ds \right) \mathrm{div}(\psi \circ \varphi^{-1}(y))| \det \nabla \varphi^{-1}(y)|\, dy \\
&= -\int_\Omega \left(\int_\Omega \eta_\varepsilon(y - s) \mathrm{div}(\psi \circ \varphi^{-1}(y))| \det \nabla \varphi^{-1}(y)|\, dy \right) u_0(s)\, ds \\
&= -\int_\Omega \eta_\varepsilon * \left(\mathrm{div}(\psi \circ \varphi^{-1})| \det \nabla \varphi^{-1}|\right)(s) u_0(s)\, ds. \qquad (3.10)
\end{aligned}$$

Since φ^{-1} is continuously differentiable, the convolved term belongs to $L^2(\Omega)$. Recall that in the two dimensional case $BV(\Omega)$ is continuously embedded into $L^2(\Omega)$, then utilizing the approximate property of mollifiers implies that the weak L^2-convergence holds. It means that (3.10) converges to

$$-\int_\Omega \mathrm{div}(\psi \circ \varphi^{-1}(s))| \det \nabla \varphi^{-1}(s)| u_0(s)\, ds$$

$$\overset{\varphi(\xi)=s}{=} -\int_{\Omega} \mathrm{div}\psi(\xi) u_0(\varphi(\xi))\, d\xi$$
$$= \int_{\Omega} \psi\, D(u_0 \circ \varphi).$$

The last equality is valid due to the Gauss-Green formula of the BV functions introduced in Chapter 2. □

Remark 3.2. Under the same assumptions of Theorem 3.3 one can derive from Theorem 2.1 that $((u_0 * \eta_\varepsilon) \circ \varphi)$ is uniformly bounded in $BV(\Omega)$ and converges to $u_0 \circ \varphi$ in $L^1(\Omega)$, actually also in $L^p(\Omega)$ with $p < 2$ and weakly in $L^2(\Omega)$ when $d = 2$ [1].

We gain in the following lemma the regularity in time of the solution to the transport equation with a smoothed BV-initial value.

Lemma 3.2. *Assume that $u_0 \in BV(\Omega)$, $\varphi(t,\cdot)$, $\varphi^{-1}(t,\cdot)$ are diffeomorphisms in Ω for every $t \in [0,T]$, and $\varphi(\cdot,x)$ is absolutely continuous in $[0,T]$ for every $x \in \Omega$. Define*

$$u_\varepsilon(t,x) = (u_0 * \eta_\varepsilon) \circ \varphi(t,x).$$

Then, $u_\varepsilon \in C([0,T]; BV(\Omega))$.

We skip the proof of Lemma 3.2, since it is a trivial result utilizing the substitution technique introduced in the proof of Theorem 3.3. Now, we are able to prove the existence and uniqueness of the weak solution to (3.1).

Theorem 3.4. *If $u_0 \in BV(\Omega)$, then there exits a unique weak solution*

$$\bar{u}(t,x) := u_0 \circ \Phi^{-1}(t,\cdot)(x) \tag{3.11}$$

to (3.1) *belonging to $L^\infty(0,T; BV(\Omega))$.*

Proof. Consider the transport equation with the initial value u_0 convolved with mollifier η_ε

$$\begin{cases} \partial_t u(t,x) + b(t,x) \cdot \nabla_x u(t,x) = 0 \quad \text{in }]0,T] \times \Omega, \\ u(0,x) = u_0 * \eta_\varepsilon(x) \quad \text{in } \Omega. \end{cases}$$

Corollary 3.4 implies that there exists a unique solution u_ε of the form

$$u_\varepsilon(t,x) = (u_0 * \eta_\varepsilon) \circ \Phi^{-1}(t,\cdot)(x).$$

Theorem 3.3 gives that $\bar{u}(t,\cdot) \in BV(\Omega)$ for every $t \in [0,T]$. By Remark 3.2 it follows that $u_\varepsilon(t,\cdot)$ converges to $\bar{u}(t,\cdot)$ in $L^2(\Omega)$ as $\varepsilon \to 0$ and $(u_\varepsilon(t,\cdot))$ is uniformly bounded in $BV(\Omega)$. And according to Lemma 3.2, it yields that (u_ε) is uniformly bounded in $L^\infty(0,T;BV(\Omega))$, which is continuously embedded into $L^2(0,T;L^2(\Omega))$. Hence, there exists a subsequence (u_{ε_k}) of (u_ε) such that

$$u_{\varepsilon_k} \rightharpoonup \bar{u} \quad \text{in } L^2(0,T;L^2(\Omega)) \tag{3.12}$$

and $\bar{u} \in L^\infty(0,T;BV(\Omega))$. Due to the weak convergence of (u_{ε_k}) in $L^2(0,T;L^2(\Omega))$, one derives for every $\varphi \in C_c^\infty([0,T[\times\Omega)$ that

$$\begin{array}{ccc}
\int_0^T \int_\Omega u_{\varepsilon_k} \left(\partial_t\varphi + b\cdot\nabla\varphi\right) dxdt & \longrightarrow & \int_0^T \int_\Omega \bar{u} \left(\partial_t\varphi + b\cdot\nabla\varphi\right) dxdt \\
\| & & \| \\
-\int_\Omega u_0 * \eta_{\varepsilon_k}\varphi(0,x)\, dx & \longrightarrow & -\int_\Omega u_0\varphi(0,x)\, dx.
\end{array}$$

The upper convergence is valid since $b \in L^2(0,T;L^2(\Omega)^2)$ and thanks to (3.12). The lower convergence is derived from the property of approximate identity. The left equality is valid for a smooth initial value according to Corollary 3.4, and hence all of them imply the right equality.

Regarding the uniqueness of weak solution, it is shown in [4] that the continuity equation, which is turned into the transport equation in the case that $\mathrm{div} b = 0$, has a unique solution in the Cauchy-Lipschitz framework, i.e. $b \in L^1(0,T;W^{1,\infty}(\mathbb{R}^d)^d)$. Definitely, it is also valid under our assumption on b.

Because of the uniqueness of the weak solution, the convergence of subsequence (u_{ε_k}) in the previous proof can be proceeded to the whole sequence (u_ε). □

3.4 Existence of a Minimizer with BV-initial Value

The goal of this subsection is to equip the cost functional (3.3) with some reasonable norm and investigate the existence of a minimizer to (3.3) restricted to (3.1) and (3.4). First of all, we give the norm of the penalty term of (3.3) concerning b. According to [2] an equivalent norm of H_0^3 is

$$\|b\|_{H_0^3(\Omega)^2} = \left(\sum_{|\alpha|=3} \|\partial^\alpha b\|^2_{L^2(\Omega)^2} \right)^{1/2}.$$

We find out that $\int_\Omega |\nabla \Delta b|^2 dx$ is equal to the norm $\|b\|_{H_0^3(\Omega)^2}$, since

$$\begin{aligned}
\int_\Omega |\nabla \Delta b|^2 \, dx &= \|\partial_{xxx} b\|^2_{L^2(\Omega)^2} + \|\partial_{xxy} b\|^2_{L^2(\Omega)^2} + \|\partial_{xyy} b\|^2_{L^2(\Omega)^2} + \|\partial_{yyy} b\|^2_{L^2(\Omega)^2} \\
&\quad + 2 \int_\Omega \partial_{xxx} b \partial_{xyy} b \, dx + 2 \int_\Omega \partial_{xxy} b \partial_{yyy} b \, dx \\
&= \|\partial_{xxx} b\|^2_{L^2(\Omega)^2} + 3 \|\partial_{xxy} b\|^2_{L^2(\Omega)^2} + 3 \|\partial_{xyy} b\|^2_{L^2(\Omega)^2} + \|\partial_{yyy} b\|^2_{L^2(\Omega)^2} \\
&= \sum_{|\alpha|=3} \|\partial^\alpha b\|^2_{L^2(\Omega)^2}.
\end{aligned}$$

Considering the regularity of b in time we give the equivalent norm of $L^2(0,T;H_0^3(\Omega)^2)$:

$$\|b\|^2_{L^2(0,T;H_0^3(\Omega)^2)} = \int_0^T \|\nabla \Delta b(t,\cdot)\|^2_{L^2(\Omega)^4} \, dt. \tag{3.13}$$

As discussed above, we assume that u_0 and u_T are BV functions. Hence, BV seems to be a proper choice for the space U. Since BV is continuously embedded in $L^2(\Omega)$ for $d = 2$, we use $U = L^2(\Omega)$. Hence, our cost functional is

$$J(b) = \frac{1}{2} \|S(u_0, b) - u_T\|^2_{L^2(\Omega)} + \frac{\lambda}{2} \int_0^T \|\nabla \Delta b(t,\cdot)\|^2_{L^2(\Omega)^4} \, dt. \tag{3.14}$$

To prove the existence of a minimizer of minimizing (3.14) restricted to (3.1) and

(3.4), we have to deal with the weak sequential closeness of the solution operator of the transport equation. Before we are able to handle that, we gain first some useful properties of the solution to the transport equation with a smooth initial value in the following lemmas:

Lemma 3.3. *If (φ_n) and (φ_n^{-1}) are sequences of diffeomorphisms in Ω and the Jacobian determinant $(\det \nabla \varphi_n)$ is uniformly bounded in $L^\infty(\Omega)$ by the upper bound C, then $((u_0 * \eta_\varepsilon) \circ \varphi_n^{-1})$ is uniformly bounded in $BV(\Omega)$ with respect to n.*

Proof. It is easy to check that $(u_0 * \eta_\varepsilon)$ is uniformly bounded in $BV(\Omega)$ according to Theorem 2.1 and Theorem 3.3. Suppose that its upper bound in $BV(\Omega)$ is $\widetilde{C}$. Let us verify the L^1-norm by setting $y = \varphi_n^{-1}(x)$

$$\begin{aligned}
&\int_\Omega |(u_0 * \eta_\varepsilon) \circ \varphi_n^{-1}| \, dx \\
&= \int_\Omega |(u_0 * \eta_\varepsilon)(y)| |\det \nabla \varphi_n(y)| \, dy \\
&\leq C \int_\Omega |(u_0 * \eta_\varepsilon)(y)| \, dy \\
&\leq C\widetilde{C}.
\end{aligned}$$

Regarding the total variation we have

$$\begin{aligned}
&\int_\Omega |\nabla(u_0 * \eta_\varepsilon) \circ \varphi_n^{-1}| \, dx \\
&= \int_\Omega |\nabla(u_0 * \eta_\varepsilon)(y)| |\det \nabla \varphi_n(y)| \, dy \\
&\leq C \int_\Omega |\nabla(u_0 * \eta_\varepsilon)(y)| \, dy \\
&\leq C\widetilde{C}.
\end{aligned}$$

□

Lemma 3.4. *If (b_n) is uniformly bounded in $L^2(0,T;H^3(\Omega)^2)$ and $u_0 \in BV(\Omega)$. Define $u_{n,\varepsilon} = (u_0 * \eta_\varepsilon) \circ \Phi_n^{-1}$ and $u_{n,\varepsilon}^t = u_{n,\varepsilon}(t)$. Then, there exists a subsequence*

$(u_{n_k,\varepsilon})$ such that $(u_{n_k,\varepsilon})$ converges to some limit u_ε in $L^2(0,T;L^p(\Omega))$ with $p<2$ and weakly to u_ε with $p=2$. $(u^t_{n_k,\varepsilon})$ converges to $u_\varepsilon(t)$ in $L^p(\Omega)$ with $p<2$ and weakly to $u_\varepsilon(t)$ with $p=2$.

Proof. Recall that for each b_n there is a corresponding Φ_n s.t. $\Phi_n(t,\cdot)\in W^{1,\infty}(\Omega)^2$ and $\|\nabla\Phi_n(t,\cdot)\|_{L^\infty(\Omega)^4}=\mathrm{Lip}(\Phi_n(t,\cdot))$. The Lipschitz continuity is implied from Gronwall's lemma:

$$\mathrm{Lip}(\Phi_n(t,\cdot))\le\exp\left(\int_0^t\mathrm{Lip}(b_n(s,\cdot))\,ds\right). \tag{3.15}$$

The boundedness of (b_n) in $L^2(0,T;H^3(\Omega)^2)$ gives the upper bound for (3.15). Hence, the Jacobian determinant $(\det\nabla\Phi_n(t,\cdot))$ is also uniformly bounded in $L^\infty(\Omega)$. According to Lemma 3.3, this implies that $(u^t_{n,\varepsilon})$ is uniformly bounded in $BV(\Omega)$ with respect to n. Then, there exists a subsequence $(u^t_{n_k,\varepsilon})$ of $(u^t_{n,\varepsilon})$ such that $(u^t_{n_k,\varepsilon})$ converges to u^t_ε in $L^p(\Omega)$ with $p<2$ (weakly for $p=2$). To derive the convergence of $(u_{n_k,\varepsilon})$ to u_ε in $L^2(0,T;L^p(\Omega))$ with $p<2$, we consider the integral over time:

$$\lim_{n_k\to\infty}\int_0^T\left\|u^t_{n_k,\varepsilon}-u^t_\varepsilon\right\|^2_{L^p(\Omega)}dt=\int_0^T\lim_{n_k\to\infty}\left\|u^t_{n_k,\varepsilon}-u^t_\varepsilon\right\|^2_{L^p(\Omega)}dt\to 0$$

with $p<2$. The exchange of the limit is valid since the integrand is bounded. The weak convergence of $(u_{n_k,\varepsilon})$ in $L^2(0,T;L^2(\Omega))$ is also valid, because $(u_{n_k,\varepsilon})$ is uniformly bounded in $L^2(0,T;L^2(\Omega))$ and $(u^t_{n_k,\varepsilon})$ converges weakly to $u_\varepsilon(t)$ in $L^2(\Omega)$ for a.e $t\in[0,T]$. □

Now we consider the minimization problem

$$\inf_{b\in L^2(0,T;H_0^{3,\mathrm{div}}(\Omega)^2)}J(b) \tag{3.16}$$

with J of the form (3.14). The existence of minimizers is usually achieved by the direct method [8], and the main part lies in the weak sequential closeness of the solution operator G with respect to u_0 and b.

Theorem 3.5 (Weak sequential closeness)**.** *Suppose that $(b_n)\subset L^2(0,T;H_0^{3,\mathrm{div}}(\Omega)^2)$ is uniformly bounded and converges weakly to b in $L^2(0,T;H^3(\Omega)^2)$. Let u_n be*

the corresponding weak solutions to (3.1) *with the flow field* b_n *and initial value* u_0*, i.e.* $u_n = G(u_0, b_n)$*. Suppose that* (u_n) *converges to* $\bar{u}$ *in* $L^2(0,T;L^1(\Omega))$ *and* $\bar{u} \in L^2(0,T;L^2(\Omega))$*, then* $\bar{u} = G(u_0, b)$*.*

Proof. Since (b_n) converges weakly to b in $L^2(0,T;H^3(\Omega)^2)$, it is also valid that

$$b_n \rightharpoonup b \quad \text{in } L^2(0,T;L^2(\Omega)^2). \tag{3.17}$$

Let us consider the difference between the weak solution u_n and $\bar{u}$ applying a test function $\varphi \in C_c^\infty([0,T[\times\Omega)$:

$$\begin{aligned} &\left| \int_0^T \int_\Omega u_n(\partial_t\varphi + b_n \cdot \nabla\varphi) - \bar{u}(\partial_t\varphi + b \cdot \nabla\varphi)\, dxdt \right| \\ &= \left| \int_0^T \int_\Omega \partial_t\varphi(u_n - \bar{u})\, dxdt + \int_0^T \int_\Omega \nabla\varphi \cdot (u_n b_n - \bar{u}b)\, dxdt \right|. \end{aligned} \tag{3.18}$$

The first summand of the right-hand side of (3.18) converges to zero, since $u_n \to \bar{u}$ in $L^2(0,T;L^1(\Omega))$. Regarding the second summand we derive that

$$\begin{aligned} &\int_0^T \int_\Omega \nabla\varphi \cdot (u_n b_n - \bar{u}b)\, dxdt \\ &= \int_0^T \int_\Omega \nabla\varphi \cdot b_n(u_n - \bar{u})\, dxdt + \int_0^T \int_\Omega \bar{u}\nabla\varphi \cdot (b_n - b)\, dxdt \\ &\leq \|\nabla\varphi\|_{L^\infty(0,T\times\Omega)^2} \|b_n\|_{L^2(0,T;L^\infty(\Omega)^2)} \|u_n - \bar{u}\|_{L^2(0,T;L^1(\Omega))} \\ &\quad + \int_0^T \int_\Omega \bar{u}\nabla\varphi \cdot (b_n - b)\, dxdt. \end{aligned}$$

Since (b_n) is uniformly bounded in $L^2(0,T;H^3(\Omega)^2)$, it is also uniformly bounded in $L^2(0,T;L^\infty(\Omega)^2)$. The convergence of (u_n) in $L^2(0,T;L^1(\Omega))$ and (3.17) imply that the right-hand side of the last inequality converges to zero.

Since u_n is the weak solutions to (3.1) for every $n \in \mathbb{N}$, the limit $\bar{u}$ is also a weak solution to (3.1), i.e. $\bar{u} = G(u_0, b)$. □

Theorem 3.6 (Existence of a minimizer)**.** *Suppose that $u_0 \in BV(\Omega)$, then the minimization problem* (3.16) *has a solution.*

Proof. Let $(b_n) \subset L^2(0,T;H_0^{3,\mathrm{div}}(\Omega)^2)$ be a minimizing sequence of the cost functional. The coercivity of (3.14) is a natural property subject to the norm (3.13). By the coercivity, (b_n) is uniformly bounded in $L^2(0,T;H^3(\Omega)^2)$, then there is a subsequence (b_{n_k}) of (b_n) converging weakly to b in $L^2(0,T;H^3(\Omega)^2)$. For each b_n there exits a unique flow Φ_n^{-1}, which is a diffeomorphism in Ω and absolutely continuous in $[0,T]$. Define

$$u_{n,\varepsilon} = (u_0 * \eta_\varepsilon) \circ \Phi_n^{-1}.$$

According to Lemma 3.4 there exists a subsequence $(u_{n_k,\varepsilon})$, which converges to $u_\varepsilon \in L^2(0,T;L^2(\Omega))$ in $L^2(0,T;L^1(\Omega))$ and converges for every $t \in [0,T]$ weakly to $u_\varepsilon(t)$ in $L^2(\Omega)$. Theorem 3.5 implies that $u_\varepsilon = (u_0 * \eta_\varepsilon) \circ \Phi^{-1}$. Hence, it yields that

$$\begin{array}{ccc} \int_\Omega u^t_{n_k,\varepsilon}\varphi\,dx & \longrightarrow & \int_\Omega u^t_\varepsilon\varphi\,dx \\ \downarrow & & \downarrow \\ \int_\Omega u^t_{n_k}\varphi\,dx & \longrightarrow & \int_\Omega u^t\varphi\,dx \end{array}$$

for every $\varphi \in L^2(\Omega)$. We just verified the upper convergence in the diagram, and the left and right convergences in the diagram are valid due to the property of approximate identities. By Theorem 3.3, it implies that $u^t = u_0 \circ \Phi^{-1}(t,\cdot)$. Hence, $(u^t_{n_k})$ converges weakly to u^t in $L^2(\Omega)$ for every $t \in [0,T]$.

The weak lower semi-continuity of the first term in (3.14) is easily derived from the fact $u^T_{n_k} - u_T \rightharpoonup u^T - u_T$ in $L^2(\Omega)$. And the weak lower semi-continuity of the second term of (3.14) is valid due to the norm-continuity of b. □

3.5 First-order Optimality Conditions System

We use the Lagrangian technique to compute the first-order optimality conditions of minimizing (3.14) restricted to (3.1) and (3.4). Let us define the Lagrange functional

with Lagrange multipliers p and q:

$$L(u,b,p,q) = J(u,b) + \int_0^T \int_\Omega (u_t + b\cdot\nabla u)p\,dxdt + \int_0^T \int_\Omega q\mathrm{div}b\,dxdt. \tag{3.19}$$

To eliminate the boundary terms by computing the functional derivative of (3.19) in b, we need the boundary conditions for b on $\partial\Omega$ such that

$$b = 0,\ \ \nabla_n b = 0,\ \ \Delta b = 0. \tag{3.20}$$

According to the characterization of $H_0^3(\Omega)$, we know that there are two equivalent formulations [41, 55]:

$$\begin{aligned} H_0^3(\Omega) &:= \overline{C_0^\infty(\Omega)}_{\|\cdot\|_{H^3(\Omega)}} \\ &= \left\{ f \in H^3(\Omega) \;\middle|\; f = 0,\ \frac{\partial f}{\partial n} = 0,\ \frac{\partial^2 f}{\partial n^2} = 0 \text{ on } \partial\Omega \right\} \\ &= \left\{ f \in H^3(\Omega) \;\middle|\; f = 0,\ \nabla f = 0,\ \Delta f = 0 \text{ on } \partial\Omega \right\}. \end{aligned}$$

Deriving (3.20) from the previous characterizations is not straightforward. However, we prove it in the following lemma.

Lemma 3.5. *If $f \in H_0^3(\Omega)$, then $f = 0, \nabla_n f = 0, \Delta f = 0$ on the boundary of Ω.*

Proof. Deriving $\partial f/\partial n = 0$ from $\nabla f = 0$ is trivial, let us prove the opposite statement. Since f is equal to zero on $\partial\Omega$, then the tangential derivative of f is equal to zero on $\partial\Omega$. Due to the fact that the normal derivative of f is equal to zero, then one obtains that the gradient of f vanishes on $\partial\Omega$, since the tangential vector and the normal vector are orthogonal each other and the gradient of f can be expressed as a linear combination of the normal and orthogonal vectors. □

Computing the functional derivatives of (3.19) in u, b and setting them to 0 yield

the first-order necessary optimality conditions of the control problem

$$\begin{cases} u_t + b \cdot \nabla u = 0 \quad \text{in } (0,T] \times \Omega, \;\; u(0) = u_0 \quad \text{in } \Omega, \\ p_t + b \cdot \nabla p = 0 \quad \text{in } [0,T) \times \Omega, \;\; p(T) = -(u(T) - u_T) \quad \text{in } \Omega, \\ \text{div} b = 0 \quad \text{in } [0,T] \times \Omega, \\ \lambda \Delta^3 b + \nabla q = p \nabla u \quad \text{in } [0,T] \times \Omega, \end{cases}, \;\; b = 0, \nabla_n b = 0, \Delta b = 0 \quad \text{on } \partial\Omega. \tag{3.21}$$

3.6 Numerical Aspects

In this section we will present some efficient numerical algorithms to discretize the optimality conditions system. The last equation of (3.21) is a triharmonic equation which stems from the use of space H_0^3 as penalty term in (3.14). There are few articles about its numerical schemes, e.g. [25]. However, the algorithms are either not efficient or difficult to be applied directly. Hence, we modify this equation as follows: The motivation of introducing the H_0^3-term is that b has to be Lipschitz continuous to obtain a unique flow Φ. If we apply some smooth initial flow b^0 in the discrete form of (3.21), then replacing Δ^3 with Δ in (3.21) still leads to smooth enough b. Indeed, under this setting b is in H^1 and according to Theorem 4.3 the L^2-regularity of u_0 is propagated to every time. Finally, if b is not only H^1 but also Lipschitz continuous, we still transport BV images to BV images. Thus, in our context we can also work with the cost functional

$$\tilde{J}(b) = \frac{1}{2} \left\| S(u_0, b) - u_T \right\|^2_{L^2(\Omega)} + \frac{\lambda}{2} \int_0^T \left\| \nabla b(t, \cdot) \right\|^2_{L^2(\Omega)^4} dt, \tag{3.22}$$

and the corresponding optimality conditions system

$$\begin{cases} u_t + b \cdot \nabla u = 0 \quad \text{in } (0,T] \times \Omega, \;\; u(0) = u_0 \quad \text{in } \Omega, \\ p_t + b \cdot \nabla p = 0 \quad \text{in } [0,T) \times \Omega, \;\; p(T) = -(u(T) - u_T) \quad \text{in } \Omega, \\ \text{div} b = 0 \quad \text{in } [0,T] \times \Omega, \\ \lambda \Delta b + \nabla q = p \nabla u \quad \text{in } [0,T] \times \Omega, \end{cases}, \;\; b = 0 \quad \text{on } \partial\Omega. \tag{3.23}$$

We remark that the assumption $u_0, u_T \in BV$ does not appear in this model. But one could easily use $U = BV$ and the BV-norm for the difference $u(T)-u_T$ in (3.22), since this would only affect the right-hand side of the adjoint equation. However, in this case we would have to ensure that the flow field b is Lipschitz-continuous. In numerical experiments we found, that the use of the BV-norm for the difference $u(T) - u_T$ did not alter the results too much, and hence we use the optimality conditions system (3.23).

With a divergence-free initial value b^0, we propose a segregation loop in the spirit of [11] to interpolate the intermediate image at time t:

Segregation loop I.
Suppose that $n = 1, \cdots, N_{\text{loop}}$ and N_{loop} is the iteration number. Given u_0, u_T, $b^{n-1}(t)$, λ^{n-1}. The iteration process for solving (3.23) on iteration n proceeds as follows:

1. Compute $u^{n-1}(t), \nabla u^{n-1}(t)$ and $u^{n-1}(T)$ by the forward transport equation using u_0 and $b^{n-1}(t)$.

2. Compute $p^{n-1}(t)$ by the backward transport equation using $-(u^{n-1}(T) - u_T)$ and $b^{n-1}(t)$.

3. Compute $b^n(t)$ by the Stokes equations with the right-hand side $p^{n-1}(t)\nabla u^{n-1}(t)$ and λ^n.

After N_{loop} iterations the intermediate image $u^{N_{\text{loop}}}(t)$ approximates $u(t)$. Moreover, we use a monotonically decreasing sequence (λ^n), which converges to a final λ^*. Thanks to the theory of Stokes equations [32], we know that

$$\|b(t)\|_{H^1(\Omega)} \leq \frac{C}{\lambda} \|p(t)\nabla u(t)\|_{H^{-1}(\Omega)}, \text{ a.e. } t \in [0,T]. \tag{3.24}$$

In practice, we find out that if we choose (λ^n) such that the norm of the right-hand side of (3.24) is monotonically increasing, then the value of $b(t)$ is also increasing. However, the final λ^* cannot be chosen too small so that the minimizing process of (3.22) becomes ill-posed.

Moreover, since the system (3.23) is a necessary condition of minimizing functional (3.22), one expects that the term $\|u(T) - u_T\|_{L^2(\Omega)}$ is not very small. But

since this is one of our final goals, we propose a modification of segregation loop I, which poses no requirement for choosing a specific sequence (λ^n) and gives better approximation of intermediate images. We modify segregation loop I as follows:

Segregation loop II.
Suppose that $n = 1, \cdots, N_{\text{loop}}$ and N_{loop} is the iteration number. Given u_0, u_T, $b^{n-1}(t)$, λ. The iteration process on iteration n proceeds as follows:

1. Compute $u^{n-1}(t), \nabla u^{n-1}(t)$ and $u^{n-1}(T)$ by the forward transport equation using u_0 and $b^{n-1}(t)$.

2. Compute $p^{n-1}(t)$ by the backward transport equation using $-(u^{n-1}(T) - u_T)$ and $b^{n-1}(t)$.

3. Compute the solution to the Stokes equations with the right-hand side $p^{n-1}(t)\nabla u^{n-1}(t)$ and λ, and denote it by $\delta b^{n-1}(t)$.

4. $b^n(t) = b^{n-1}(t) + \delta b^{n-1}(t)$.

In segregation loop II we utilize the system (3.23) to estimate the update of the flow field and update the flow field in step 4. This point of view is different from the original problem (3.23), but interestingly this modification actually solves the necessary conditions of another minimizing problem. If the segregation loop II converges, then the update $\delta b^{n-1}(t)$ converges to zero. Since the initial value b^0 is divergence-free and in each iteration the update flow $\delta b^{n-1}(t)$ is divergence-free, the limit of $(b^n(t))$ is also divergence-free.

We denote by u^*, p^*, b^*, q^* the limits of particular sequences and in this case $\delta b^* = 0$. Setting the limits into (3.23) we derive

$$\begin{cases} u_t^* + b^* \cdot \nabla u^* = 0 \quad \text{in } (0,T] \times \Omega, \;\; u^*(0) = u_0 \quad \text{in } \Omega, \\ p_t^* + b^* \cdot \nabla p^* = 0 \quad \text{in } [0,T) \times \Omega, \;\; p^*(T) = -(u^*(T) - u_T) \quad \text{in } \Omega, \\ \text{div} b^* = 0 \quad \text{in } [0,T] \times \Omega, \;\; b^* = 0 \quad \text{on } \partial\Omega, \\ \nabla q^* = p^* \nabla u^* \quad \text{in } [0,T] \times \Omega. \end{cases} \tag{3.25}$$

Actually, (3.25) is the optimality conditions system of another constrained mini-

mization problem, namely

$$\inf_{b^*} \frac{1}{2} \|u^*(T) - u_T\|^2_{L^2(\Omega)} \tag{3.26}$$

subject to

$$\begin{cases} u^*_t + b^* \cdot \nabla u^* = 0 \quad \text{in } (0,T] \times \Omega, \;\; u^*(0) = u_0 \quad \text{in } \Omega, \\ \text{div} b^* = 0 \quad \text{in } [0,T] \times \Omega, \;\; b^* = 0 \quad \text{on } \partial\Omega. \end{cases} \tag{3.27}$$

Compared to (3.14) or (3.22) the functional (3.26) is not regularized. But if we stop the segregation loop II on time, i.e. the interpolation error does not vary too much, then it is not surprising that segregation loop II gives good approximation results. From the point of view of regularization theory, one may see the segregation loop II as a kind of a Landweber method for minimizing $\|u(T) - u_T\|^2_{L^2(\Omega)}$ which is inspired by a Tikhonov-functional.

In most cases the forward interpolation from u_0 to u_T and the backward interpolation from u_T to u_0 are complementary, since the flow is only able to transport objects from one place to another place, but not able to create some new objects. If, in the forward case, some new objects appear, then in the backward case the new objects disappear, implying that backward interpolation is more suitable in this case. In practice, we take the average of forward and backward interpolations to achieve better interpolation results.

3.6.1 Hierarchical Method

In order to get a start value b^0 for the optimality conditions system, the hierarchical processing is a good approach [10]:

1. Down-sample the images into level l.
2. Solve system (3.23) in level l out and get b^l.
3. Up-sample the optical flow into level $l-1$ and get b^{l-1}.

The estimated optical flow b^{l-1} is a start value of the hierarchical method in level $l-1$. In coarsest level we assume the start value to be zero. The down- and up-sampling methods are decisive, i.e. it is important to preserve the local structures

and small objects as well as possible while down- and up-sampling the images or the optical flow.

In practice, we apply bicubic interpolation [45] for the sampling, since it has fewer interpolation artifacts than bilinear interpolation or nearest-neighbor interpolation. Compared to the Gaussian pyramid [15] the down-sampled images by bicubic interpolation do not look as blurred.

3.6.2 Numerical Schemes

To discretize the Stokes equations in (3.23) we apply the P2-P1 finite element method introduced in Chapter 2. To discretize the transport equations we employ two approaches: The first one follows [35, 40, 11] and it is a second-order total-variation diminishing scheme (TVD scheme). The second one is utilizing the method of characteristics. Both are also applicable for the backward transport equation, since we can reformulate it as a forward problem by setting $t' := T - t$:

$$p_{t'} - b \cdot \nabla p = 0, \;\; p(0) = -(u(0) - u_T).$$

For the sake of completeness, we present the TVD scheme from [11]: Suppose that the image size is $N \times M$, h and Δt are the mesh sizes in space and time, respectively with mesh index $i = 1, \cdots, N, j = 1, \cdots, M$ in space and $k = 1, \cdots, K$ in time. Setting $b = (v, w)$, the stability condition of the scheme, usually called CFL condition [8], is

$$\sigma_{\text{CFL}} := \max(|v|_{\max}, |w|_{\max}) \frac{\Delta t}{h} \leq 1.$$

In practice we choose Δt such that $\sigma_{\text{CFL}} = 0.1$. The TVD scheme of the forward transport equation is given by

$$\begin{aligned}
u_t|_{i,j}^k &= \frac{u_{i,j}^{k+1} - u_{i,j}^k}{\Delta t}, \\
-v u_x|_{i,j}^k &= \frac{v_{i,j}^+}{h} \left[1 + \frac{1}{2} \chi(r_{i-\frac{1}{2},j}^+) - \frac{1}{2} \frac{\chi(r_{i-\frac{3}{2},j}^+)}{r_{i-\frac{3}{2},j}^+} \right] (u_{i-1,j}^k - u_{i,j}^k) \\
&\quad - \frac{v_{i,j}^-}{h} \left[1 + \frac{1}{2} \chi(r_{i+\frac{1}{2},j}^-) - \frac{1}{2} \frac{\chi(r_{i+\frac{3}{2},j}^-)}{r_{i+\frac{3}{2},j}^-} \right] (u_{i+1,j}^k - u_{i,j}^k),
\end{aligned}$$

where $v^+_{i,j} = \max(v_{i,j}, 0), v^-_{i,j} = \min(v_{i,j}, 0)$ and the flux difference ratios are defined as

$$r^+_{i-\frac{1}{2},j} = \frac{u^k_{i+1,j} - u^k_{i,j}}{u^k_{i,j} - u^k_{i-1,j}},\ r^+_{i-\frac{3}{2},j} = \frac{u^k_{i,j} - u^k_{i-1,j}}{u^k_{i-1,j} - u^k_{i-2,j}},$$
$$r^-_{i+\frac{1}{2},j} = \frac{u^k_{i,j} - u^k_{i-1,j}}{u^k_{i+1,j} - u^k_{i,j}},\ r^-_{i+\frac{3}{2},j} = \frac{u^k_{i+1,j} - u^k_{i,j}}{u^k_{i+2,j} - u^k_{i+1,j}}.$$

In a similar way we can discretize the term $-wu_y$. The super-bee limiter function is given by

$$\chi(r) = \max(0, \min(2r, 1), \min(r, 2)).$$

To compute the spatial derivatives of images we use the standard three-point formula:

$$pu_x|_{i,j} = \frac{1}{2h}(-u_{i-1,j} + u_{i+1,j})p_{i,j},$$
$$pu_y|_{i,j} = \frac{1}{2h}(-u_{i,j-1} + u_{i,j+1})p_{i,j}.$$

Another way for solving the transport equation is to utilize the characteristic solution. From (3.8) we know that the key point is to solve the backward flow starting from (t, x)

$$\begin{cases} \dfrac{\partial \Phi}{\partial s} = b(s, \Phi) \quad \text{in } [0, t[\times\Omega, \\ \Phi(t, x) = x \quad \text{in } \Omega. \end{cases} \tag{3.28}$$

To solve (3.28) numerically efficiently we use Runge-Kutta 4th order method [45]. We discretize $[0, t]$ with time step $\Delta t = 0.1$ and utilize a constant flow b over $[0, t]$ to save memory and computational cost. In this scheme we have to interpolate the flow $b(t, x)$ with some non-integer x, since only the flow $b(t, \cdot)$ with integer coordinates is given. For this we use bilinear interpolation (a bicubic interpolation leads to almost the same results). Then, we warp the image u_0 with the coordinates calculated by (3.28) using the cubic spline predefined in Matlab to approximate $u(t, x)$.

3.6.3 Experiments

To illustrate the effect of our intermediate interpolated images, we apply the interpolation error (IE) introduced in [9]. The IE measures the root-mean-square (RMS) difference between the ground-truth image u_{GT} and the interpolated image u:

$$IE = \left(\frac{1}{NM} \sum_{i=1}^{N} \sum_{j=1}^{M} \left(u(x_i, y_j) - u_{\mathrm{GT}}(x_i, y_j) \right)^2 \right)^{\frac{1}{2}},$$

where $N \times M$ is the image size. We test our methods on the datasets generated by Middlebury College[1] with public ground-truth interpolations:

– Dimetrodon with size 584×388;

– Venus with size 420×380.

Every dataset is composed of three images and the mid-image is the ground-truth interpolation at time $T/2$ if we assume the evolution process of three images lasts time $T = 1$. To evaluate the interpolation we can compare our interpolation results with the ground-truth by means of the IE measure. The interpolation results calculated by segregation loop I and II are shown in Table 3.1. As mentioned in [9], the Pyramid LK method and Mediaplayer$^{\mathrm{TM}}$ are significantly better for image sequence interpolation than for ground-truth motion estimation. Because, e.g. Mediaplayer$^{\mathrm{TM}}$, tends to overly extend the flow into textureless regions, which are not significantly affected by image sequence interpolation. According to Table 3.1 segregation loop II works better than some classic methods and more accurately than segregation loop I. The places where the interpolation errors take place are plotted in Figure 3.2. As a result, our methods, especially segregation loop II, work in image sequence interpolation effectively.

Dealing with the convergence history of the proposed methods we can expect that segregation loop I minimizes the cost functional (3.22) and segregation loop II minimizes the data error $\|u(T) - u_T\|_{L^2(\Omega)}$ according to the explanation in Section 3.6. In Figure 3.3 we observe this phenomenon for the test image sequence Dimetrodon from Figure 3.1. Segregation loop I reduces the value of the cost functional considerably in the first iterates (see subfigure (a)) while the data error is

[1] `http://vision.middlebury.edu/flow/data/`

	Dimetrodon	Venus
Segregation loop I	**2.25**	**6.67**
Segregation loop II	**1.95**	**3.63**
Stich et al.	1.78	2.88
Pyramid LK	2.49	3.67
Bruhn et al.	2.59	3.73
Black and Anandan	2.56	3.93
Mediaplayer^{TM}	2.68	4.54
Zitnick et al.	3.06	5.33

Table 3.1: Interpolation errors calculated by our methods with comparison to the ground-truth interpolation of Middlebury datasets, and the other IE results taken from [51].

only reduced mildly (see subfigure (b)). Segregation loop II reduces the value of the data error faster and this is responsible for the quality of image interpolation (see subfigure (c)).

In addition to the accuracy, we demonstrate in Figures 3.4 and 3.5 how segregation loop II deals with noisy images. In Figure 3.4 the same images as in Figure 3.1 are polluted with salt and pepper noises with density 0.5. Compared to the interpolation results without noises we can distinguish that in subfigure (d) of Figure 3.5 are mainly only the noises left. Hence, this method works stably with respect to perturbation by noises.

In another kind of tests, we tried segregation loop II with nonrigid objects and large displacements. Figure 3.6 demonstrates an artificially warped hand and the zoomed-in regions of the hand is viewed in Figure 3.7. Compared to the blend method, i.e. the mean values of u_0 and u_T, we can observe that our method is able to generate reasonable intermediate images without ghosting-effect, which is characterized by using the blend method. The reason is that the divergence-free flow preserves only the volume but not the shape. Thus, the objects in the interpolated image can be warped by the optical flow.

Finally, even a more challenging problem, we test our method with images with varying illumination. We tried to interpolate between two different head sections with different geometry. Here the assumption that the image intensity is constant along the characteristics generated by the optical flow breaks down. We can not

create the new pixels, which belong to u_T, but do not belong to u_0.Viewing Figure 3.8 we can observe this phenomenon, but we still get a reasonable registered image. It means that the warped contours of the template image (a) match the contours of target image (c) well. From this point of view our interpolation method is deemed to be useful in image registration. Actually, this kind of illumination varying interpolation can be classified into image morphing. To get the morphing-like interpolation we apply the forward interpolation from time 0 to $T/2$ and the backward interpolation from time T to $T/2$. Then, we take the mean values of the forward and backward interpolation at time $T/2$. We demonstrate the morphing-like interpolation in Figure 3.9.

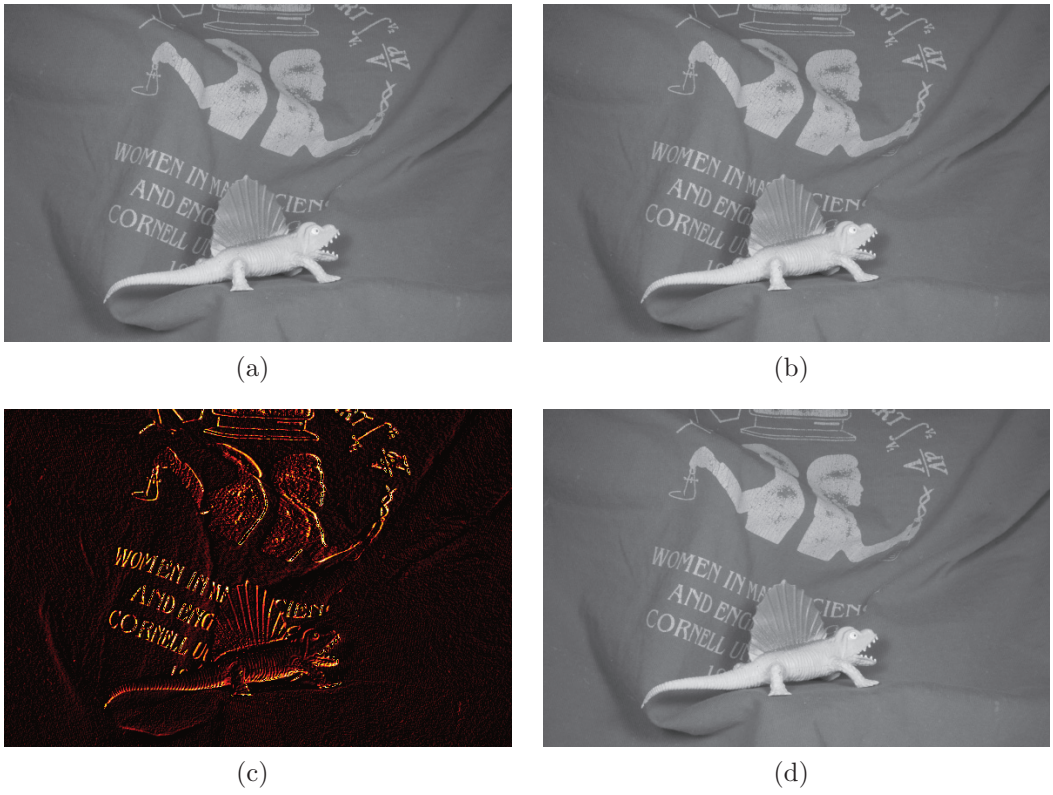

(a) (b)

(c) (d)

Figure 3.1: Dataset Dimetrodon. (a) u_0. (b) u_T. (c) The absolute difference between (a) and (b). (d) The ground-truth interpolation at time $T/2$.

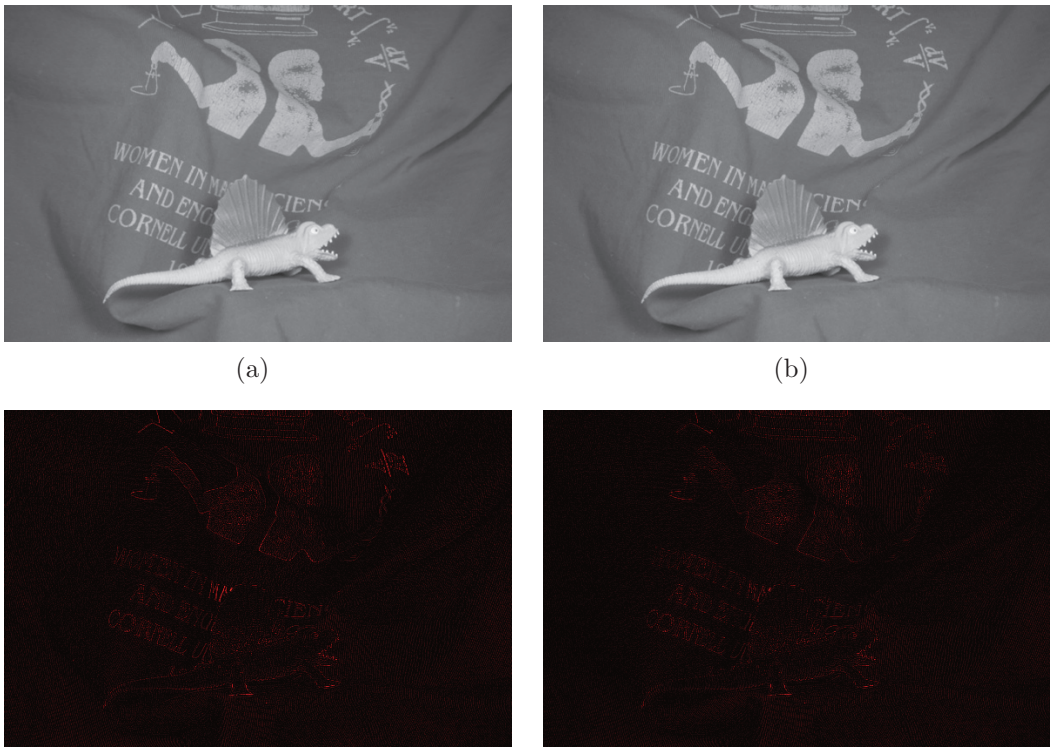

(a) (b)

(c) (d)

Figure 3.2: (a) The generated interpolation at time $T/2$ by segregation loop I. (b) The generated interpolation at time $T/2$ by segregation loop II. (c) The absolute difference between (a) and the ground-truth. (d) The absolute difference between (b) and the ground-truth.

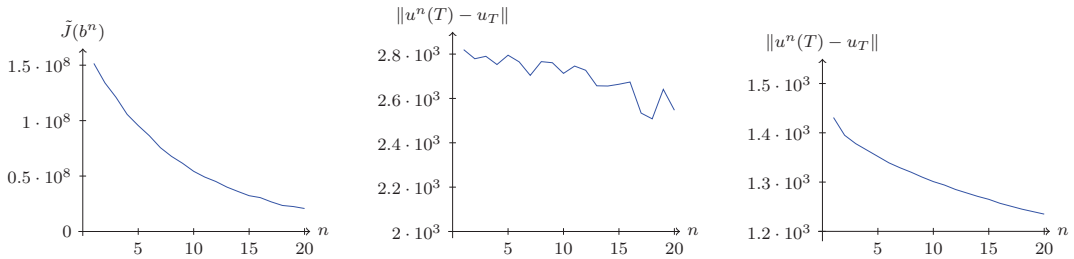

(a) (b) (c)

Figure 3.3: Applied on dataset Dimetrodon. (a) Values of the cost functional for segregation loop I. (b) Values of the data error for segregation loop I. (c) Values of the data error for segregation loop II.

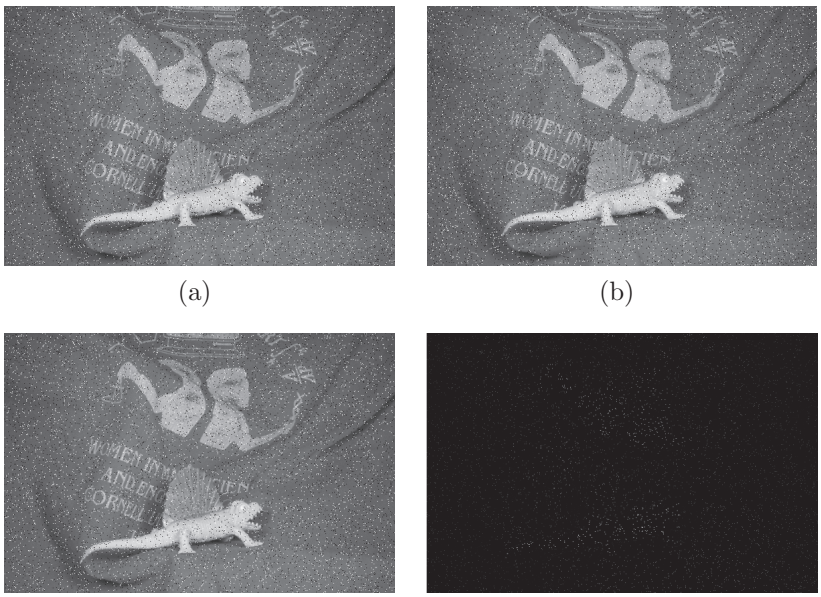

(a) (b)

(c) (d)

Figure 3.4: (a) Noisy u_0. (b) Noisy u_T. (c) $u(T/2)$ calculated by segregation loop II. (d) Absolute difference between (c) and the ground-truth without noise.

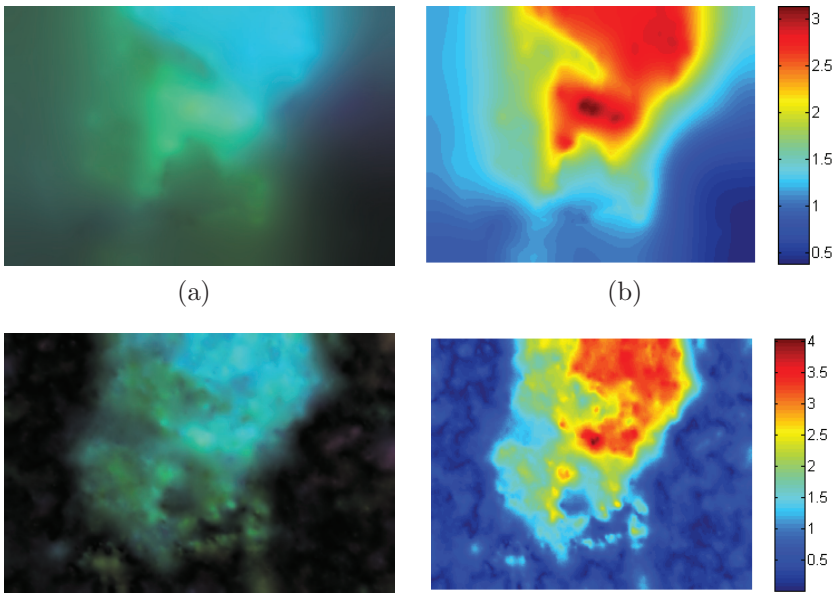

(a) (b)

(c) (d)

Figure 3.5: (a) The optical flow of dataset Dimetrodon. (b) The intensities of (a). (c) The optical flow of dataset noisy Dimetrodon. (d) The intensities of (c).

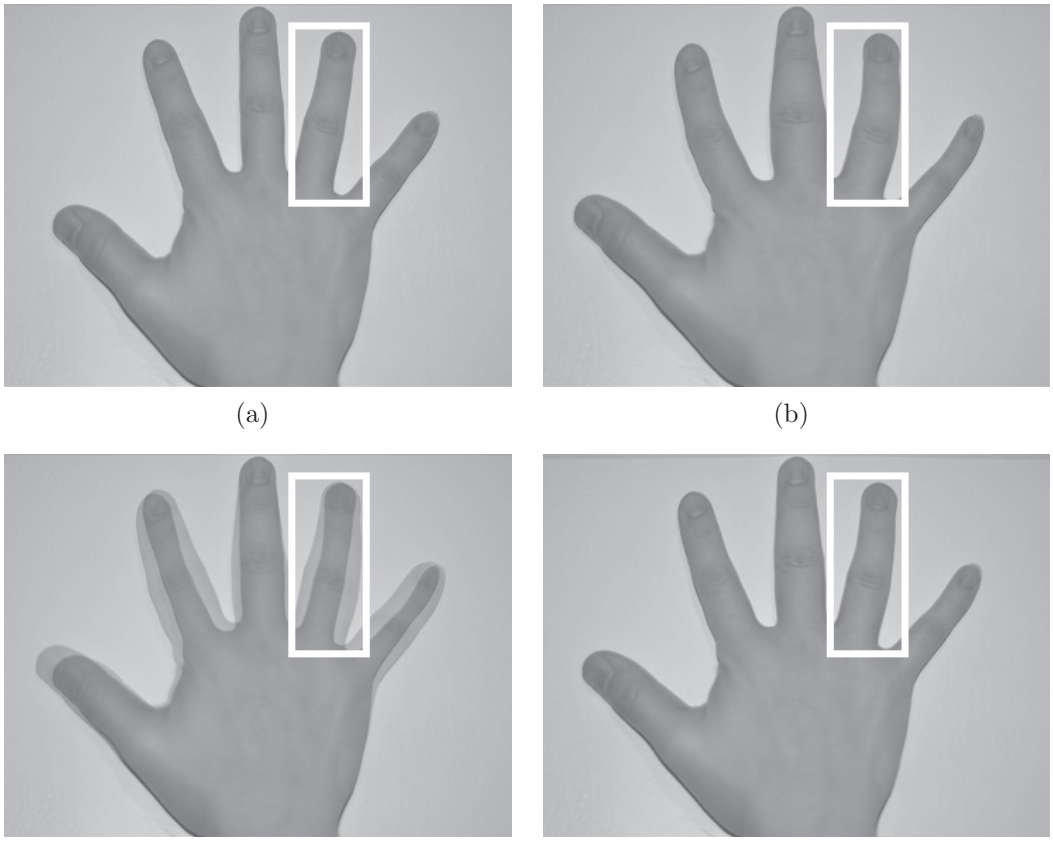

(a) (b)

(c) (d)

Figure 3.6: (a) u_0. (b) u_T. (c) $u(T/2)$ calculated by the blend method. (d) $u(T/2)$ calculated by segregation loop II.

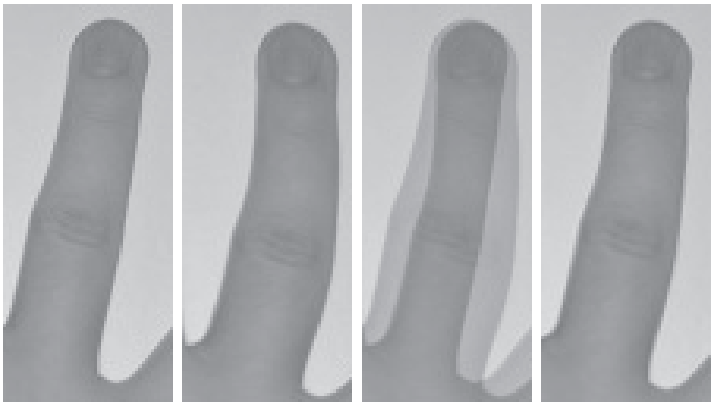

(a) (b) (c) (d)

Figure 3.7: Zoomed-in regions of Figure 3.6. (a) Zoomed-in region of (a). (b) Zoomed-in region of (b). (c) Zoomed-in region of (c). (d) Zoomed-in region of (d).

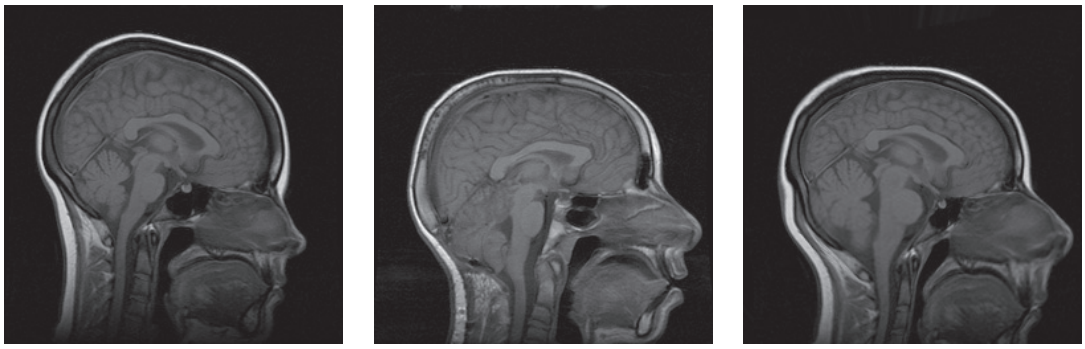

(a) (b) (c)

Figure 3.8: Illumination varying brain. (a) The template image. (b) The target image. (c) The registered image.

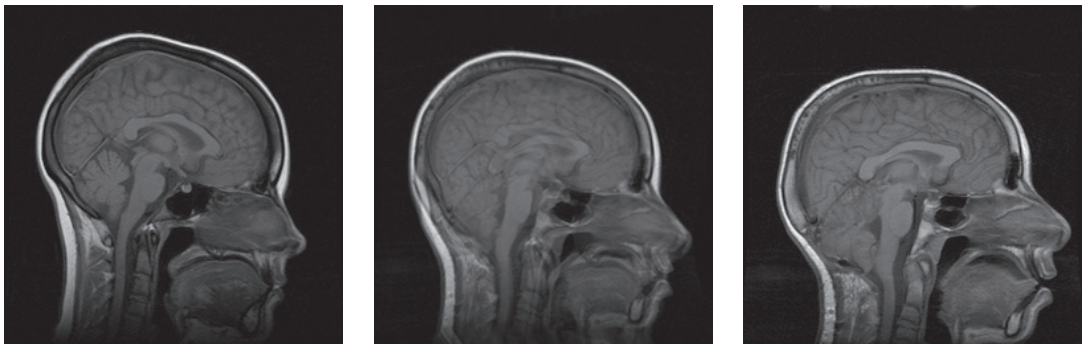

(a) (b) (c)

Figure 3.9: Illumination varying brain. (a) u_0. (b) The morphed image at time $T/2$. (c) u_T.

Chapter 4

TV_ε-Flow based Optimal Control

4.1 Problem Statement and Modeling

In the last chapter we introduced the image sequence interpolation method in the framework of optimal control governed by an H^1 optical flow. However, the H^1-regularization produces a homogeneous smooth flow field, i.e. the flow field is equally penalized across the flow edges. As a result, the shape of objects in the image sequence may not be preserved well in the case that objects are moving faster or slower than the background. To deal with such problem, it is common to substitute the H^1-regularization with the TV-regularization. As introduced in Chapter 2, the space of bounded variation involves functions which are discontinuous across hypersurfaces, i.e. a line in 2 dimension. Thus, the minimizer to TV regularization problem is piece-wise constant, i.e. the smoothing is not permitted to cross flow edges. Since the solution operator of transport equations is non-linear with respect to the optical flow, it is difficult to utilize the projection method [17] to solve the TV minimization problem. To get ride of that we relax the BV semi-norm with the ε-smooth total variation functional introduced in Section 4.2, and the non-differentiable BV semi-norm becomes differentiable with this relaxation.

Let us model image interpolation using the ε-smooth total variation in the framework of optimal control. We assume that

$$u_0, u_T \in L^\infty(\Omega), \tag{4.1}$$

$$b \in L^2(0, T; W_0^{1,1+\tau}(\Omega)^d), \tag{4.2}$$

with a sufficient small τ, i.e. $\tau > 0$ satisfies for an $f \in W_0^{1,1+\tau}(\Omega)$ and a given $\varepsilon > 0$

$$|\Omega|^{\frac{\tau}{1+\tau}} \|\nabla f\|_{L^{1+\tau}(\Omega)^d} \leq \int_\Omega \sqrt{|\nabla f|^2 + \varepsilon}\, dx, \tag{4.3}$$

where the constant $|\Omega|^{\frac{\tau}{1+\tau}}$ is the norm of the embedding operator from $L^{1+\tau}(\Omega)$ to $L^1(\Omega)$. Then, we consider the minimization problem

$$\inf J(b) = \frac{1}{2} \|u(T) - u_T\|^2_{L^2(\Omega)} + \lambda \int_0^T \int_\Omega \sqrt{|\nabla b|^2 + \varepsilon}\, dxdt \tag{4.4}$$

restricted to

$$\mathrm{div} b = 0, \tag{4.5}$$

$$\begin{cases} \partial_t u(t,x) + b(t,x) \cdot \nabla_x u(t,x) = 0 \quad \text{in } (0,T] \times \Omega, \\ u(0,x) = u_0(x) \quad \text{in } \Omega. \end{cases} \tag{4.6}$$

To analyze the control problem we apply the existing theory of transport equations with non-Lipschitz flow introduced in Section 4.4. To make it possible, we shall extend the range of u_0, u_T, b in $\mathbb{R}^d \setminus \Omega$ with 0 extension in this chapter if necessary.

4.2 Introduction of TV_ε

The BV semi-norm, or total variation is defined by

$$J_0(u) = \sup_{v \in \mathcal{V}} \int_\Omega -u \mathrm{div} v\, dx, \tag{4.7}$$

where Ω is a bounded open subset of $\mathbb{R}^d$ and the set of test functions

$$\mathcal{V} := \left\{ v \in C_0^1(\Omega)^d \;\middle|\; \|v(x)\|_{L^\infty(\Omega)^d} \leq 1 \right\}.$$

In the case that u belongs to $C^1(\Omega)$, then $\int_\Omega u \mathrm{div} v\, dx = -\int_\Omega v \cdot \nabla u\, dx$ and $J_0(u) =$

$\int_\Omega |\nabla u(x)|\, dx$. We define an extension of $J_0(u)$:

$$J_\varepsilon(u) = \int_\Omega \sqrt{|\nabla u|^2 + \varepsilon}\, dx, \tag{4.8}$$

which is called the ε-smooth total variation functional and notice that it is not a semi-norm. Based on the concept of bidual formulation we gain an another way to represent a convex functional.

Definition 4.1. *Let X be a real Banach space and $f : X \to \overline{\mathbb{R}}$. Then $f^* : X^* \to \overline{\mathbb{R}}$, defined by*

$$f^*(y) = \sup_{x \in X} \{y(x) - f(x)\}$$

is called the Fenchel transform *of f. $f^{**} : X \to \overline{\mathbb{R}}$ defined by*

$$f^{**}(x) = \sup_{y \in X^*} \{y(x) - f^*(y)\}$$

is called second conjugate *of f.*

Example 4.1. We denote by V a norm space endowed with norm $\|\cdot\|$ and V^* its topological dual endowed with norm $\|\cdot\|_*$. We define $F : V \to \mathbb{R}$ by

$$F(x) = \varphi\left(\|x\|\right), \text{ with } \varphi(t) = \frac{1}{\alpha}|t|^\alpha \text{ and } \alpha \in]1, \infty[,$$

then the Fenchel transform of F gives

$$F^*(y) = \varphi^*(\|y\|_*), \text{ with } \varphi^*(t) = \frac{1}{\alpha^*}|t|^{\alpha^*} \text{ and } \frac{1}{\alpha} + \frac{1}{\alpha^*} = 1.$$

Proof.

$$\begin{aligned} F^*(y) &= \sup_{x \in V} \{< y, x > -\varphi(\|x\|)\} \\ &= \sup_{t \geq 0} \sup_{\substack{x \in V \\ \|x\| = t}} \{< y, x > -\varphi(\|x\|)\} \\ &= \sup_{t \geq 0} \{t \|y\|_* - \varphi(t)\} \\ &\overset{\varphi \text{ even}}{=} \sup_{t \in \mathbb{R}} \left\{ t \|y\|_* - \frac{1}{\alpha}|t|^\alpha \right\}. \end{aligned}$$

The last expression has a maximum at $t = \|y\|_*^{\alpha^*-1}$, and hence $\varphi^*(\|y\|_*) = \frac{1}{\alpha^*}\|y\|_*^{\alpha^*}$. □

Remark 4.1. If f is a lower semi-continuous convex functional, then $f^{**} = f$. The details of the proof refer to [26].

Given a continuous and convex function $f(x) = \sqrt{|x|^2 + \varepsilon}$, the Fenchel transform of f yields

$$f^*(y) = -\sqrt{\varepsilon\,(1 - |y|^2)}, \;\; |y| \leq 1,$$

the second conjugate of f yields

$$f^{**}(x) = \sup_{y\in\mathbb{R}} \left\{ xy + \sqrt{\varepsilon\left(1 - |y|^2\right)} \;\middle|\; |y| \leq 1 \right\}, \tag{4.9}$$

and it is equal to $f(x)$ due to Remark 4.1. Motivated by this and (4.8) we define

$$J_\varepsilon^{**}(u) = \sup_{v\in\mathcal{V}} \int_\Omega -u\mathrm{div}v + \sqrt{\varepsilon\left(1 - |v\,(x)|^2\right)}dx.$$

The question on under which assumption $J_\varepsilon(u) = J_\varepsilon^{**}(u)$ is answered in the following theorem [1].

Theorem 4.1. *If $u \in W^{1,1}(\Omega)$, then $J_\varepsilon(u) = J_\varepsilon^{**}(u)$.*

Proof. Since $C^1(\Omega)$ is dense in $W^{1,1}(\Omega)$, it suffices to show that the statement is valid for $u \in C^1(\Omega)$. For any $v \in \mathcal{V}$ yields

$$\begin{aligned}\int_\Omega -u\mathrm{div}v + \sqrt{\varepsilon\left(1 - |v|^2\right)}\,dx &= \int_\Omega \nabla u \cdot v + \sqrt{\varepsilon\left(1 - |v|^2\right)}\,dx \\ &\leq \int_\Omega \sqrt{|\nabla u|^2 + \varepsilon}\,dx.\end{aligned}$$

The last inequality holds due to (4.9). Taking the supremum of both sides over $v \in \mathcal{V}$ yields

$$J_\varepsilon^{**}(u) \leq \int_\Omega \sqrt{|\nabla u|^2 + \varepsilon}\,dx.$$

Regarding the reserve inequality we take $\overline{v} = \nabla u/\sqrt{|\nabla u|^2 + \varepsilon}$, and get

$$\int_\Omega \nabla u \cdot \overline{v} + \sqrt{\varepsilon\left(1 - |\overline{v}|^2\right)}dx = \int_\Omega \sqrt{|\nabla u|^2 + \varepsilon}\, dx \tag{4.10}$$

and $\overline{v} \in C(\Omega)^d$ with $|\overline{v}(x)| < 1$ for all $x \in \Omega$. Multiplying $\overline{v}$ by a suitable characteristic function compactly supported in Ω and then mollifying, denoted by v, one obtains $v \in \mathcal{V} \cap C_0^\infty(\Omega)^d$ for which the left-hand side of (4.10) substituting $\overline{v}$ with v is arbitrarily close to $\int_\Omega \sqrt{|\nabla u|^2 + \varepsilon}\, dx$. □

Theorem 4.2. *Let (u_n) converge weakly to $\overline{u}$ in $L^p(\Omega)$ for $1 < p < \infty$. Then, $(J_\varepsilon(u_n))$ is weakly lower semi-continuous for any $\varepsilon \geq 0$.*

Proof. For any $v \in \mathcal{V}, \mathrm{div}v \in C(\Omega)$ we have

$$\begin{aligned}\int_\Omega -\overline{u}\mathrm{div}v + \sqrt{\varepsilon\left(1 - |v|^2\right)}\, dx &= \lim_{n\to\infty} \int_\Omega -u_n \mathrm{div}v + \sqrt{\varepsilon\left(1 - |v|^2\right)}\, dx \\ &= \liminf_{n\to\infty} \int_\Omega -u_n \mathrm{div}v + \sqrt{\varepsilon\left(1 - |v|^2\right)}\, dx \\ &\overset{\text{Theorem 4.1}}{\leq} \liminf_{n\to\infty} J_\varepsilon(u_n).\end{aligned}$$

Taking supremum over $v \in \mathcal{V}$ gives $J_\varepsilon(\overline{u}) \leq \liminf_{n\to\infty} J_\varepsilon(u_n)$. □

We can also extend Theorem 4.2 to the case that the weak lower semi-continuity of $(J_\varepsilon(u_n))$ involves time.

Corollary 4.1. *Assume that $1 < p < \infty$ and (u_n) converges weakly to $\overline{u}$ in $L^2(0, T; L^p(\Omega))$, then*

$$\int_0^T J_\varepsilon(\overline{u}(t))\, dt \leq \liminf_{n\to\infty} \int_0^T J_\varepsilon(u_n(t))\, dt.$$

Proof. By the weak convergence of (u_n) we can deduce that

$$J_\varepsilon(\overline{u}(t)) \leq \liminf_{n\to\infty} J_\varepsilon(u_n(t)) \tag{4.11}$$

for a.e. $t \in (0,T)$. Taking the integral of (4.11) over t and applying the Fatou's lemma [30] derives the statement. □

4.3 Solution Theory of Transport Equation with H^1-Flow

We consider the transport equation in $[0,T] \times \mathbb{R}^d$

$$\begin{cases} \partial_t u(t,x) + b(t,x) \cdot \nabla_x u(t,x) = 0 \quad \text{in } (0,T] \times \mathbb{R}^d, \\ u(0,x) = u_0(x) \quad \text{in } \mathbb{R}^d. \end{cases} \tag{4.12}$$

According to the theorem of Picard-Lindelöf, the well-posedness of (4.12) needs that b enjoys at least Lipschitz regularity in space. In this case, the transport equation propagates the regularity of u_0 to $t \in [0,T]$ according to the solution theory of the transport equation with the smooth setting introduced in Chapter 3. However, the well-posedness of the transport equation related to weakly differentiable vector field was an open problem until DiPerna and Lions published the celebrated work [27]. They introduced the notion of renormalized solution, roughly speaking, the solution enjoys the chain rule. They relaxed the assumption on b to $W^{1,p}_{\text{loc}}\left(\mathbb{R}^d\right)^d$ in space, as a result the transport equation does not propagate the BV regularity. As a counterexample we refer to [23]. Recently, Ambrosio extended the assumption on b to $BV_{\text{loc}}\left(\mathbb{R}^d\right)^d$ in space, such that the solution to the transport equation is still unique. More details refer to [3, 4].

Applying the theory of DiPerna and Lions to obtain the uniqueness of the solution to the transport equation, the chain rule plays a decisive role. To explain this we argue first formally: Multiplying (4.12) by $2u$ and applying the chain rule yields

$$\partial_t u^2 + b \cdot \nabla u^2 = 0.$$

Assume $\text{div} b = 0$ and integrating over Ω gives

$$\frac{d}{dt} \int_\Omega u^2(t,x)\, dx = -\int_\Omega \text{div} b(t,x) u^2(t,x)\, dx = 0. \tag{4.13}$$

To obtain the uniqueness, it suffices to show that if the initial value $u_0 = 0$, then the only solution $u = 0$. This is clear from (4.13). However, the formal argument has two gaps. Firstly, in the case that the solutions to (4.12) are not smooth, so we can not use the chain rule

$$\partial_t u^2 = 2u\partial_t u \text{ and } \nabla u^2 = 2u\nabla u.$$

Secondly, applying (4.13) to show that $\|u(t,\cdot)\|_{L^2(\Omega)} = 0$ for every t, we need to know that

$$\|u(t,\cdot)\|_{L^2(\Omega)} \to \|u_0\|_{L^2(\Omega)}.$$

However, the continuity in norm can not be deduced only from the weak formulation [24].

To face the uniqueness issue, DiPerna and Lions introduced the notion of renormalized solution [4, 27]:

Definition 4.2 (Renormalized solution)**.** *Let b be a locally summable vector field such that* div$b$ *is locally summable. We say that $u \in L^\infty(0,T;L^p(\mathbb{R}^d))$ is a* renormalized solution *to a transport equation if the following equation holds in the sense of distributions*

$$\frac{\partial}{\partial t}\beta(u) + b\cdot\nabla\beta(u) = 0$$

for all $\beta \in C^1(\mathbb{R})$.

The importance of the renormalized solution is summarized in the following theorems, which corresponds to the rough statement "the vector field b which gives the renormalized solution to (4.12), implies the well-posedness of (4.12)". We assume first that

$$b \in L^1(0,T;W^{1,1}_{\text{loc}}\left(\mathbb{R}^d\right)^d),\ \ \text{div}b \in L^1(0,T;L^\infty(\mathbb{R}^d)), \tag{4.14}$$

$$\frac{|b(t,x)|}{1+|x|} \in L^1(0,T;L^1(\mathbb{R}^d)^d) \cap L^1(0,T;L^\infty(\mathbb{R}^d)^d). \tag{4.15}$$

Under the assumption (4.2) it is clear that b belongs to $L^1(0,T;W^{1,1}(\mathbb{R}^d)^d)$, and since b is divergence-free, (4.14) is satisfied. Furthermore, b satisfies (4.15) because b is assumed to have the trivial extension in $\mathbb{R}^d\setminus\Omega$ and b belongs to $L^1(0,T;L^\infty(\Omega)^d)$, then from the fact $0 < 1/(1+|x|) \le 1$ we derive this statement.

Theorem 4.3. *We assume* (4.14) *and* (4.15).

1. *(Consistency). Let* $u \in L^\infty(0,T;L^p(\mathbb{R}^d))$ *and let* $b \in L^1(0,T;L^p(\mathbb{R}^d)^d)$ *with* $1 \le p \le \infty$. *If* u *is a renormalized solution to* (4.12), *then* u *is a solution to* (4.12). *If* u *is a solution to* (4.12) *and* $b \in L^1(0,T;W^{1,q}_{\mathrm{loc}}(\mathbb{R}^d)^d)$ *with* $\frac{1}{p}+\frac{1}{q}=1$, *then* u *is a renormalized solution.*

2. *(Existence and uniqueness). Let* $u_0 \in L^p(\mathbb{R}^d)$, *then there exists a unique renormalized solution* u *to* (4.12) *in* $C([0,T];L^p(\mathbb{R}^d))$ *for* $1 \le p \le \infty$.

Due to the settings (4.1), (4.2), and (4.5) of b. The observing state $u(T) \in L^2(\Omega)$ makes sense, since $u \in C([0,T];L^\infty(\mathbb{R}^d))$ and $u(T) \in L^\infty(\Omega)$, which is continuously embedded into $L^2(\Omega)$. Next, we establish the stability results of the renormalized solution to (4.12) with respect to b.

Theorem 4.4 (Stability)**.** *Let* $b_n \in L^1(0,T;L^1_{\mathrm{loc}}\left(\mathbb{R}^d\right)^d), \mathrm{div} b_n \in L^1(0,T;L^1_{\mathrm{loc}}\left(\mathbb{R}^d\right))$ *and* $(b_n), (\mathrm{div} b_n)$ *converge to* $b, \mathrm{div} b$ *where* b *satisfies* (4.14) *and* (4.15). *Let* $u_0 \in L^p(\mathbb{R}^d)$ *and* (u_n) *be bounded sequence in* $L^\infty(0,T;L^p_{\mathrm{loc}}\left(\mathbb{R}^d\right))$ *such that* u^n *is a renormalized solution to* (4.12) *with* b *replaced by* b_n *corresponding to* u_0, *and* u *is a renormalized solution to* (4.12). *Then,* (u_n) *converges to* u *in* $C([0,T];L^p_{\mathrm{loc}}\left(\mathbb{R}^d\right))$.

4.4 Existence of a Minimizer

Lemma 4.1 (Maximum Principle)**.** *Let* b *and* u_0 *be smooth and let* u *be a smooth solution to* (4.6). *Then,* $\|u(t,\cdot)\|_{L^\infty(\mathbb{R}^d)} \le \|u_0\|_{L^\infty(\mathbb{R}^d)}$.

Proof. The lemma is a trivial consequence of the method of characteristics. Indeed, arguing as $u(t,x) = u_0(\Phi^{-1}(t,x))$, where Φ is the solution to the ODE corresponding to b. □

Now, we are able to prove the existence of a minimizer to (4.4) restricted to (4.5) and (4.6) in the following theorem:

Theorem 4.5. *Assume that* u_0, u_T *satisfy* (4.1) *and* b *satisfies* (4.2). *Then, the minimization problem* (4.4) *governed by* (4.5) *and* (4.6) *has a solution.*

Proof. Define a minimizing sequence $(b_n) \subset L^2(0,T;W_0^{1,1+\tau}(\Omega)^d)$ with $\mathrm{div} b_n = 0$. The coercivity of (4.4) in $L^2(0,T;W_0^{1,1+\tau}(\mathbb{R}^d)^d)$ is clear under the assumption (4.3), then one obtains that (b_n) is uniformly bounded in $L^2(0,T;W_0^{1,1+\tau}(\Omega)^d)$. Then, one deduces that there exist a $b \in L^2(0,T;W_0^{1,1+\tau}(\Omega)^d)$ and of a subsequence (b_{n_j}) such that (b_{n_j}) converges weakly to b in $L^2(0,T;W_0^{1,1+\tau}(\Omega)^d)$.

The weak lower semi-continuity of the regularization term of (4.4) is clear from Corollary 4.1. The weak lower semi-continuity of the data term of (4.4) we argue in the following:

Since b belongs to $L^2(0,T;W_0^{1,1+\tau}(\mathbb{R}^d)^d)$ with $\mathrm{div} b = 0$, and u_0 belongs to $L^\infty(\mathbb{R}^d)$, according to Theorem 4.3 there exists a unique (renormalized) solution $u \in C([0,T];L^\infty(\mathbb{R}^d))$. Let ρ_ε be a convolution kernel on $\mathbb{R}^d$ and η_ε be a convolution kernel on $\mathbb{R}^{d+1}$. We define $u_0^\varepsilon = u_0 * \rho_\varepsilon$, $b_{n_j}^\varepsilon = b_{n_j} * \eta_\varepsilon$ and $u_{n_j}^\varepsilon$ is the unique solution to

$$\begin{cases} \partial_t u(t,x) + b_{n_j}^\varepsilon(t,x) \cdot \nabla_x u(t,x) = 0 \quad \text{in } (0,T] \times \mathbb{R}^d, \\ u(0,x) = u_0^\varepsilon(x) \quad \text{in } \mathbb{R}^d. \end{cases} \tag{4.16}$$

Due to the fact that $u_{n_j}^\varepsilon$ is smooth and supported in a bounded domain, and according to Lemma 4.1 we deduce that for every $t \in [0,T]$

$$\begin{aligned} \left\| u_{n_j}^\varepsilon(t,\cdot) \right\|_{L^2(\mathbb{R}^d)} &\le \left\| u_{n_j}^\varepsilon(t,\cdot) \right\|_{L^\infty(\mathbb{R}^d)} \\ &\le \| u_0^\varepsilon \|_{L^\infty(\mathbb{R}^d)} \\ &= \operatorname*{esssup}_{x \in \mathbb{R}^d} \int_{\mathbb{R}^d} u_0(x-y) \rho_\varepsilon(y)\, dy \\ &\le \operatorname*{esssup}_{x \in \mathbb{R}^d} \operatorname*{esssup}_{y \in \mathbb{R}^d} |u_0(x-y)| \int_{\mathbb{R}^d} \rho_\varepsilon\, dy \\ &\le \| u_0 \|_{L^\infty(\mathbb{R}^d)}. \end{aligned}$$

Let ε converge to 0 and it follows that (u_{n_j}) is uniformly bounded in $L^\infty(0,T;L^2(\mathbb{R}^d))$. By Theorem 4.4 it is clear that (u_{n_j}) converges to u in $C([0,T];L^2_{\mathrm{loc}}(\mathbb{R}^d))$, and then we derive the statement. □

4.5 First-order Optimality Conditions System

The Lagrange multiplier equation of (4.4) restricted to (4.6) and (4.5) is given by

$$\begin{aligned} L(u,b,p,q) = \frac{1}{2}\left\|u(T)-u_T\right\|^2_{L^2(\Omega)} + \lambda \int_0^T \int_\Omega \sqrt{|\nabla b|^2+\varepsilon}\, dxdt \\ + \int_0^T \int_\Omega \left(\partial_t u + b\cdot\nabla u\right) p\, dxdt + \int_0^T \int_\Omega q \mathrm{div} b\, dxdt, \end{aligned} \tag{4.17}$$

where p is the adjoint state of u and q is the adjoint state of b. We denote

$$|\nabla b|_\varepsilon = \sqrt{|\nabla b|^2+\varepsilon}$$

in the following context. We derive the necessary optimality conditions system by setting the functional derivatives of (4.17) in u, b, p, q equal to 0, and then we have

$$\begin{cases} u_t + b\cdot\nabla u = 0 \quad \text{in } (0,T]\times\Omega, \;\; u(0)=u_0 \quad \text{in } \Omega, \\ p_t + b\cdot\nabla p = 0 \quad \text{in } [0,T)\times\Omega, \;\; p(T) = -(u(T)-u_T) \quad \text{in } \Omega, \\ \mathrm{div} b = 0 \quad \text{in } [0,T]\times\Omega, \\ \lambda\nabla\cdot\left(\dfrac{\nabla b}{|\nabla b|_\varepsilon}\right) + \nabla q = p\nabla u \quad \text{in } [0,T]\times\Omega, \end{cases}, \;\; b=0 \quad \text{on } \partial\Omega. \tag{4.18}$$

4.6 Numerical Aspects

4.6.1 Numerical Schemes

Numerically, the challenged part is how to discretize the TV_ε-Stokes equations [54] in (4.18) effectively. We apply the time marching scheme, also called method of gradient-descent, introduced in [54, 46] and it requires to solve the following

unsteady-state equation with a long evolution time:

$$\begin{cases} \partial_t b - \nabla \cdot \left(\dfrac{\nabla b}{|\nabla b|_\varepsilon} \right) - \dfrac{1}{\lambda} \nabla q = -\dfrac{1}{\lambda} p \nabla u \quad \text{in } (0,\infty) \times \Omega, \\ b = 0 \quad \text{on } \partial\Omega, \\ b(0,\cdot) = 0 \quad \text{in } \Omega, \\ \partial_t q - \text{div} b = 0 \quad \text{in } (0,\infty) \times \Omega. \end{cases} \tag{4.19}$$

where $|\nabla b|_\varepsilon = \sqrt{|v_x|^2 + |v_y|^2 + |w_x|^2 + |w_y|^2 + \varepsilon}$. Actually, the TV_ε-Stokes equations of (4.18) is the steady state of (4.19). The algorithm uses the following iterative procedure to update b and q on active iterative $n+1$ with given $p^n, \nabla u^n$ and time step Δt:

$$\begin{aligned} b^{n+1} &= b^n + \Delta t \left(\nabla \cdot \left(\frac{\nabla b^n}{|\nabla b^n|_\varepsilon} \right) + \frac{1}{\lambda} \nabla q^n - \frac{1}{\lambda} p^n \nabla u^n \right), \\ q^{n+1} &= q^n + \Delta t \nabla \cdot b^n. \end{aligned} \tag{4.20}$$

In [56] is shown that the explicit (forward Euler) time marching scheme is conditionally stable, i.e. the time step Δt should be selected in a manner which gives sufficient decrease in the functional (4.4). However, the forward scheme has rather undesirable asymptotic convergence properties which may make it very inefficient. Vogel and Oman introduced the lagged diffusivity fixed point iteration, denoted by FP-iteration, in [56]. The FP-iteration linearizes the nonlinear diffusion part in (4.20) on iteration $n+1$, i.e. we apply the diffusion operator

$$DF(b^n)v := \nabla \cdot \left(\frac{\nabla v}{|\nabla b^n|_\varepsilon} \right)$$

on the active iteration $n+1$. Hence, we can formulate it into an implicit scheme

$$\left(1 - \Delta t DF(b^n)\right) b^{n+1} = z,$$

where z denotes the rest terms not involving b^{n+1}. It is shown in [18] that this algorithm is very robust and globally linearly convergent. The details of the scheme concerning v read as follows, and similarly we can also derive the scheme concerning

w.

$$\begin{aligned}\partial_x\left(\frac{v_x^{n+1}}{|\nabla b^n|_\varepsilon}\right) &= \partial_x\left(|\nabla b^n|_\varepsilon^{-1}\right) v_x^{n+1} + \frac{v_{xx}^{n+1}}{|\nabla b^n|_\varepsilon} \\ &= -|\nabla b^n|_\varepsilon^{-3}\left(v_x^n v_{xx}^n + v_y^n v_{xy}^n + w_x^n w_{xx}^n + w_y^n w_{xy}^n\right) v_x^{n+1} + \frac{v_{xx}^{n+1}}{|\nabla b^n|_\varepsilon},\end{aligned}$$

$$\begin{aligned}\partial_y\left(\frac{v_y^{n+1}}{|\nabla b^n|_\varepsilon}\right) &= \partial_y\left(|\nabla b^n|_\varepsilon^{-1}\right) v_y^{n+1} + \frac{v_{yy}^{n+1}}{|\nabla b^n|_\varepsilon} \\ &= -|\nabla b^n|_\varepsilon^{-3}\left(v_x^n v_{xy}^n + v_y^n v_{yy}^n + w_x^n w_{xy}^n + w_y^n w_{yy}^n\right) v_y^{n+1} + \frac{v_{yy}^{n+1}}{|\nabla b^n|_\varepsilon}.\end{aligned}$$

Altogether the implicit scheme of (4.20) in v yields

$$\begin{aligned}&v^{n+1} + \Delta t\,|\nabla b^n|_\varepsilon^{-3}\left(v_x^n v_{xx}^n + v_y^n v_{xy}^n + w_x^n w_{xx}^n + w_y^n w_{xy}^n\right) v_x^{n+1} - \Delta t\frac{v_{xx}^{n+1}}{|\nabla b^n|_\varepsilon} \\ &\quad + \Delta t\,|\nabla b^n|_\varepsilon^{-3}\left(v_x^n v_{xy}^n + v_y^n v_{yy}^n + w_x^n w_{xy}^n + w_y^n w_{yy}^n\right) v_y^{n+1} - \Delta t\frac{v_{yy}^{n+1}}{|\nabla b^n|_\varepsilon} \\ &= v^n + \frac{\Delta t}{\lambda} q_x^n - \frac{\Delta t}{\lambda} p u_x.\end{aligned}$$

4.6.2 Image Denoising

In the first experiment we use the imposed FP-iteration for discretizing the nonlinear diffusion operator to denoise an image. Given a noised image $z(x) = u_0(x) + \sigma(x)$, where u_0 denotes the uncontaminated image and σ denotes some additive noise, we reconstruct u by minimizing the following functional

$$E(u) = \frac{\lambda}{2}\|u - z\|_{L^2(\Omega)}^2 + \int_\Omega |\nabla u|_\varepsilon \, dx.$$

The necessary optimality condition is

$$\lambda\,(u - z) - \nabla \cdot \left(\frac{\nabla u}{|\nabla u|_\varepsilon}\right) = 0. \tag{4.21}$$

To solve (4.21) we also time-march the equation as we handled the TV_ε-Stokes equations in (4.18), namely

$$\begin{cases} \partial_t u = \nabla \cdot \left(\dfrac{\nabla u}{|\nabla u|_\varepsilon} \right) - \lambda (u - z) \quad \text{in } (0, \infty) \times \Omega, \\ u(0, x) = z(x) \quad \text{in } \Omega, \\ u_n(t, x) = 0 \quad \text{on } \partial\Omega. \end{cases} \tag{4.22}$$

If the diffusion process lasts long enough, then the noise will be removed and the edges will be preserved by the property of TV_ε minimization. In practice, we choose a monotonously decreasing sequence (ε_n) for iterations of the discrete system of (4.22), since a large ε results in a fast convergence of the system but blurred edges of the image, and a small ε results in a slow convergence of the system but preserving the edges better. Thus, such a choice of (ε_n) is a good tradeoff between efficiency and accuracy.

In Figure 4.1 we iterate the system 50 times, choose (ε_n) to be an equiv-distant sequence from 1 to 0.01 and select $\Delta t = 5, \lambda = 10^{-3.5}$. Because the FP-iteration is unconditionally stable, we can select a large time step and a small iteration number such that the whole computational cost keeps low.

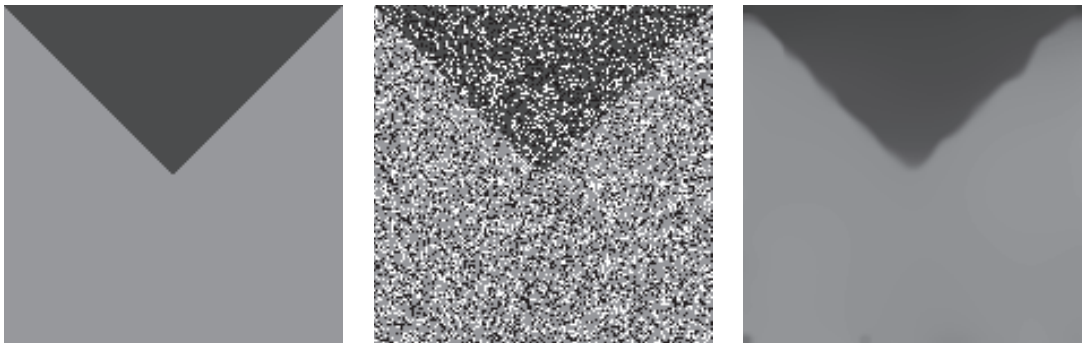

(a) (b) (c)

Figure 4.1: (a) The uncontaminated image. (b) The image is perturbed by the "salt and pepper" noise with density 0.4. (c) The denoised image by (4.22).

4.6.3 Experiments

Let us denote the interpolation method (3.23) with segregation loop II by the smooth method. Actually, the smooth method works better than the TV_ε method in the smooth regions in which the displacement is not small. Because the image gradient of this regions is small, the smooth diffusion has a fill-in effect such that the motion of this regions can be recognized. To combine the advantage of both methods we make a smooth diffusion at the coarsest level and step by step shorten the diffusion time to get better interpolation of the non-smooth regions.

	T	$T/2$	$T/2$ merging
smooth	5.17	4.01	3.63
TV_ε	3.96	3.69	3.50

Table 4.1: IE of the interpolation at time T, $T/2$ and merging the forward & backward interpolation at time $T/2$ by the smooth method and the TV_ε method applied on dataset Venus.

To demonstrate the difference between the smooth method and the TV_ε method we apply them on dataset Venus, see Figure 4.2. Viewing Figure 4.5 it is obvious that the TV_ε method keeps the flow edges better than the smooth method. Consequently, the shape of objects is preserved better in the case that the objects are moving faster or slower than the background, see Figure 4.4. In Table 4.1 we observe that the smooth method works more inconsistent than the TV_ε method if the interpolation time is larger. In contrast, the TV_ε method works more accurately and more robustly over the time. In Table 4.2 and 4.3 we list the parameter setting of both methods in this experiment. It is worth mentioning that the TV_ε method does not require too many iterations on each level, since the long to short diffusion time strategy from the coarse level to fine level is able to detect the optical flow both in smooth regions and non-smooth regions, effectively.

We also demonstrate the merging at time $T/2$. It means that we merge the forward interpolation that the interpolation starts from u_0 to $u(T/2)$, and the backward interpolation that the interpolation starts from u_T to $u(T/2)$. From the results of Table 4.1 we find out that the forward and backward interpolation are somehow compatible. This phenomenon we will explain in next chapter and it shall arouse

	λ	N_{loop}
L3	$10^{5.3}$	100
L2	$10^{5.5}$	100
L1	$10^{5.8}$	100
L0	$10^{6.7}$	10

Table 4.2: Parameters of the smooth method.

	λ	N_{loop}	Δt	ε
L3	$10^{4.8}$	20	10^{3}	1
L2	$10^{4.4}$	20	10^{2}	1
L1	$10^{4.4}$	20	10^{1}	1
L0	$10^{4.2}$	20	10^{0}	1

Table 4.3: Parameters of the TV_ε method.

us a new idea to improve the modeling.

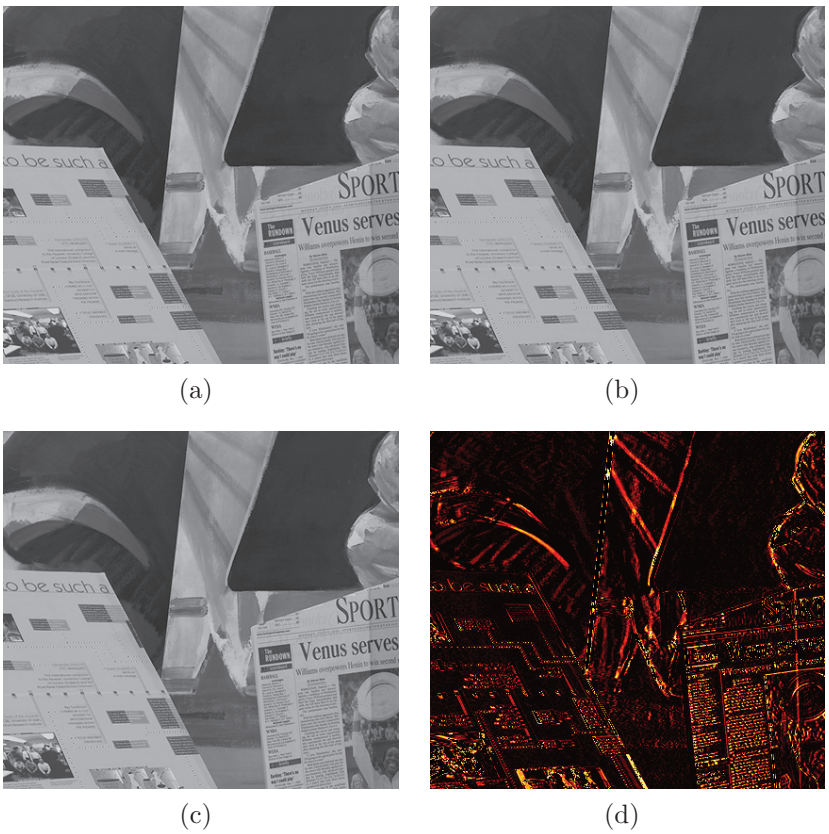

(a) (b)

(c) (d)

Figure 4.2: (a) u_0 (b) u_T (c) The ground-truth interpolation $u_{T/2}$ at time $T/2$. (d) The absolute difference between u_0 and u_T.

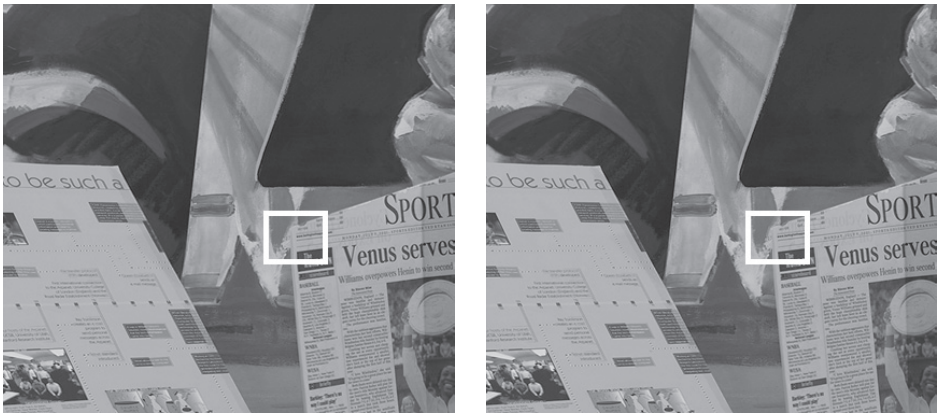

(a) (b)

Figure 4.3: (a) $u(T/2)$ interpolated by the smooth method. (b) $u(T/2)$ interpolated by the TV_ε method.

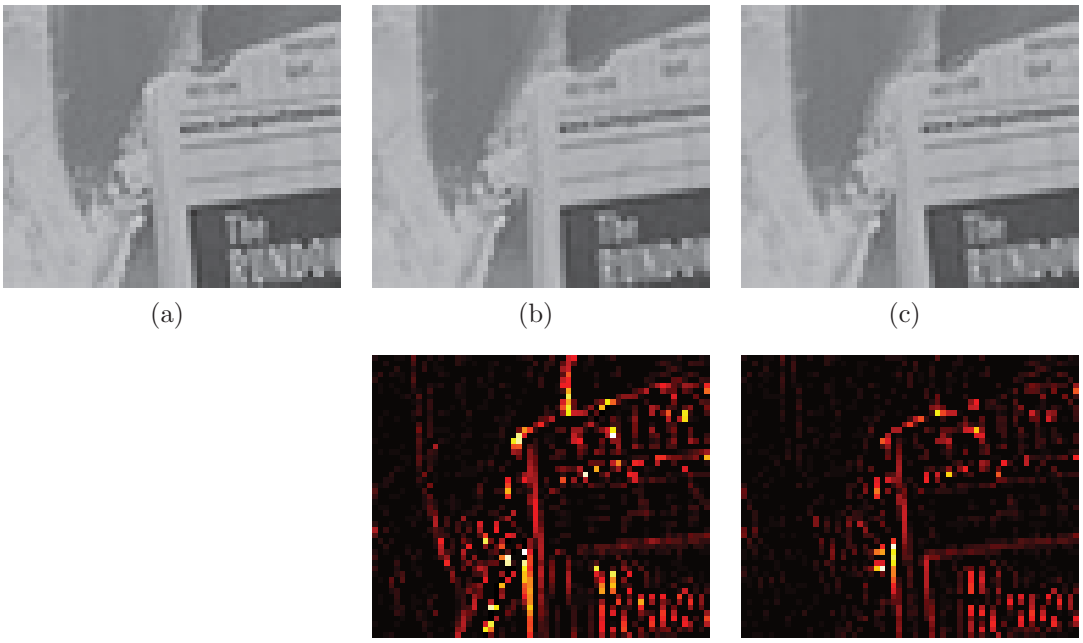

(a) (b) (c)

(d) (e)

Figure 4.4: (a) The zoomed-in region of ground-truth. (b) The zoomed-in region of (a) of Figure 4.3. (c) The zoomed-in region of (b) of Figure 4.3. (d) The absolute difference between (a) and (b). (e) The absolute difference between (a) and (c).

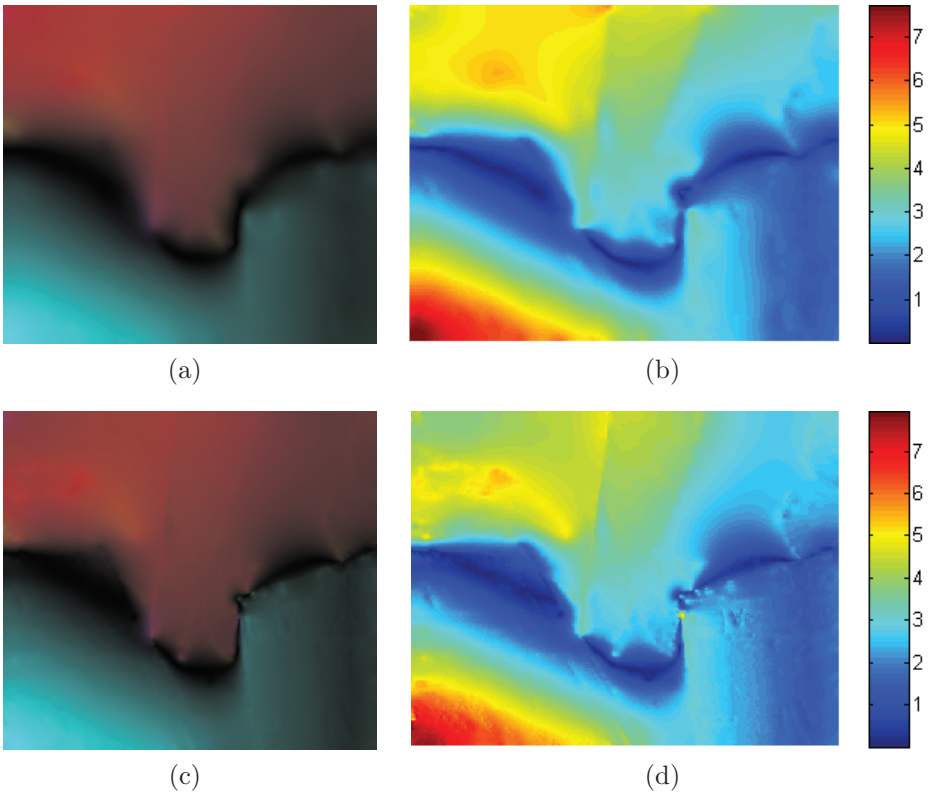

Figure 4.5: (a) The optical flow calculated by the smooth method. (b) The intensity of the optical flow calculated by the smooth method. (c) The optical flow calculated by the TV_ε method. (d) The intensity of the optical flow calculated by the TV_ε method.

Chapter 5

TV_ε-Flow and Segmentation based Optimal Control

5.1 Problem Statement

So far we used the forward interpolation in the smooth method and TV_ε method, i.e. interpolation from time 0 to T. According to the introduced algorithms, we generate the intermediate images by taking pixels only from u_0 in the forward interpolation process. Obviously, it is not nature since the new disclosed objects in the evolution process are unknown with respect to u_0 at time $t > 0$. We illustrate this phenomenon more clearly in Figure 5.1. In the zoomed-in regions we can observe that the disclosed black regions in the middle and upper right of subfigure (d) are new with respect to subfigure (c).

Attentively, we find out that from subfigure (d) to subfigure (c) the black regions in the middle and upper right of subfigure (d) are getting covered, not disclosed any more. More precisely speaking, the backward interpolation is suitable for the disclosed regions and the forward interpolation is suitable for the covered regions. From this point of view some segmentation tool is desired to segment the domain into disclosed parts and covered parts.

(a) (b) (c) (d)

Figure 5.1: (a) u_0. (b) u_T. (c) The zoomed-in region of (a). (d) The zoomed-in region of (b).

5.2 Introduction of Active Contours for Segmentation

The classical active contours models or snakes [16, 38] are widely used in image segmentation. However, in these models an edge detector related to the image gradient is required to stop the evolving curve on the boundaries of objects. In [20] Chan and Vese introduced a model based on active contours and the Mumford-Shah segmentation model [43], which does not require an edge detector. Consequently, this model is able to detect contours with or without gradient, i.e. objects with discontinuous boundaries or even with very smooth boundaries. We give here a brief overview of the model of active contours without edges.

Let us define a curve C as the boundary of an open subset ω of a bounded domain $\Omega \subset \mathbb{R}^2$. Now we consider the following fitting term

$$F_1(C) + F_2(C) = \int_{\omega} (u - c_1)^2 \, dx + \int_{\Omega \setminus \overline{\omega}} (u - c_2)^2 \, dx,$$

where $u : \Omega \to \mathbb{R}$, C segments the domain into ω and $\Omega \setminus \overline{\omega}$, and the constants c_1, c_2 depending on C, are the average of u inside C and outside of C, respectively. In this case, the boundary C_0 of the object minimizes the fitting term

$$\inf_C \left(F_1(C) + F_2(C)\right) \approx 0 \approx F_1(C_0) + F_2(C_0).$$

In the active contours model [20] some regularizing terms are appended to the fitting term, namely the length of C and the area of the region ω segmented by C.

Therefore,

$$F(c_1, c_2, C) = \mu|C| + \nu|\omega| + \lambda_1 \int\limits_{\omega} |u - c_1|^2 \, dx + \lambda_2 \int\limits_{\Omega\setminus\overline{\omega}} |u - c_2|^2 \, dx, \tag{5.1}$$

where $\mu \geq 0, \nu \geq 0, \lambda_1, \lambda_2 > 0$ are the regularization parameters. To minimize (5.1) one can reformulate it by means of the level set formulation. Suppose that C is represented by the zero level set of a Lipschitz function $\phi : \Omega \to \mathbb{R}$, such that

$$\begin{cases} C = \partial\omega = \{x \in \Omega \mid \ \phi(x) = 0\}, \\ \omega = \{x \in \Omega \mid \ \phi(x) > 0\}, \\ \Omega \setminus \overline{\omega} = \{x \in \Omega \mid \ \phi(x) < 0\}. \end{cases}$$

Recall that the Heaviside function H and one-dimensional Dirac measure δ_0 are defined as

$$H(z) = \begin{cases} 1 & \text{if } z \geq 0 \\ 0 & \text{if } z < 0 \end{cases}, \ \ \delta_0(z) = \frac{d}{dz} H(z). \tag{5.2}$$

Then, we reformulate the terms of (5.1) by means of (5.2):

$$\begin{aligned} |C| &= \int\limits_{\Omega} |\nabla H(\phi(x))| \, dx \\ &= \int\limits_{\Omega} \delta_0(\phi(x)) \, |\nabla\phi(x)| \, dx, \\ |\omega| &= \int\limits_{\Omega} H(\phi(x)) \, dx, \\ \int\limits_{\omega} |u - c_1|^2 \, dx &= \int\limits_{\Omega} |u - c_1|^2 \, H(\phi(x)) \, dx, \\ \int\limits_{\Omega\setminus\overline{\omega}} |u - c_2|^2 \, dx &= \int\limits_{\Omega} |u - c_2|^2 \, (1 - H(\phi(x))) \, dx. \end{aligned}$$

With this notation the cost functional (5.1) becomes

$$F(c_1,c_2,\phi) = \mu \int_\Omega \delta_0\left(\phi(x)\right)\left|\nabla\phi(x)\right| dx + \nu \int_\Omega H\left(\phi(x)\right) dx + \lambda_1 \int_\Omega \left|u-c_1\right|^2 H\left(\phi(x)\right) dx + \lambda_2 \int_\Omega \left|u-c_2\right|^2 \left(1-H\left(\phi(x)\right)\right) dx. \tag{5.3}$$

Keeping ϕ fixed and minimizing the energy $F(c_1,c_2,\phi)$ with respect to c_1 and c_2, it is easy to express the constant functions by

$$c_1(\phi) = \frac{\int_\Omega u(x) H\left(\phi(x)\right) dx}{\int_\Omega H\left(\phi(x)\right) dx}, \tag{5.4}$$

if $\int_\Omega H\left(\phi(x)\right) dx > 0$, i.e. the curve C has a nonempty interior in Ω and

$$c_2(\phi) = \frac{\int_\Omega u(x)\left(1-H\left(\phi(x)\right)\right) dx}{\int_\Omega \left(1-H\left(\phi(x)\right)\right) dx}, \tag{5.5}$$

if $\int_\Omega \left(1-H\left(\phi(x)\right)\right) dx > 0$, i.e. the curve C has a nonempty exterior in Ω. For the corresponding degenerate cases, namely $|\omega| = 0$ or $|\Omega \setminus \overline{\omega}| = 0$, there are no constraints on c_1 or c_2 respectively. Then, c_1 and c_2 are in fact given by

$$\begin{cases} c_1(\phi) = \text{mean}(u) \text{ in } \left\{x \in \Omega \mid \ \phi(x) \geq 0\right\}, \\ c_2(\phi) = \text{mean}(u) \text{ in } \left\{x \in \Omega \mid \ \phi(x) < 0\right\}. \end{cases}$$

In order to compute the associated Euler-Lagrange equation with respect to ϕ, we choose the smooth approximation H_s and δ_s, which converge to H and δ as $s \to 0$. Assume that H_s enjoys the $C^2(\overline{\Omega})$ regularity and $\delta_s = H_s'$. We denote by F_s the smooth version of (5.3) given by

$$F_s(c_1,c_2,\phi) = \mu \int_\Omega \delta_s\left(\phi(x)\right)\left|\nabla\phi(x)\right| dx + \nu \int_\Omega H_s\left(\phi(x)\right) dx + \lambda_1 \int_\Omega \left|u-c_1\right|^2 H_s\left(\phi(x)\right) dx + \lambda_2 \int_\Omega \left|u-c_2\right|^2 \left(1-H_s\left(\phi(x)\right)\right) dx.$$

Minimize F_s with respect to ϕ and we deduce the associated Euler-Lagrange equa-

tion for ϕ and parameterize the descent direction by an artificial time $t \geq 0$, the equation in $\phi(t, x)$ with the initial contour $\phi(0, x) = \phi_0(x)$ is given by

$$\begin{cases} \dfrac{\partial \phi}{\partial t} = \delta_s(\phi) \left(\mu \mathrm{div} \left(\dfrac{\nabla \phi}{|\nabla \phi|} \right) - \nu - \lambda_1 (u - c_1)^2 + \lambda_2 (u - c_2)^2 \right) \text{ in } (0, \infty) \times \Omega, \\ \phi(0) = \phi_0 \text{ in } \Omega, \\ \dfrac{\delta_s(\phi)}{|\nabla \phi|} \dfrac{\partial \phi}{\partial n} = 0 \text{ on } \partial\Omega. \end{cases} \tag{5.6}$$

5.2.1 Algorithm

We introduce the smooth regularization of H

$$H_s(z) = \frac{1}{2} \left(1 + \frac{2}{\pi} \arctan \left(\frac{z}{s} \right) \right), \tag{5.7}$$

and its derivative

$$\delta_s(z) = \frac{1}{s\pi} \cos^2 \left(\arctan \left(\frac{z}{s} \right) \right). \tag{5.8}$$

The graphs of H_s and δ_s are illustrated in Figure 5.2.

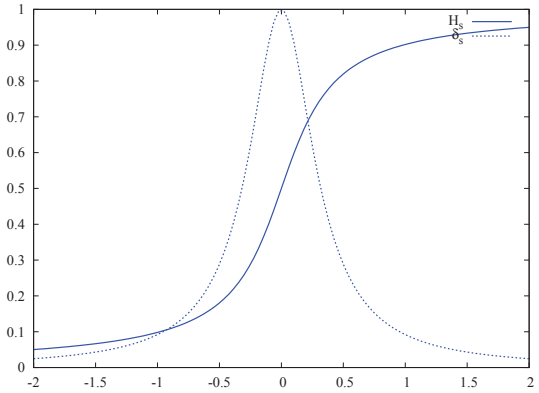

Figure 5.2: The graphs of the Heaviside function and its derivative with $s = 1/\pi$.

In the discretization of (5.6) we use the Neumann boundary condition of ϕ, since it is a sufficient boundary condition of (5.6). The rest we follow the FP-iteration

introduced in Chapter 4, and we list the algorithm of the active contours without edges. Assume that N is the number of iterations and the procedure is

1. Initialize ϕ^0 by ϕ_0 as $n = 0$.

2. Compute $c_1(\phi^n)$ and $c_2(\phi^n)$ by (5.4) and (5.5).

3. Solve (5.6) and obtain ϕ^{n+1}.

4. If $n < N$, then go back to 2.

We gain the binary segmentation by modification of c_1 and c_2 for an $x \in \Omega$:

$$\begin{cases} c_1(x) = 0 & \text{if } \phi(x) \geq 0, \\ c_2(x) = 1 & \text{if } \phi(x) < 0. \end{cases}$$

In Figure 5.3 we demonstrate the binary segmentation on dataset Eagle[1]. We set $\phi_0(x) = -100$ on the boundary of the image and $\phi_0(x) = 100$ otherwise. It is worth mentioning that we gain a reasonable segmentation of the corners while the edges of the image near the corners are not clear.

(a) (b)

Figure 5.3: $\mu = 10, \nu = 10, \lambda_1 = \lambda_2 = 100$. (a) The original image. (b) The binary segmented image.

[1] http://www.eecs.berkeley.edu/Research/Projects/CS/vision/grouping/segbench/BSDS300/html/dataset/images.html

5.3 Modeling

Based on the phenomenon demonstrated in Section 5.1 we may divide the domain into the covered domain and the disclosed domain. The covered domain refers to the regions in which the characteristics of two different pixels starting at time 0 end up at time T in a same place. Obviously, the covered domain is suitable for the forward interpolation from 0 to T. In contrast, the disclosed domain refers to the regions in which no characteristic of a pixel starting at time 0 ends up at time T. Since our interpolation method under the framework of optimal control produces a continuous optical flow, the disclosed domain will be filled-in with the neighboring optical flow. The filling-in process in the forward interpolation normally "guesses" wrong what actually happens in the disclosed domain. To overcome this drawback we apply a backward interpolation from T to 0 in the disclosed domain, i.e. the disclosed domain is turned to the covered domain in this case. In Figure 5.1 the backward interpolation is supposed to be occurred to detect the disclosed black color in the middle and upper right of the zoomed-in regions in the subfigures.

Combining the introduced active contours without edges and the TV_ε method, we achieve this locally selecting process of the regions for the forward or backward interpolation. Let us model the image sequence interpolation using the ε-smooth total variation of optical flow and active contours in the framework of optimal control. We assume that

$$u_0, u_T \in L^\infty(\Omega), \tag{5.9}$$

$$b \in L^2(0,T; W_0^{1,1+\tau}(\Omega)^d), \tag{5.10}$$

with a sufficient small τ, i.e. $\tau > 0$ satisfies for an $f \in W_0^{1,1+\tau}(\Omega)$ and a given $\varepsilon > 0$

$$|\Omega|^{\frac{\tau}{1+\tau}} \|\nabla f\|_{L^{1+\tau}(\Omega)^d} \leq \int_\Omega \sqrt{|\nabla f|^2 + \varepsilon}\, dx, \tag{5.11}$$

where the constant $|\Omega|^{\frac{\tau}{1+\tau}}$ is the norm of the embedding operator from $L^{1+\tau}(\Omega)$ to $L^1(\Omega)$, and the evolving curve C in Ω is defined as the boundary of an open subset ω of Ω. The cost functional is defined as

$$J(b, C, \omega) = \frac{1}{2} \|\hat{u}(T) - u_T\|^2_{L^2(\omega)} + \frac{1}{2} \|\tilde{u}(0) - u_0\|^2_{L^2(\Omega\setminus\overline{\omega})} + \lambda \int_0^T \int_\Omega \sqrt{|\nabla b|^2 + \varepsilon}\, dxdt$$

$$+ \mu |C| + \nu |\omega| \tag{5.12}$$

restricted to the forward transport equation

$$\begin{cases} \hat{u}_t + b \cdot \nabla_x \hat{u} = 0 \quad \text{in } (0,T] \times \Omega, \\ \hat{u}(0) = u_0 \quad \text{in } \Omega, \end{cases} \tag{5.13}$$

the backward transport equation

$$\begin{cases} \tilde{u}_t + b \cdot \nabla_x \tilde{u} = 0 \quad \text{in } [0,T) \times \Omega, \\ \tilde{u}(T) = u_T \quad \text{in } \Omega, \end{cases} \tag{5.14}$$

and the divergence-free equation

$$\text{div} b = 0 \quad \text{in } [0,T] \times \Omega. \tag{5.15}$$

The desired interpolation u at time t is estimated by

$$u(t,x) = \begin{cases} \hat{u}(t,x) & \text{if } x \in \omega, \\ \tilde{u}(t,x) & \text{if } x \in \Omega \setminus \overline{\omega}. \end{cases}$$

5.4 Existence of a Minimizer

We investigate the existence of a minimizer of minimizing (5.12) restricted to (5.13) − (5.15). First of all, we formulate (5.12) in terms of the characteristic function χ_ω of the set ω by the fact $\chi_\omega = H(\phi)$:

$$\begin{aligned} J(b, \chi_\omega) = \frac{1}{2} \int_\Omega |\hat{u}(T) - u_T|^2 \chi_\omega \, dx + \frac{1}{2} \int_\Omega |\tilde{u}(0) - u|^2 (1 - \chi_\omega) \, dx \\ + \lambda \int_0^T \int_\Omega \sqrt{|\nabla b|^2 + \varepsilon} \, dx dt + \mu \int_\Omega |D\chi_\omega| + \nu \int_\Omega \chi_\omega \, dx. \end{aligned} \tag{5.16}$$

Besides b we also search for a characteristic function of ω with finite perimeter in Ω (see Chapter 2), i.e. χ_ω has bounded variation. Assume in the following contexts that $d = 2$ and $\partial\Omega$ is Lipschitz.

Theorem 5.1 (Existence of a minimizer)**.** *Suppose* $\chi_\omega \in BV(\Omega)$*, then minimizing* (5.16) *restricted to* (5.13) – (5.15) *has a minimizer under* (5.9) – (5.11)*.*

Proof. We define a minimizing sequence (b_n, χ_{ω_n}) belonging to $L^2(0,T;W_0^{1,1+\tau}(\Omega)^2)$ and $BV(\Omega)$. The coercivity of (5.16) is obvious due to (5.10), (5.11) and the BV norm of χ_ω in the functional. From the coercivity we gain a minimizing subsequence $\left(b_{n_k}, \chi_{\omega_{n_k}}\right)$, which converges to (b, χ_ω) in the weak topology of $L^2(0,T;W_0^{1,1+\tau}(\Omega)^2)$ and the $BV - w^*$ topology respectively. The $BV - w^*$ convergence yields the L^1-convergence of $(\chi_{\omega_{n_k}})$, and hence if χ_ω is not a characteristic function, then this contradicts the fact of the L^1-convergence of $(\chi_{\omega_{n_k}})$.

The weak lower semi-continuity of last two terms of (5.16) is clear in the $BV - w^*$ topology. In Chapter 4 it is shown that the term of b is weakly lower semi-continuous. The rest is to show the weak lower semi-continuity of the first two terms in (5.16). The proof of both terms are similar, so we verify the first one:

$$
\begin{aligned}
&\int_\Omega |\hat{u}(T) - u_T|^2 \chi_\omega \, dx - \int_\Omega |\hat{u}(T) - u_T|^2 \chi_{\omega_{n_k}} \, dx \\
&\quad + \int_\Omega |\hat{u}(T) - u_T|^2 \chi_{\omega_{n_k}} \, dx - \int_\Omega |\hat{u}_{n_k}(T) - u_T|^2 \chi_{\omega_{n_k}} \, dx \\
&\leq \int_\Omega |\hat{u}(T) - u_T|^2 |\chi_{\omega_{n_k}} - \chi_\omega| \, dx + \int_\Omega \left| |\hat{u}_{n_k}(T) - u_T|^2 - |\hat{u}(T) - u_T|^2 \right| \chi_{\omega_{n_k}} \, dx \\
&\leq \|\hat{u}(T) - u_T\|^2_{L^\infty(\Omega)} \int_\Omega |\chi_{\omega_{n_k}} - \chi_\omega| \, dx \\
&\quad + \int_\Omega |\hat{u}_{n_k}(T) + \hat{u}(T) - 2u_T| \, |\hat{u}_{n_k}(T) - \hat{u}(T)| \, dx \\
&\leq \|\hat{u}(T) - u_T\|^2_{L^\infty(\Omega)} \left\| \chi_{\omega_{n_k}} - \chi_\omega \right\|_{L^1(\Omega)} \\
&\quad + \|\hat{u}_{n_k}(T) + \hat{u}(T) - 2u_T\|_{L^2(\Omega)} \, \|\hat{u}_{n_k}(T) - \hat{u}(T)\|_{L^2(\Omega)} \, .
\end{aligned}
$$

The second summand of the right-hand side of last inequality converges to zero, since $(\hat{u}_{n_k}(T))$ converges to $\hat{u}(T)$ in $L^2(\Omega)$ because of the stability of the solution to the transport equation clarified in Chapter 4. The first summand converges to zero, since in the $BV - w^*$ topology $(\chi_{\omega_{n_k}})$ converges to χ_ω in $L^1(\Omega)$ and u propagates the L^∞-regularity of u for all the time due to the propagation results of transport equations given in Chapter 4. □

5.5 Smooth Minimization Functional

5.5.1 Level Set Formulation

Assume that C is the zero level set of ϕ introduced in Section 5.2. Applying the Heaviside function we can reformulate (5.12) in terms of the level set:

$$J(b,\phi) = \frac{1}{2}\int_\Omega |\hat{u}(T) - u_T|^2 H(\phi)\,dx + \frac{1}{2}\int_\Omega |\tilde{u}(0) - u_0|^2 (1 - H(\phi))\,dx + \lambda \int_0^T \int_\Omega \sqrt{|\nabla b|^2 + \varepsilon}\,dxdt + \mu \int_\Omega \delta(\phi)\,|\nabla\phi|\,dx + \nu \int_\Omega H(\phi)\,dx. \quad (5.17)$$

To make it computationally possible, we replace the Heaviside and its derivative with the smooth version (5.7) and (5.8):

$$J_s(b,\phi) = \frac{1}{2}\int_\Omega |\hat{u}(T) - u_T|^2 H_s(\phi)\,dx + \frac{1}{2}\int_\Omega |\tilde{u}(0) - u_0|^2 (1 - H_s(\phi))\,dx + \lambda \int_0^T \int_\Omega \sqrt{|\nabla b|^2 + \varepsilon}\,dxdt + \mu \int_\Omega \delta_s(\phi)\,|\nabla\phi|\,dx + \nu \int_\Omega H_s(\phi)\,dx. \quad (5.18)$$

5.5.2 Convergence Property of Smooth Minimization Functional

We want to investigate under which assumptions (5.18) converges to (5.17) for every b, ϕ as $s \to 0$. We give the concept of intermediate convergence of BV functions [5]:

Definition 5.1 (Intermediate convergence)**.** *Let (u_n) be a sequence in $BV(\Omega)$ and $u \in BV(\Omega)$. We say that (u_n) converges to u in the sense of the intermediate convergence if and only if*

$$u_n \to u \text{ in } L^1(\Omega),$$
$$\int_\Omega |Du_n| \to \int_\Omega |Du|.$$

In [5] it is proven that the topology induced by the intermediate convergence is finer than the topology induced by the weak* convergence of BV. Thus, from a

in $BV(\Omega)$ bounded sequence (u_n) we only deduce that (Du_n) converges weakly* to Du, but we can not ensure that the total variation of (Du_n) converges to the total variation of Du. To gain this property we assume additionally that $H_s = H * \eta_s$ and the level set function $\phi : \Omega \to K$ is a diffeomorphism, where K is a bounded subset of $\mathbb{R}$. Then, we have

Lemma 5.1. $\int_\Omega |D(H_s \circ \phi)| \longrightarrow \int_\Omega |D(H \circ \phi)|$ *as* $s \to 0$.

Proof. Theorem 2.4 implies that $H_s \to H$ almost everywhere as $s \to 0$. Set $y = \phi(x)$, then for every $\varphi \in C_c^1(\Omega)^d$ with $\|\varphi\|_{L^\infty(\Omega)^d} \leq 1$ gives

$$\begin{aligned}
&\int_\Omega (H * \eta_s) \circ \phi(x) \operatorname{div}\varphi(x)\, dx \\
&= \int_K H * \eta_s(y) \operatorname{div}\varphi(\phi^{-1}(y)) \left|\det\left(\nabla\phi^{-1}(y)\right)\right| dy \\
&\to \int_K H(y) \operatorname{div}\varphi(\phi^{-1}(y)) \left|\det\left(\nabla\phi^{-1}(y)\right)\right| dy \\
&= \int_\Omega (H \circ \phi(x)) \operatorname{div}\varphi(x)\, dx.
\end{aligned}$$

Taking supremum over φ gives the statement. □

Theorem 5.2 (Point-wise convergence)**.** *Under* (5.9) – (5.11) *the functional* (5.18) *converges point-wise to* (5.17)*.*

Proof. Subtracting the functionals point-wise we gain that

$$\begin{aligned}
|L_s(b,\phi) - L(b,\phi)| \leq\ & \frac{1}{2}\int_\Omega |\hat{u}(T) - u_T|^2 \,|H_s(\phi) - H(\phi)|\, dx \\
&+ \frac{1}{2}\int_\Omega |\tilde{u}(0) - u_0|^2 \,|H_s(\phi) - H(\phi)|\, dx \\
&+ \mu \left| \int_\Omega |D\,(H_s \circ \phi)| - \int_\Omega |D\,(H \circ \phi)| \right| \\
&+ \nu \int_\Omega |H_s(\phi) - H(\phi)|\, dx.
\end{aligned} \tag{5.19}$$

Since ϕ is a diffeomorphism, $(H_s \circ \phi)$ is uniformly bounded in $BV(\Omega)$. The approximate properties of mollifiers yield that $(H_s \circ \phi)$ converges to $H \circ \phi$ in $L^1(\Omega)$ (similar to proof of Theorem 3.3). We know that the transport equation propagates the L^∞-regularity for every $t \in [0,T]$. Then, together with Lemma 5.1 it is obvious that the right-hand side of (5.19) converges to 0. □

5.5.3 First-order Optimality Conditions System

The associated Lagrange equation of (5.18) restricted to (5.13) − (5.15) is given by

$$\begin{aligned} L(\hat{u},\tilde{u},b,\phi,\hat{p},\tilde{p},q) = {} & \frac{1}{2}\int_\Omega |\hat{u}(T)-u_T|^2 H_s(\phi)\,dx + \frac{1}{2}\int_\Omega |\tilde{u}(0)-u_0|^2 (1-H_s(\phi))\,dx \\ & + \lambda \int_0^T\int_\Omega \sqrt{|\nabla b|^2+\varepsilon}\,dxdt + \int_0^T\int_\Omega (\hat{u}_t + b\cdot\nabla\hat{u})\,\hat{p}\,dxdt \\ & + \int_0^T\int_\Omega (\tilde{u}_t + b\cdot\nabla\tilde{u})\,\tilde{p}\,dxdt + \int_0^T\int_\Omega q\mathrm{div}b\,dxdt \\ & + \mu\int_\Omega \delta_s(\phi)\,|\nabla\phi|\,dx + \nu\int_\Omega H_s(\phi)\,dx, \end{aligned} \tag{5.20}$$

where $\hat{p},\tilde{p},q$ are the adjoint states of $\hat{u},\tilde{u},b$ respectively.

Compute the functional derivatives of (5.20) according to $\hat{u},\hat{p},\tilde{u},\tilde{p},b,q,\phi$ and set them to 0, then we gain the first-order necessary optimality conditions system and it consists of

1. The forward transport equation and its adjoint equation

$$\begin{cases} \hat{u}_t + b\cdot\nabla\hat{u} = 0 \quad \text{in } (0,T]\times\Omega, \;\; \hat{u}(0) = u_0 \quad \text{in } \Omega, \\ \hat{p}_t + b\cdot\nabla\hat{p} = 0 \quad \text{in } [0,T)\times\Omega, \;\; \hat{p}(T) = -(\hat{u}(T)-u_T)\,H_s(\phi) \quad \text{in } \Omega; \end{cases} \tag{5.21}$$

2. The backward transport equation and its adjoint equation

$$\begin{cases} \tilde{u}_t + b \cdot \nabla \tilde{u} = 0 \quad \text{in } [0,T) \times \Omega, \;\; \tilde{u}(T) = u_T \quad \text{in } \Omega, \\ \tilde{p}_t + b \cdot \nabla \tilde{p} = 0 \quad \text{in } (0,T] \times \Omega, \;\; \tilde{p}(0) = (\tilde{u}(0) - u_0)\,(1 - H_s(\phi)) \quad \text{in } \Omega; \end{cases} \tag{5.22}$$

3. The TV$_\varepsilon$-Stokes equations

$$\begin{cases} \lambda \nabla \cdot \left(\dfrac{\nabla b}{|\nabla b|_\varepsilon} \right) + \nabla q = \hat{p} \nabla \hat{u} + \tilde{p} \nabla \tilde{u} \quad \text{in } [0,T] \times \Omega, \;\; b = 0 \quad \text{on } \partial\Omega, \\ \mathrm{div} b = 0 \quad \text{in } [0,T] \times \Omega; \end{cases} \tag{5.23}$$

4. The equation for segmentation

$$\begin{cases} \delta_s(\phi) \Big(\mu \nabla \cdot \left(\dfrac{\nabla \phi}{|\nabla \phi|} \right) - \nu - \dfrac{1}{2} \left| \hat{u}(T) - u_T \right|^2 + \dfrac{1}{2} \left| \tilde{u}(0) - u_0 \right|^2 \Big) = 0 \quad \text{in } \Omega, \\ \dfrac{\delta_s(\phi)}{|\nabla \phi|} \dfrac{\partial \phi}{\partial n} = 0 \quad \text{on } \partial\Omega. \end{cases} \tag{5.24}$$

5.6 Numerical Aspects

5.6.1 Segregation Loop

To solve the optimality conditions (5.21) – (5.24) at time t numerically, we apply a modified segregation loop similar to segregation loop II introduced in Chapter 3. We suppose $n = 1, \cdots, N_{\text{loop}}$ and N_{loop} is the iteration number. Given $u_0, u_T, b^{n-1}(t), \phi^{n-1}, \lambda, \mu, \nu$, the iteration process on iteration n proceeds as follows:

1. Compute $\hat{u}^{n-1}(t), \nabla \hat{u}^{n-1}(t)$ and $\hat{u}^{n-1}(T)$ using u_0 and $b^{n-1}(t)$.

2. Compute $\hat{p}^{n-1}(t)$ using $\hat{u}^{n-1}(T), u_T$ and $H_s(\phi^{n-1})$.

3. Compute $\tilde{u}^{n-1}(t), \nabla \tilde{u}^{n-1}(t)$ and $\tilde{u}^{n-1}(0)$ using u_T and $b^{n-1}(t)$.

4. Compute $\tilde{p}^{n-1}(t)$ using $\tilde{u}^{n-1}(0), u_0$ and $H_s(\phi^{n-1})$.

5. Compute the solution to the TV$_\varepsilon$-Stokes equations with right-hand side $\hat{p}^{n-1}(t)\nabla\hat{u}^{n-1}(t) + \tilde{p}^{n-1}(t)\nabla\tilde{u}^{n-1}(t)$, and denote it by $\delta b^{n-1}(t)$.

6. Compute solution ϕ^n to (5.24) using $\hat{u}(T), u_T, \tilde{u}(0), u_0$ and ϕ^{n-1} as the initial value of the time-marching scheme.

7. $b^n(t) = b^{n-1}(t) + \delta b^{n-1}(t)$.

Set the initial value b^0 divergence-free, and denote by $\hat{u}^*, \tilde{u}^*, \hat{p}^*, \tilde{p}^*, b^*, q^*, \phi^*$ the limits of particular sequences. In this case $\delta b^* = 0$, and setting the limits into $(5.21) - (5.24)$ we derive

$$\begin{cases} \hat{u}_t^* + b^* \cdot \nabla\hat{u}^* = 0 \quad \text{in } (0,T] \times \Omega, \;\; \hat{u}^*(0) = u_0 \quad \text{in } \Omega, \\ \hat{p}_t^* + b^* \cdot \nabla\hat{p}^* = 0 \quad \text{in } [0,T) \times \Omega, \;\; \hat{p}^*(T) = -\left(\hat{u}^*(T) - u_T\right) H_s(\phi^*) \quad \text{in } \Omega; \end{cases} \tag{5.25}$$

$$\begin{cases} \tilde{u}_t^* + b^* \cdot \nabla\tilde{u}^* = 0 \quad \text{in } [0,T) \times \Omega, \;\; \tilde{u}^*(T) = u_T \quad \text{in } \Omega, \\ \tilde{p}_t^* + b^* \cdot \nabla\tilde{p}^* = 0 \quad \text{in } (0,T] \times \Omega, \;\; \tilde{p}^*(0) = \left(\tilde{u}^*(0) - u_0\right)\left(1 - H_s(\phi^*)\right) \quad \text{in } \Omega; \end{cases} \tag{5.26}$$

$$\begin{cases} \nabla q^* = \hat{p}^*\nabla\hat{u}^* + \tilde{p}^*\nabla\tilde{u}^* \quad \text{in } [0,T] \times \Omega, \\ \mathrm{div} b^* = 0 \quad \text{in } [0,T] \times \Omega, \;\; b^* = 0 \quad \text{on } \partial\Omega; \end{cases} \tag{5.27}$$

$$\begin{cases} \delta_s(\phi^*)\Big(\mu\nabla\cdot\left(\dfrac{\nabla\phi^*}{|\nabla\phi^*|}\right) - \nu - \dfrac{1}{2}\left|\hat{u}^*(T) - u_T\right|^2 + \dfrac{1}{2}\left|\tilde{u}^*(0) - u_0\right|^2\Big) = 0 \quad \text{in } \Omega, \\ \dfrac{\delta_s(\phi^*)}{|\nabla\phi^*|}\dfrac{\partial\phi^*}{\partial n} = 0 \quad \text{on } \partial\Omega. \end{cases} \tag{5.28}$$

Although the segregation loop is different from the original problem, $(5.25) - (5.28)$ is actually the optimality conditions system of another constrained minimization

problem when $s = 0$, namely

$$\inf_{(b^*,\omega)} \frac{1}{2} \|\hat{u}^*(T) - u_T\|^2_{L^2(\omega)} + \frac{1}{2} \|\tilde{u}^*(0) - u_0\|^2_{L^2(\Omega\setminus\overline{\omega})}$$

subject to

$$\begin{cases} \hat{u}^*_t + b^* \cdot \nabla \hat{u}^* = 0 \quad \text{in } (0,T] \times \Omega, \;\; \hat{u}^*(0) = u_0 \quad \text{in } \Omega, \\ \tilde{u}^*_t + b^* \cdot \nabla \tilde{u}^* = 0 \quad \text{in } [0,T) \times \Omega, \;\; \tilde{u}^*(T) = u_T \quad \text{in } \Omega, \\ \text{div} b^* = 0 \quad \text{in } [0,T] \times \Omega, \;\; b^* = 0 \quad \text{on } \partial\Omega. \end{cases}$$

From the point of view of regularization theory, one may see the segregation loop as a kind of a Landweber method for minimizing $\frac{1}{2}\|\hat{u}(T) - u_T\|^2_{L^2(\omega)} + \frac{1}{2}\|\tilde{u}(0) - u_0\|^2_{L^2(\Omega\setminus\overline{\omega})}$, which is inspired by a Tikhonov-functional.

5.6.2 Experiments

First of all, we compare the new introduced method, denoted by the TV_ε-segment method, with the smooth method introduced in Chapter 3. To illustrate the difference we apply them on the dataset Mequon. In Figure 5.4 we can distinguish that the flow field of the TV_ε-segment preserves the flow edges better than the smooth method. Consequently, the interpolation by the TV_ε-segment keeps the boundary of objects (shape) better than the smooth method. Additionally, the associated active contours for segmentation are also shown in Figure 5.4. In Figure 5.5 we present the interpolated image applied on Mequon at time $T/2$ by the smooth method and TV_ε-segment method. In the associated zoomed-in subfigures in Figure 5.6 we can observe that the TV_ε-segment method interpolated the disclosed black regions better than the smooth method. Referring to its zoomed-in contours (see subfigure (c)) we can coordinate the disclosed regions with the black color, which refers to the regions where the backward interpolation occurred.

To evaluate our image sequence interpolation method we design an experiment based on human visual perception. We choose 4 datasets (see Figure 5.7) from `ftp://graphics.tu-bs.de/pub/public/people/lipski/stimuli/` and list 7 methods introduced in [52] and [51] to be compared with. We design the experiment in the follwing way: For each of the scenes we compare all 8 interpolation methods

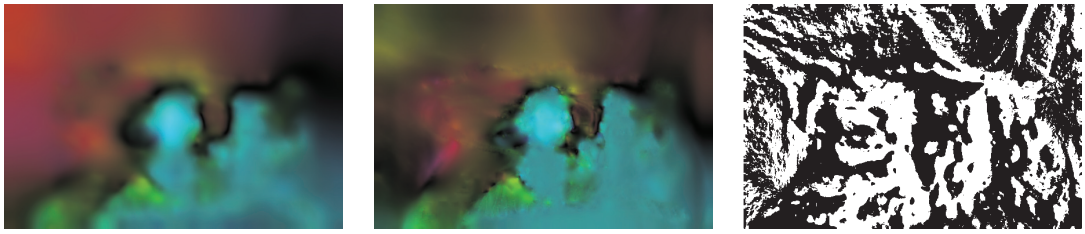

(a) (b) (c)

Figure 5.4: Experiment on Mequon. (a) The optical flow calculated by the smooth method. (b) The optical flow calculated by the TV_ε-segment method. (c) The active contours calculated by the TV_ε-segment method. The black refers to the backward interpolation regions and the white refers to the forward interpolation regions.

(a) (b)

Figure 5.5: Experiment on Mequon. (a) The interpolated frame calculated by the smooth method at time $T/2$. (b) The interpolated frame calculated by the TV_ε-segment method at time $T/2$.

(a) (b) (c)

Figure 5.6: (a) The zoomed-in region of (a) of Figure 5.5. (b) The zoomed-in region of (b) of Figure 5.5. (c) The corresponding zoomed-in region of its contours generated by the TV_ε-segment method.

against each other (only AB, not AA and BA comparisons), yields a total of $4 \cdot (8 \cdot 7/2) = 112$ trials. We denote the number of participants by N and in each trial the perceptually better image sequence gets 1 point. After all trials we divide the score of every algorithm applied on each dataset by $7N$ and all datasets by $35N$ to get the normalized score for every dataset and all datasets. The range of the score is in $[0, 1]$ and the image sequence with the higher score is better for human visual perception.

	Face	Earth	Bunny	Dragon	**average**
original	0.90	0.86	0.88	0.96	**0.90**
blend	0.24	0.14	0.32	0.26	**0.24**
opticalflow	0.01	0.02	0.02	0.02	**0.02**
nofeathering	0.49	0.50	0.35	0.50	**0.46**
nooptim	0.26	0.32	0.39	0.21	**0.29**
full	0.50	0.53	0.42	0.51	**0.49**
multiscale	0.82	0.82	0.84	0.82	**0.82**
TV_ε-segment	0.77	0.82	0.78	0.73	**0.78**

Table 5.1: The normalized score of every algorithm applied on every dataset and the average of all scores of every algorithm.

We appreciate 17 participants took part in this experiment, and in Table 5.1 we observe that the multiscale and TV_ε-segment methods perform visually perceptually better than the other methods. We also give out the evaluation results by the interpolation error in Table 5.2 and find out that the TV_ε-segment method does not outperform the nooptim and full methods. The interpolation error measure can not reveal human visual perception due to two reasons. Firstly, the human eyes are sensitive for the shocks which are the common drawbacks of the opticalflow, nofeathering, full methods (see Figure 5.11), and also sensitive for the ghosting effects, which are characterized by the blend method. Secondly, the original dataset can not be regarded as the ground-truth since the interpolation between two images may not be unique.

We also test our algorithm in the field of image registration. Since image registration is one-way interpolation, we set μ, ν equal to 0 to avoid the segmentation. Under this setting the TV_ε-segment method turns into the TV_ε method. In this point of view we can also consider the TV_ε-segment method as a generalization of

	Face	Earth	Bunny	Dragon	**average**
blend	3.73	4.18	2.41	3.49	**3.45**
opticalflow	3.11	4.25	2.36	3.38	**3.28**
nofeathering	2.29	2.15	1.95	2.58	**2.24**
nooptim	1.72	1.52	1.40	2.02	**1.67**
full	1.72	1.52	1.40	2.02	**1.67**
multiscale	1.31	0.75	1.16	1.97	**1.31**
TV_ε-segment	2.08	1.91	1.65	2.40	**1.99**

Table 5.2: The interpolation error of every algorithm applied on every dataset and the average of all interpolation errors of every algorithm.

the TV_ε method. As an example we apply a synthetically warped image [44] and register it according to the unwarped image. In Figure 5.12 we find out that the contours of the skull are matched well. However, the brain tissues are not well registered because the tissue edges are not significant and the locally varying optical flow of every neighboring tissue segment influences each other.

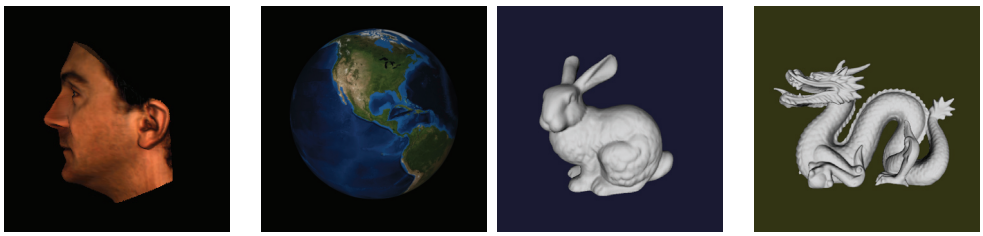

(a) (b) (c) (d)

Figure 5.7: Datasets of Stich. (a) Face. (b) Earth. (c) Bunny. (d) Dragon.

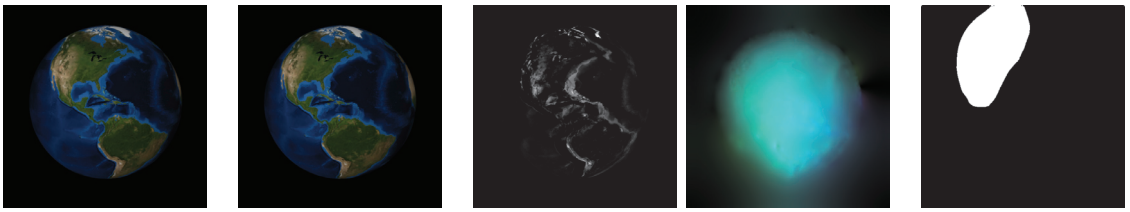

(a) (b) (c) (d) (e)

Figure 5.8: (a) Frame 9 of Earth. (b) Frame 12 of Earth. (c) The absolute difference between (a) and (b). (d) The optical flow calculated by the TV_ε-segment method. (e) The active contours calculated by the TV_ε-segment method.

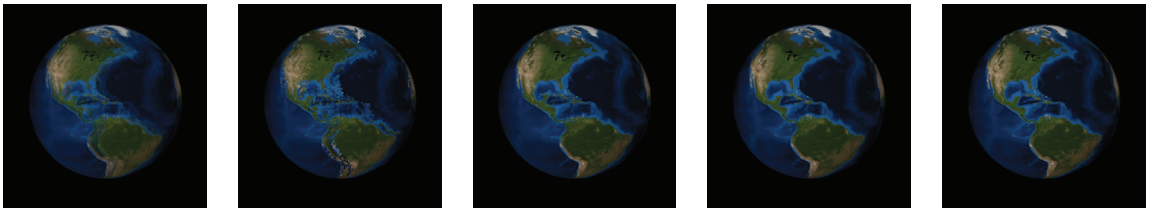

(a) (b) (c) (d) (e)

Figure 5.9: Frame 11 calculated by (a) the blend method, (b) the opticalflow method, (c) the full method, (d) the multiscale method, (e) the TV_ε-segment method.

(a) (b) (c) (d) (e)

Figure 5.10: (a) Frame 15 of Bunny. (b) Frame 18 of Bunny. (c) The absolute difference of (a) and (b). (d) The optical flow calculated by the TV_ε-segment method. (e) The active contours calculated by the TV_ε-segment method.

(a) (b) (c) (d) (e)

Figure 5.11: Frame 16 calculated by (a) the blend method, (b) the optical flow method, (c) the full method, (d) the multiscale method, (e) the TV_ε-segment method.

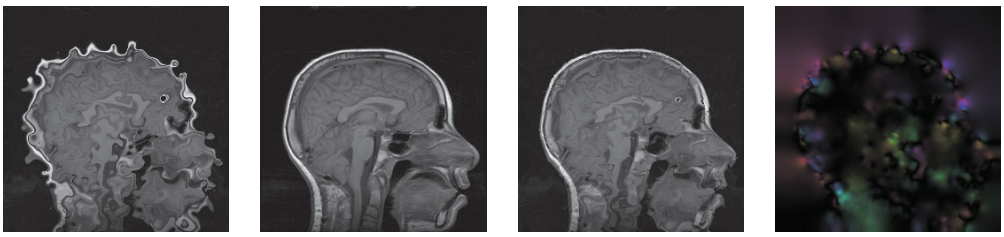

(a) (b) (c) (d)

Figure 5.12: (a) The template frame. (b) The target frame. (c) The registered frame calculated by the TV_ε-segment method. (d) The associated optical flow.

Chapter 6

Conclusion

In this work we investigate the image sequence interpolation problem with an optimal control of the optical flow governing a transport equation. With a priori optical flow we are able to utilize the transport equation to "transport" a given image to a certain moment. To identify the optical flow we seek a interpolated image to fit another given image in the sense of a cost functional and minimize it. Inspired by the solution theory of transport equations, we first set up the optical flow enjoying the Lipschitz regularity in space and the given images belong to BV. However, under these assumptions the estimated flow are too smooth to show the local features of the optical flow. To fix it we use the H^1-regularization instead, which is not so smooth and the transport equation still propagates the L^2-regularity of the initial image. Therefore, the validity term endowed with the L^2-norm still makes sense.

In the second model we consider the ε-smooth total variation instead of the H^1-regularization. The ε-smooth total variation is "a little bit" smoother than the TV-norm, and hence the minimizer to the associated minimization problem is supposed to be "a little bit" smoother than $W^{1,1}$, namely in $W^{1,1+\tau}$ where τ depends on the smooth variable ε. As a result, the optical flow estimated by the ε-smooth regularity has better edges preserving property than the H^1-regularization. And the well-posedness of transport equations under these settings still works according to the theory of DiPerna-Lions [27].

Inspired by the experiments we find out that the forward interpolation is not suitable in the disclosed regions. Thus, we utilize the active contours to segment the domain into the covered regions and disclosed regions. Moreover, we add another control, namely a level set function, whose zero level set is the contours segmenting

the covered regions and disclosed regions. In the associated cost functional we add the total variation of the level set function to regularize the level set function, hence the minimizer of the level set function exists in BV.

The introduced image sequence methods in the frame work of optimal control have several advantages compared to the per-pixel-wise methods introduced in Chapter 1: Firstly, our methods are stable, i.e. they avoid the shocks, ghosting effects, which are typically characterized by the per-pixel-wise methods. Secondly, they work robust against noise in the given images, because the optical flow field is continuous, and hence the local oscillations in the optical flow created by noises are dumped by the neighboring dominated optical flow. Thirdly, they solve a quite large range of image sequence interpolation problems, simple rigid movements interpolation and non-rigid movements interpolation are able to be handled.

On the other hand, our methods have also several disadvantages. The major problem lies in the definition of optical flow, since it does not reveal the real motion fields in 2d, it only figures an apparent motion field created by variation of image intensities. Thus, we have to assume that the intensity of objects do not change in time. If the images intensities of the background vary in time, then the flow field estimated by our methods are not really true, it could lead to some non-sense interpolation results. Thinking of the way out we may consider a transport equation with right-hand side f, which is another control and describes the variation of image intensities:

$$\begin{cases} u_t + b \cdot \nabla_x u = f \quad \text{in } (0,T] \times \Omega, \\ u(0) = u_0 \quad \text{in } \Omega, \\ u_n = 0 \quad \text{on } \partial\Omega. \end{cases}$$

Regarding the modeling and the regularization theory we know that b and f affect each other, since a strong weighted regularization of b leads to high-valued output f and low-valued output b, and a mildly weighted regularization of b converses. But what kind of combination of b and f creating the real interpolation is still not clear.

Secondly, although the ε-smooth total variation produces the optical flow with better edge preserving properties, however in some cases it is still too smooth for generating the intermediate images, since the discontinuous flow edges are important to keep shape of the objects not warped near the edges. To our knowledge, the effective methods solving the total variation minimization problems, e.g. [17]

is only available to the linear problem and [18] is available in the case that the adjoint operator of (3.2) is known. Hence, it is still a challenge to solve our imposed non-linear problems penalized by the total variation numerically.

References

[1] R. Acar and C.R. Vogel. Analysis of bounded variation penalty methods for ill-posed problems. *Inverse Problems*, 10:1217–1229, 1994.

[2] R.A. Adams and J.J.F. Fournier. *Sobolev Spaces*. Academic Press, 2003.

[3] L. Ambrosio. Transport equation and Cauchy problem for BV vector fields. *Inventiones mathematicae*, 158:227–260, 2004.

[4] L. Ambrosio, G. Crippa, C.D. Lellis, F. Otto, and M. Westdickenberg. *Transport Euqations and Multi-D Hyperbolic Conservation Laws*. Springer, 2008.

[5] L. Ambrosio, N. Fusco, and D. Pallara. *Functions of Bounded Variation and Free Discontinuity Problems*. Clarendon Press Oxford, 2000.

[6] L. Ambrosio, P. Tilli, and L. Zambotti. Introduzione allla teoria della misura ed alla probabilitá. Lecture notes of a course given at the Scuola Normale Superiore.

[7] H. Attouch, G. Buttazzo, and G. Michaille. *Variational Analysis in Sobolev and BV Spaces*. SIAM, 2006.

[8] G. Aubert and P. Kornprobst. *Mathematical Problems in Image Processing*. Springer, 2002.

[9] S. Baker, D. Scharstein, J.P. Lewis, S. Roth, M.J. Black, and R. Szeliski. A database and evaluation methodology for optical flow. *International Conference on Computer Vision*, pages 1–8, 2007.

[10] J. Barron and M. Khurana. Determining optical flow for large motions using parametric models in a hierarchical framework. *Vision Interface*, pages 47–56, 1994.

[11] A. Borzí, K. Ito, and K. Kunisch. Optimal control formulation for determining optical flow. *SIAM Journal of Scientific Computing*, 24:818–847, 2002.

[12] D. Braess. *Finite Elemente Theorie, schnelle Löser und Anwendungen in der Elastizitätstheorie*. Springer, fourth edition, 2007.

[13] F. Brezzi and M. Fortin. *Mixed and Hybrid Finite Element Methods*. Springer, 1991.

[14] A. Bruhn, J. Weickert, and C. Schnörr. Lucas/Kanade meets Horn/Schunck: Combining local and global optic flow methods. *International Journal of Computer Vision*, 61:211–231, 2005.

[15] P.J. Burt and E.H. Adelson. The Laplacian pyramid as a compact image code. *IEEE Transactions on Communications*, 31.

[16] V. Caselles, F. Catté, T. Coll, and F. Dibos. A geometric model for active contours in image processing. *Numerische Mathematik*, 66:1–31, 1993.

[17] A. Chambolle. An algorithm for total variation minimization and applications. *Journal of Mathematical Imaging and Vision*, 20:89–97, 2004.

[18] T.F. Chan and P. Mulet. On the convergence of the lagged diffusivity fixed point method in total variation image restoration. *SIAM Journal on Numerical Analysis*, 36(2):354–367, 1999.

[19] T.F. Chan and J. Shen. Variational image inpainting. *Communications on Pure and Applied Mathematics*, 58, 2005.

[20] T.F. Chan and L.A. Vese. Active contours without edges. *IEEE transactions on image processing*, 10(2), 2001.

[21] T.F. Chan and C. Wong. Total variation blind deconvolution. *IEEE Transactions on Image Processing*, 7, 1998.

[22] K. Chen and D.A. Lorenz. Image sequence interpolation using optimal control. *Journal of Mathematical Imaging and Vision*, pages 1–17, 2011.

[23] F. Colombini, T. Luo, and J. Rauch. Nearly Lipschitzean divergence free transport propagates neither continuity nor BV regularity. *Communications in Mathematical Sciences*, 2(2):207–212, 2004.

[24] G. Crippa. *The flow associated to weakly differentiable vector fields*. PhD thesis, Universität Zürich, 2007.

[25] Q.A. Dang. Using boundary-operator method for approximate solution of a boundary value problem (bvp) for triharmonic equation. *Vietnam Journal of Mahtematics*, 33(1):9–18, 2005.

[26] K. Deimling. *Nonlinear Functional Analysis*. Springer, 1985.

[27] R.J. DiPerna and P.L. Lions. Ordinary differential equations, transport theory and Sobolev spaces. *Inventiones mathematicae*, 98:511–547, 1989.

[28] H. Elman, D. Silvester, and A. Wathen. *Finite Elements and Fast Iterative Solvers*. Oxford University Press, 2005.

[29] L.C. Evans. *Partial Differential Equations*. Oxford University Press, 1998.

[30] L.C. Evans and R.F. Gariepy. *Measure Theory and Fine Properties of Functions*. CRC Press, 1992.

[31] J.M. Fitzpatrick and M. Sonka. *Handbook of Medical Imaging, Volume 2. Medical Image Processing and Analysis*. SPIE, 1 edition, 2000.

[32] V. Girault and P.A. Raviart. *Finite Element Methods for Navier-Stokes Equations*. Springer, 1986.

[33] P. Hartman. *Ordinary Differential Equations*. SIAM, second edition, 2002.

[34] W. Hinterberger and O. Scherzer. Models for image interpolation based on the optical flow. *Computing*, 66(3):231–247, 2001.

[35] C. Hirsch. *Numerical Computation of Internal & External Flows*. Elsevier, 2007.

[36] B.K.P. Horn and B.G. Schunck. Determining optical flow. *Artifical Intelligence*, 17:185–203, 1981.

[37] Y. Kameda and A. Imiya. The William Harvey code: Mathematical analysis of optical flow computation for cardiac motion. *Computational Imaging and Vision*, 36:81–104, 2007.

[38] M. Kass, D. Terzopoulos, and A. Witkin. Snakes: Active contour models. *International Journal of Computer Vision*, 1(4):321–331, 1988.

[39] S.L. Keeling and W. Ring. Medical image registration and interpolation by optical flow with maximal rigidity. *Journal of Mathematical Imaging and Vision*, 23(1):47–65, 2005.

[40] D. Kuzmin and S. Turek. High-resolution FEM-TVD schemes based on a fully multidimensional flux limiter. *Journal of Computational Physics*, 198, 2004.

[41] J.L. Lions. *Optimal Control of Systems Governed by Partial Differential Equations*. Springer, 1971.

[42] D. Mahajan, F. Huang, W. Matusik, R. Ramamoorthi, and P. Belhumeur. Moving gradients: a path-based method for plausible image interpolation. *ACM Transactions on Graphics*, 28(3), 2009.

[43] D. Mumford and J. Shah. Optimal approximations by piecewise smooth functions and associated variational problems. *Communications on Pure and Applied Mathematics*, 42(5):577–685, 1989.

[44] S. Periaswamy and H. Farid. Differential elastic image registration. Technical Report TR2001-413, Dartmouth College, Computer Science, 2001.

[45] W.H. Press, S.A. Teukolsky, W.T. Vetterling, and B.P. Flannery. *Numerical Recipes*. Cambridge University Press, third edition, 2007.

[46] T. Rahman, X.C. Tai, and S. Osher. A TV-Stokes denoising algorithm. In *Scale-Space Theories in Computer Vision*, pages 473–483, 2007.

[47] K.F. Riley, M.P. Hobson, S.J. Bence, and S. Bence. *Mathematical methods for physics and engineering*. Cambridge University Press, 2006.

[48] L.I. Rudin, S. Osher, and E. Fatemi. Nonlinear total variation based noise removal algorithms. *Physica D*, 60, 1992.

[49] W. Rudin. *Functional analysis*. International Series in Pure and Applied Mathematics. McGraw-Hill, second edition, 1991.

[50] D. Rueckert, L.I. Sonoda, C. Hayes, D.L.G. Hill, M.O. Leach, and D.J. Hawkes. Nonrigid registration using free-form deformations: Application to breast MR images. *IEEE Transactions on Medical Imaging*, 18:712–721, 1999.

[51] T. Stich, C. Linz, G. Albuquerque, and M. Magnor. View and time interpolation in image space. *Pacific Graphics*, 27(7):1781–1787, 2008.

[52] T. Stich, C. Linz, C. Wallraven, D. Cunningham, and M. Magnor. Perception-motivated interpolation of image sequences. *ACM Transactions on Applied Perception*, 2010.

[53] D. Suter. Mixed-finite element based motion estimation. *Innovation and Technology in Biology and Medicine*, 15(3):292–307, 1994.

[54] X.C. Tai, S. Osher, and I. Holm. Image inpainting using a TV-Stokes equation. In *Image Processing on Partial Differential Equations*. Springer, 2006.

[55] F. Tröltzsch. *Optimale Steuerung partieller Differentialgleichungen*. Vieweg, 2005.

[56] C.R. Vogel and M.E. Oman. Iterative methods for total variation denoising. *SIAM Journal on Scientific Computing*, 17:227–238, 1996.

[57] J. Watkinson. *The MPEG Handbook*. Focal Press, second edition, 2004.

[58] A. Wedel, T. Pock, C. Zach, H. Bischof, and D. Cremers. An Improved Algorithm for TV-L1 Optical Flow. In *Statistical and Geometrical Approaches to Visual Motion Analysis*, page 45, 2009.

[59] C. Zach, T. Pock, and H. Bischof. A duality based approach for realtime TV-L1 optical flow. In *Annual Symposium of the German Association for Pattern Recognition*, pages 214–223, 2007.

[60] O.C. Zienkiewicz and R.L. Taylor. *The Finite Element Method*, volume 1. Butterworth-Heinemann, fourth edition, 1997.